2011

Electromagnetic Propagation Anomalies In Waveguiding Structures And Scattering Systems

Alessandro Salandrino
University of Central Florida

ELECTROMAGNETIC PROPAGATION ANOMALIES IN WAVEGUIDING STRUCTURES AND SCATTERING SYSTEMS

by

ALESSANDRO SALANDRINO
laurea degree (M.S.) University of Rome ROMATRE, 2003
M.S. University of Central Florida, 2010

A dissertation submitted in partial fulfillment of the requirements
for the degree of Doctor of Philosophy
in the College of Optics and Photonics
at the University of Central Florida
Orlando, Florida

Summer Term
2011

Major Professor: Demetrios N. Christodoulides

ABSTRACT

The effects related to diffraction and interference are ubiquitous in phenomena involving electromagnetic wave propagation, and are accurately predicted and described within the framework of classical electrodynamics. In the vast majority of the cases the qualitative features of the evolution of a propagating wave can be inferred even without detailed calculations. A field distribution will spread upon propagation, will accumulate phase along the direction of power flow, will exert mechanical forces upon scattering objects in the direction of propagation etc. When such predictions fail, counterintuitive effects and new functionalities can be engineered. In this work a series of exceptional cases under different degrees of field confinement have been isolated. In such instances the electromagnetic behavior significantly deviates from conventional cases. In particular, considering structures with monodimensional field confinement, the only possible class of diffraction free surface waves has been introduced. Again within the context of surface waves the mechanism of Enhanced Evanescent Tunneling (EET) has been proposed, which allows a net power flow to be sustained by evanescent fields only with applications to sub-diffraction imaging. Increasing the degree of field confinement, a unique class of fully dielectric waveguide arrays able to support negative effective index modes has been theoretically demonstrated. Finally the opto-mechanical consequences of such effective negative index environments have been studied, highlighting counterintuitive properties. Instrumental to these findings was the introduction of a general theory of optical forces in terms of vector spherical harmonics.

AKNOWLEDGEMENTS

I would like here to express my gratitude to all the people who helped me and supported me during my studies.

I would like to thank my advisor Prof.Christodoulides for guiding me through my research. It was a great honor for me to work with him.

I thank all the members of my committee for the useful and stimulating discussions.

I would like to thank all the CREOL staff, in particular Rachel, Amy, Gail and Maria for their invaluable help and kindness.

But most of all I would like to express all my gratitude to my family: my dear Shima, my Mother, my Father and my Grandmother. They supported me with all their love and care. And since I know very well how annoying I can be when I am stressed, I thank them even more. What really I want say can only be properly expressed in Italian, so…

Grazie Shima, Game', Gazzu' e Nonna. Vi voglio tanto bene. Questa non e' la mia, ma e' la vostra tesi.

TABLE OF CONTENTS

LIST OF FIGURES

CHAPTER 1
INTRODUCTION

The development of the theory Classical Electrodynamics may be considered as one of the highest achievements in Classical Physics. The very fact that Maxwell's theory survived, and as a matter of fact ushered, the era of Relativistic Physics is by itself unique and impressive. The enormous predictive power of the theory of Classical Electrodynamics may be interpreted as a clear indication that this field has reached a stage complete maturity. This is certainly true as far as the foundations of the Electromagnetic Theory are concerned, nevertheless a great wealth of exotic phenomena and counterintuitive effects are still hidden in the fine details of specific systems carefully designed to isolate them. As a patent example, the whole field of Metamaterials emerged in the past decade, and engaged scientists and engineers in the quest of achieving media with negative index of refraction. Besides the achievement of this ultimate goal, along the way a whole body of knowledge has been created and new concepts such as hyperbolic dispersion and transformation optics have been introduced.

The complexity of the electromagnetic problem is directly related to the material properties and the dimensionality of the structures interacting with, or confining the fields. Different effects and richer dynamics emerge in the electromagnetic propagation as the system complexity increases from unbound dielectric spaces to waveguide structures and ultimately coupled systems.

In this work we have explored anomalous propagation dynamics in waveguiding structures with mono-dimensional and two-dimensional field confinement, and in coupled waveguide systems.

Chapters 2 and 3 are devoted to surface waves. In the chapter 2 diffraction free propagation of surface plasmons is theoretically demonstrated. We introduced a new class of non-diffracting surface plasmonic wave: the Airy Plasmon. The propagation properties of such field configuration are unique among the family of surface waves and could lead to interesting applications in plasmonic energy routing. The self-bending and self-healing behavior of these solutions is discussed. Schemes for experimental realization and potential applications are proposed.

Chapter 3 is devoted to the manipulation of surface waves. In particular we propose the concept of enhanced evanescent tunneling (EET). Our analysis indicates, that by means of a suitable control field, the transmission of evanescent waves across a forbidden gap can be enhanced by several orders of magnitude-well beyond the ordinary frustrated total internal reflection case. We show how such phenomenon can be used to probe both the amplitude and phase of the evanescent portion of the angular spectrum, thereby allowing target superresolution.

In the fourth chapter we add another degree of field confinement. A class of dielectrically loaded metallic waveguides supporting negative index modes in the far infrared and terahertz regime is presented. Principles of operation, modal structure and appropriate coupling schemes are analytically and numerically investigated. The extreme simplicity of the proposed design, along with the non conventional and counter intuitive electromagnetic properties of this class of waveguides, makes of these structures excellent candidates for the practical realization of far

infrared and terahertz devices with new and interesting functionalities. Generalizations and extensions of the current design are also discussed.

In the fifth chapter coupled systems are considered. We present an analytical description of a new class of three-core adiabatic following directional couplers. Using a multiple-scale WKB method we obtain closed-form expressions describing the optical field dynamics in such structures. The adiabatic evolution occurring in this particular three-core configuration can lead to a spatial switch over of local supermodes and to an irreversible power transfer.

The sixth chapter is devoted to the opto-mechanical consequences of the exotic properties of the structures presented in chapter 4. In particular we show that the negative index environment constituted by an array of Clarricoats-Waldron waveguides has the unique property of inducing longitudinally invariant reverse force fields on dipolar scatterers.

In chapter 7 a general formulation of optical forces, beyond the electric dipole approximation, is developed in terms of spherical electromagnetic multipoles. The interaction mechanisms between multipoles of different parity, order and degree are highlighted. This general formulation is used in chapter 8 to analyze the optical forces exerted on a dielectric sphere illuminated by a very particular superposition of two non-interfering plane waves able to generate a transverse Poynting vector flow.

CHAPTER 2
UNIDIMENSIONAL FIELD CONFINEMENT: SURFACE PLASMONS

Introduction

In recent years, advances in nanotechnology have led to an increased interest in surface plasmons as a means to manipulate light at the nanoscale. The part of optics which deals with surface plasmons has grown into a discipline of its own, commonly referred to as plasmonics. Several peculiar properties of surface plasmons have been experimentally demonstrated and successfully exploited in waveguides [1-7], plasmonic nanoantennas[8-15], and plasmonic collimators [16-19], to cite a few.

While a great deal of attention has been devoted to surface plasmon guidance, propagation and diffraction, to the best of our knowledge no diffraction free field configurations have been so far suggested for these plasmon waves. In this paper, inspired by recent developments in diffraction free beams, we present the only possible class of surface plasmons compatible with paraxial diffraction-free, surface bound propagation, and exhibiting a unique self-bending behavior.

Diffraction-free beams are associated with field configurations (exhibiting a definite peak in amplitude) for which the transverse intensity profiles at any two locations along the propagation direction remain invariant. In free space several families of diffraction-free beams have been identified in the literature, such as Bessel beams [20], Mathieu beams [21] and more recently Airy beams [22-30].

In general however, the surface wave nature of plasmons does not allow a straightforward extension of these ideas to a metal/dielectric interface. In this case, the exponential decay of the transverse field distribution is fixed, and hence the plasmon propagation properties are exclusively dictated by its 1D angular spectrum. Along these very lines, one may ask whether a 1D projection of the conical angular spectrum of a 2D diffraction-free solution could yield a surface wave of similar characteristics. In this regard, the answer is negative since a "conical" superposition in 1D leads to a sinusoidal interference pattern, which is by no means a localized beam.

Lately, non-diffracting Airy beams have been suggested and observed in optics [22, 23]. As first indicated by Berry and Balazs [31], the Airy wavepacket happens to be unique: it represents the only non-spreading solution to the one-dimensional potential-free quantum Schrödinger equation. Given the isomorphism between the quantum mechanical Schrödinger equation and the paraxial wave equation, the Airy beam indeed represents the only non-diffracting 1D beam profile [27, 32]. But perhaps the most intriguing feature of this solution is its very ability to freely self-bend even in the absence of any external potential [22]. This aspect has thus far been exploited in several physical settings such as in microparticle manipulation [33], plasma filamentation in air [34], nonlinear Airy beam generation [29, 30], and optical Airy bullets [35] to mention a few.

Analysis

The problem of surface plasmon propagation at the planar interface $y = 0$ between a dielectric medium of permittivity ε_d placed over a metallic substrate of permittivity ε_m is polarization dependent and therefore strictly vectorial. It is however possible to select a Cartesian component of the field to be used as a scalar potential, from which all the other field component may be deduced. Without loss of generality, the problem may be effectively formulated in terms of the component of the electric field normal to the boundary, which obeys the scalar Helmholtz equation (1.1):

$$\nabla^2 E_{dy} + k_0^2 \varepsilon_d E_{dy} = 0 \qquad (2.1)$$

For a surface Plasmon, the field exponentially decays away from the interface, leading to a functional dependence of the form $E_y(x, y, z) = A(x, z)\exp(ik_z z)\exp(-\alpha_d y)$, where the parameters k_z and α_d are be related through the dispersion relations $\alpha_d^2 = k_z^2 - k_0^2 \varepsilon_d$ and $k_z = k_0 \sqrt{\varepsilon_d \varepsilon_m / (\varepsilon_d + \varepsilon_m)}$. Assuming that the transverse beam profile is slowly varying with respect to the propagation coordinate z, it is straightforward to show that the problem reduces to the 1D free-particle Schrödinger equation:

$$\frac{\partial^2 A}{\partial x^2} + 2ik_z \frac{\partial A}{\partial z} = 0 \qquad (2.2)$$

In this case, one can directly show that the complex amplitude of the normal component of the electric field associated with a finite energy plasmon-Airy beam solution is described by:

$$A(x,z)=\mathrm{Ai}\left[\frac{x}{x_0}-\left(\frac{z}{2k_z x_0^2}\right)^2+i\frac{az}{k_z x_0^2}\right]\exp\left[i\left(\frac{x+a^2x_0}{2x_0}\frac{z}{k_z x_0^2}-\frac{1}{12}\left(\frac{z}{k_z x_0^2}\right)^3\right)\right]\exp\left[a\frac{x}{x_0}-\frac{a}{2}\left(\frac{z}{k_z x_0^2}\right)^2\right] \tag{2.3}$$

Of importance is the angular spectrum of this solution which is given by:

$$\tilde{A}(k_x,z)=x_0\exp\left(\frac{a^3}{3}\right)\exp\left(-ia^2x_0k_x\right)\exp\left(-ax_0^2k_x^2\right)\exp\left(\frac{ix_0^3k_x^3}{3}\right)\exp\left(-i\frac{k_x^2z}{2k_z^2}\right) \tag{2.4}$$

In expression(2.4), the Gaussian spectrum arises from the exponential apodization of the beam (in Eq.(2.3)) while the cubic phase term is associated with the Fourier transform of the Airy wave itself. Given the Gaussian spectrum of this Airy plasmon, the paraxial treatment will hold provided that:

$$\sqrt{\ln 2\Big/\left(ax_0^2\right)}<<k_0\sqrt{\frac{\varepsilon_d\varepsilon_m}{\left(\varepsilon_d+\varepsilon_m\right)}} \tag{2.5}$$

In this case, the k-spectrum of the remaining electromagnetic field components can be written in terms of the angular spectrum $\tilde{E}_y(k_x)$, e.g.:

$$
\begin{aligned}
\tilde{E}_z &= -\frac{i\alpha_d}{k_0^2\varepsilon_d + \alpha_d^2} k_z \tilde{E}_y \approx -\frac{i\alpha_d}{\sqrt{k_0^2\varepsilon_d + \alpha_d^2}} \tilde{E}_y \\
\tilde{E}_x &= \frac{\alpha_d}{k_0^2\varepsilon_d + \alpha_d^2}\left(-ik_x\right)\tilde{E}_y \\
\tilde{H}_x &= -\frac{\omega\varepsilon_0\varepsilon_d}{k_0^2\varepsilon_d + \alpha_d^2} k_z \tilde{E}_y \approx -\frac{\omega\varepsilon_0\varepsilon_d}{\sqrt{k_0^2\varepsilon_d + \alpha_d^2}} \tilde{E}_y \\
\tilde{H}_z &= \frac{i\omega\varepsilon_0\varepsilon_d}{k_0^2\varepsilon_d + \alpha_d^2}\left(-ik_x\right)\tilde{E}_y
\end{aligned}
\qquad (2.6)
$$

Based on the expressions (1.6) the electromagnetic field associated with the Airy plasmon in the dielectric region can be finally written as:

$$
\begin{aligned}
\mathbf{E}_d &= \frac{1}{\varepsilon_d}\left[\left(\hat{\mathbf{y}} - \frac{i\alpha_d}{\sqrt{k_0^2\varepsilon_d + \alpha_d^2}}\hat{\mathbf{z}}\right)A(x,z) + \hat{\mathbf{x}}\frac{\alpha_d}{k_0^2\varepsilon_d + \alpha_d^2}\frac{\partial A(x,z)}{\partial x}\right]\exp\left(i\sqrt{k_0^2\varepsilon_d + \alpha_d^2}\,z\right)\exp(-\alpha_d y) \\
\mathbf{H}_d &= \frac{1}{\varepsilon_d}\left[-\hat{\mathbf{x}}\frac{\omega\varepsilon_0\varepsilon_d}{\sqrt{k_0^2\varepsilon_d + \alpha_d^2}}A(x,z) + \hat{\mathbf{z}}\frac{i\omega\varepsilon_0\varepsilon_d}{k_0^2\varepsilon_d + \alpha_d^2}\frac{\partial A(x,z)}{\partial x}\right]\exp\left(i\sqrt{k_0^2\varepsilon_d + \alpha_d^2}\,z\right)\exp(-\alpha_d y)
\end{aligned}
\qquad (2.7)
$$

The corresponding electromagnetic fields in the metal region can be readily obtained from equations (7) using the substitutions $\varepsilon_d \to \varepsilon_m$ and $\alpha_d \to \alpha_d(\varepsilon_m / \varepsilon_d)$. Plots of the intensity distribution of an Airy plasmon on the interface plane and on transverse cuts are presented in Figs.1a and 1b respectively.

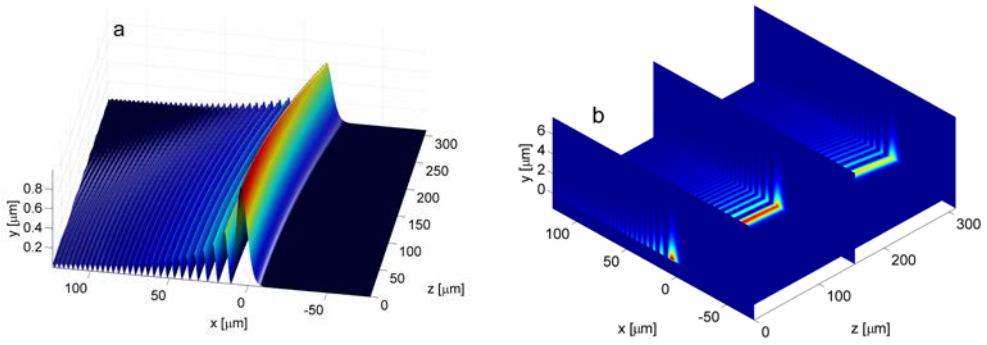

Figure 1 (a) Normalized intensity distribution at a metal dielectric interface.(b) Intensity distribution on the interface plane and on three transverse cuts along propagation.

The diffraction-free character of this Airy plasmon wave is evident. In addition, the self-bending features of this solution are clearly depicted in this same figure.

The parabolic self-deflection experienced by the Airy plasmon during propagation can be estimated from Eq. (3). Taking the quantity $2x_0$ as a measure of the width of the main lobe, one can define a characteristic propagation length $Z_c = 2\sqrt{2}k_z x_0^2$ for which the beam is approximately displaced by one full width (of the main lobe). This characteristic parameter can be used to estimate an upper limit of propagation losses that can be tolerated in an experimental setup aimed to observe Airy plasmons. Given the losses of the system, this behavior can only be detected provided that the $1/e$ power decay is comparable to Z_c. This particular choice leads to the condition $\max\left[\mathrm{Im}\left(k_z\right)\right] = 1/[4\sqrt{2}\,\mathrm{Re}\left(k_z\right)x_0^2]$. Based on this criterion, Fig.2 depicts the

$\{\lambda, x_0\}$ region where such Airy plasmons are practically allowed to propagate along a silver-air interface.

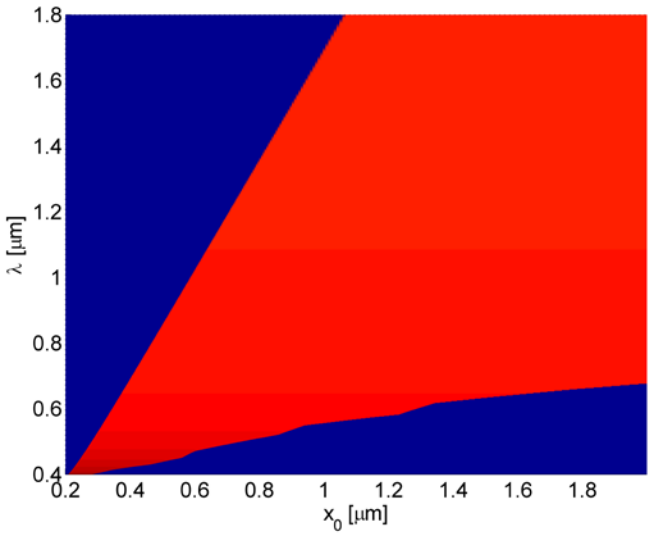

Figure 2 The red area represents the region in the parameter space over which the criterion is met for a silver-air interface.

As previously indicated, apart from its characteristic self bending, Airy plasmons remain essentially diffraction-free during propagation. This important feature can be more easily appreciated by directly comparing this solution with a Gaussian plasmon wave whose width is comparable to that of the Airy main lobe. In the numerical example shown in Fig.3 we considered an Airy and a Gaussian plasmon wave propagating at an interface between silver and

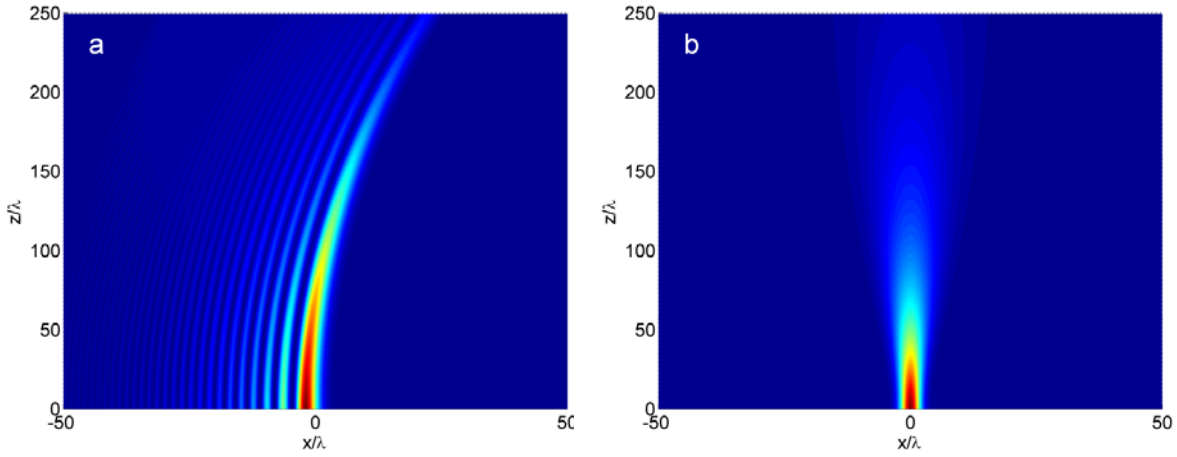

Figure 3 Comparison between the propagation of an Airy Plasmon (a) and a Guassian plasmon at a silver-air interface.

air at a wavelength of 1.55μm. As it becomes apparent from the simulations, both plasmons experience attenuation due to the loss in the metal, but while the Gaussian undergoes significant spreading, the Airy plasmon propagates almost undiffracted. Furthermore, as theoretically and experimentally shown in [25] for the 2D counterpart, the Airy plasmon shares one of the most attractive properties typical of non-diffracting waves: an inherent resilience against perturbations and a self-healing behavior. This concept translated into the plasmonic realm leads to a field configuration which is relatively unaffected by surface roughness and fabrication defects of the metallic layer. Based on these properties the Airy plasmon could find applications as an effective means to route energy over a metallic interface between plasmonic devices.

It is important to notice that the aforementioned interesting features of an Airy plasmon can only be displayed provided that a sufficiently long range of propagation is possible. In this respect, while the idea of a sub-wavelength Airy beam appears extremely attractive in principle, the high losses of strongly confined surface plasmons would most likely prevent the practical realization of such a concept. At this stage, perhaps only weakly guided plasmons hold promise as far as the experimental implementation of the Airy plasmon is concerned.

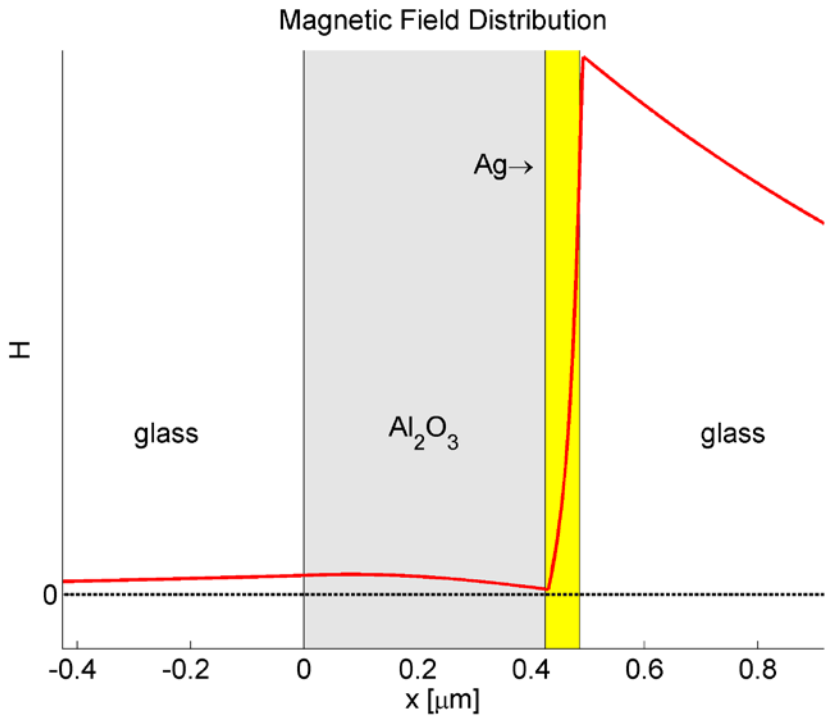

Figure 4 Magnetic field distribution over the cross-section of a multilayer structure. The surface plasmon at the Ag-Glass interface is excited by the first TM mode of the aluminum oxide layer.

The commonly used schemes for the excitation of surface plasmons over a metallic block, such as for instance the Otto configuration [36] or the grating coupling, are not without challenges in this specific case in which a carefully imprinted transverse profile is necessary. From a practical standpoint, thin metallic films deposited over dielectric substrates could represent a more viable route towards the excitation and the observation of Airy plasmons. Power could be effectively coupled into the surface plasmon by using the substrate as a waveguide, provided that the thickness of the dielectric is chosen so as to support just the first TM mode properly phase matched to the mode of the metallic film. One such example of plasmonic launcher for operation at 1.5μm is shown in Fig.4. Using this scheme an Airy beam could be generated in free space as done in [23] and then focused down into the input facet of the substrate with a cylindrical lens, exciting only the TM mode coupled to the surface plasmon.

In conclusion, a novel class of surface plasmons capable of propagating almost diffraction-free was introduced. Our analysis indicates that this class of solutions can freely self-bend during propagation-a unique property among all other surface waves. Such field configurations may find interesting applications in energy routing over plasmonic boards. The associated electromagnetic field distribution was analyzed and suitable coupling schemes were discussed.

CHAPTER 3
EVANESCENT WAVE INTERACTION: ENHANCED EVANESCENT TUNNELING (EET)

Introduction

In the previous chapter we dealt with surface plasmons which, as modes of a metal dielectric interface, represent one very specific instance of evanescent electromagnetic fields. In this chapter we treat evanescent waves from a more general perspective. In particular we study the interaction of multiple evanescent waves. This subject has major implications in the field of imaging, where the resolution of an ideal instrument is ultimately limited by the evanescent nature of part of the angular spectrum of any finite size target to be resolved. The question that we tried to answer is whether or not a far field measurement technique could be devised in order to recover an evanescent spectrum, therefore increasing the resolving power of an imaging system.

Since the early days of physics, imaging has always been a subject of intense research activity with crucial implications in many other disciplines ranging from biology and material sciences to astronomy. Over the centuries, starting from the “oculo vitreo” of the English friar Thomas Waleys (1349) to the modern confocal microscopes, endless efforts have been devoted to either improve existing techniques or to invent new approaches -based on completely different principles- in order to achieve higher resolving power. The resolution limitations of conventional far-field optics are well known and they are fundamental by nature. The physics of

free space electromagnetic propagation itself prevents the possibility of resolving features (or focusing light) beyond the so-called Abbe-Rayleigh limit [37].

In the past decades several new ideas have been put forward in order to alleviate or entirely circumvent the shortcomings of conventional imaging. A true revolution in the field came about with the demonstration of the first near field scanning microscope (working in the microwaves regime) in 1972 by Ash and Nicholls [38], which eventually led to the implementation of the first near field optical microscope (NSOM) in 1984 [39, 40]. Interestingly enough, the concept behind this important device can be traced back to 1928, when Synge [41] proposed the idea of scanning a sub-wavelength aperture in close proximity of a target in order to totally avoid propagation and diffraction effects. In fact resolutions down to the 10-100nm scale are these days within the reach of modern NSOMs.

Despite the success of near field optics, the pursuit of a far field sub-diffraction microscope never stopped. Interesting and effective contributions came from the most diverse perspectives. The STED method devised by Hell and co-workers [42] exploits stimulated emission to overcome the diffraction limit in fluorescence microscopy. Another successfully demonstrated approach was developed within the metamaterials community, with the introduction of artificial media with hyperbolic dispersion [43-48], supporting diffraction free propagation. Other information theoretic methods utilizing sparsity have also been suggested in order to attain a higher resolving power in post-processing [49]. From a physical point of view, the mechanism that ultimately limits the resolution of an optical instrument is the spatial frequency cut-off

imposed by free space propagation on the electromagnetic angular spectrum of the source field. The information associated with the finer (subwavelength) details of an illuminated object is in fact carried by evanescent waves, which decay exponentially with the distance of propagation and are eventually lost, as far as any far field detection scheme is concerned.

In this chapter we introduce the concept of enhanced evanescent tunneling (EET) and show how it can be used to probe both amplitude and phase of the evanescent portion of the angular spectrum of a field distribution. As we will see, this process effectively exploits the peculiar features of the evanescent waves themselves. In this case, interference effects alone are responsible for boosting the power tunneled over a forbidden gap. This is accomplished through an auxiliary beam that is appropriately matched to the signal. As opposed to other arrangements, this effect can be employed to extract the evanescent information even when direct contact with the target is impossible, e.g. when is submerged few wavelengths below the accessible surface. Even more importantly, this enhancement is possible without invoking any amplification or fluorescent markers. In principle enhanced evanescent tunneling can be manifested in other areas of physics where wave tunneling is involved as for example in quantum mechanical scattering.

We begin our analysis by considering the propagation dynamics of a monochromatic electromagnetic field $\mathbf{E}_s(x, y, z)$ in a linear homogeneous isotropic medium, taking place between two parallel planes, say $z = 0$ and $z = d$. This can be conveniently described in terms of the angular spectrum $\mathbf{A}_S(k_x, k_y)$ of the electric field at $z = 0$:

$$\mathbf{A}_S\left(k_x,k_y\right)=\frac{1}{2\pi}\iint\mathbf{E}_S\left(x,y,0\right)e^{-i\left(k_xx+k_yy\right)}dxdy \qquad (3.1)$$

$$\mathbf{E}_S\left(x,y,d\right)=\frac{1}{2\pi}\iint\mathbf{A}_S\left(k_x,k_y\right)e^{id\left[k^2-k_x^2-k_y^2\right]^{1/2}}e^{i\left(k_xx+k_yy\right)}dk_xdk_y \quad (3.2)$$

In Eqs. (2.1)and (2.2) a harmonic time dependence of the form $\exp\left(-i\omega t\right)$ was assumed. As usual, k in a linear homogeneous isotropic medium of refractive index n is given by $k=\omega n/c$. In this plane-wave expansion the transition from homogeneous to evanescent components occurs for $k_x^2+k_y^2>k^2$. As previously indicated, it is the exponential decay of the evanescent part of the angular spectrum that is ultimately responsible for limiting the resolution of an ideal far field imaging system. Such shortcomings may be overcome if and only if a scheme is devised that enables one to measure the cut-off components of the angular spectrum.

The differences between evanescent waves and their homogeneous counterparts are profound in many respects and of course these characteristics are reflected in the anomalous ways these waves interfere or can be detected. In a lossless medium, the spatial evolution of evanescent waves along the direction of decay is such that there is no phase variation and the net power flow is zero. The origin of this phenomenon can be easily traced back to the relative phase between the electric and magnetic field components-orthogonal to the decay direction. While for homogeneous waves these components are in phase, in the evanescent case they are in quadrature, thus having a Poynting vector with a vanishing real part.

Nevertheless there are instances in which evanescent waves can support a net power flow. Probably the first example that comes to mind is the phenomenon of frustrated total internal reflection (FTIR) which is schematically illustrated in Fig.5.

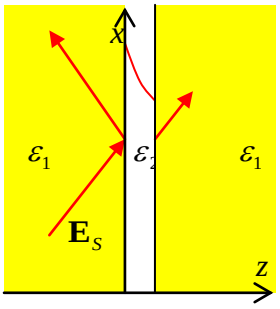

Figure 5 Evanescent tunneling through a gap by frustrated total internal reflection

In this case two dielectric half-spaces having equal relative permittivities ε_1 are separated by a gap of lower permittivity ε_2 and of length d. Assuming that a TE polarized plane wave is incident upon the first interface under total internal reflection conditions, then the electromagnetic field distribution in the intermediate layer is given by:

$$\mathbf{E} = \hat{\mathbf{y}}\left[A_D e^{-\alpha z} + A_R e^{\alpha(z-d)}\right] e^{ik_x x}$$
$$\mathbf{H} = \left[\left(\frac{k_x \hat{\mathbf{z}} - i\alpha\hat{\mathbf{x}}}{k_0\eta_0}\right) A_D e^{-\alpha z} + \left(\frac{k_x \hat{\mathbf{z}} + i\alpha\hat{\mathbf{x}}}{k_0\eta_0}\right) A_R e^{\alpha(z-d)}\right] e^{ik_x x} \qquad (3.3)$$

where $k_0 = \omega / c$ and η_0 is the vacuum characteristic impedance. In addition $\alpha = \sqrt{k_x^2 - k_0^2 \varepsilon_2}$ represents the evanescent wave decay constant.

As indicated in (2.3), the field in the gap is given by the superposition of two evanescent waves, each one decaying away from its corresponding interface at $z = 0$ and at $z = d$. We will refer to these two components as "direct" A_D and "reflected" waves A_R. As pointed out before none of the two evanescent fields can separately contribute to the power transfer across the gap. Nevertheless the cooperative action of the two evanescent components does lead to net power flow in the z direction, which in terms of the Poynting vector reads:

$$\mathbf{S} \cdot \hat{\mathbf{z}} = \frac{1}{2} \mathrm{Re}\left[\left(\mathbf{E} \times \mathbf{H}^* \right) \cdot \hat{\mathbf{z}} \right] = \frac{\alpha \exp\left(-\alpha d\right)}{k_0 \eta_0} A_D \, \mathrm{Im}\left[A_R \right] \quad (3.4)$$

Where we assumed without loss of generality that $A_D \in \Re$. The presence of the interference factor $A_D \, \mathrm{Im}\left[A_R \right]$ in the expression (2.4) lends itself to a simple interpretation of the physics behind this power flow. Depending on the relative phase of the coefficients A_D and A_R, the magnetic field of the reflected wave can actually provide a component which is in phase with the electric field of the direct wave. As a result, the electric field of the direct wave A_D, "rides" across the gap by using the in phase component of the reflected magnetic field, proportional to $\mathrm{Im}[A_R]$.In this example the relation between the direct and the reflected evanescent wave is fully dictated by the geometry of the system and it is straightforward to show that:

$$\frac{A_R}{A_D} = \frac{\alpha + i\sqrt{k_0^2(\varepsilon_1 - \varepsilon_2) - \alpha^2}}{\alpha - i\sqrt{k_0^2(\varepsilon_1 - \varepsilon_2) - \alpha^2}} \exp(-\alpha d) \qquad (3.5)$$

As it may be deduced from (2.4) and (2.5) the fraction of incident power that could tunnel is at best on the order of $\exp(-2\alpha d)$. The concept of enhanced evanescent tunneling (EET) emerges here as a way of imitating the power transfer mechanism of Eq.(2.4) in a fully controllable fashion, without the limitations imposed by equation(2.5).The main idea behind EET is to apply an auxiliary control field so as to induce a net power flow from an evanescent signal. The FTIR scheme discussed before is a particularly suitable framework for the illustration of the EET working principle, as all the relevant quantities can be computed in analytical form. Let us then consider a similar geometry in the presence of an additional control field, as schematically shown in Fig.6.

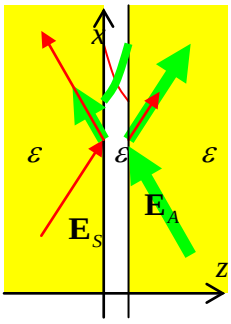

Figure 6 Enhanced Evanescent Tunneling

With reference to Fig.6, the following applied fields are considered:

$$\begin{aligned} \mathbf{E}_S &= \hat{\mathbf{y}} A_S e^{i\varphi_S} e^{ik_z z} e^{ik_x x}; \qquad (z \le 0) \\ \mathbf{E}_A &= \hat{\mathbf{y}} A_A e^{i\varphi_A} e^{-ik_z (z-d)} e^{ik_x x}; \quad (z \ge d) \end{aligned} \tag{3.6}$$

with $A_S, A_A \in \Re$ representing the amplitude of the signal and of the auxiliary fields respectively and with φ_S, φ_A being their phases evaluated at the appropriate interface.

The auxiliary field $\mathbf{E}_A$ is considered here to fall upon the second interface ($z = d$) at the same angle of incidence, polarization, and under the same total internal reflection conditions with the signal field $\mathbf{E}_S$, and therefore having identical Fresnel's coefficients. The field in the intermediate gap is now a superposition of the evanescent waves produced by the total internal reflection of both the signal and the auxiliary field. It is worth stressing the fact that, because of their evanescent nature, none of these fields undergoes any longitudinal phase shift across the gap. This effectively allows a univocal definition of the relative phase $\Delta\varphi_{AS} = \varphi_A - \varphi_S$ between similar field components due to the signal and the auxiliary wave. In these terms, the auxiliary field and the signal will be considered "in phase" if the tangential components of the respective electric fields evaluated at the two interfaces are in phase.

It is intuitively clear that if the auxiliary field and the signal have the same amplitude ($A_A = A_S$) and are in phase ($\varphi_A = \varphi_S$), then the power flow across the gap (through any $z = const$ plane) will vanish. More interesting and counterintuitive is the instance for which $\mathbf{E}_S$ and $\mathbf{E}_A$ are

$\pm\pi/2$ out of phase. In this case the electric field $\mathbf{E}_S$ of the signal is in phase with the magnetic field $\mathbf{H}_A$ of the auxiliary field and vice versa. As a consequence the combination of the two evanescent fields will sustain a net power flow across the structure, given in the most general case by:

$$P_z = \frac{2k_z^2\alpha}{k_0\eta_0}\frac{\left[k_z\alpha\left(A_S^2 - A_A^2\right) + \left(k_z^2+\alpha^2\right)\sinh\left(\alpha d\right)A_S A_A \sin\left(\Delta\varphi_{AS}\right)\right]}{\left[2k_z\alpha\cosh\left(\alpha d\right)\right]^2 + \left[\left(k_z^2-\alpha^2\right)\sinh\left(\alpha d\right)\right]^2} \quad (3.7)$$

By inspection it is possible to identify in equation (2.7) three different components. The quadratic term in A_S describes the power transfer due to the FTIR of the signal alone. The analogous quadratic term in A_A, bearing a negative sign, is associated with an energy flow in the opposite direction due to the FTIR of the auxiliary field. More interesting is the mixed term proportional to $A_A A_S$, which will be referred to as "Poynting interference". This term accounts for the cooperative power transfer effects enabled by the electric field of one wave and the in-phase magnetic field component of the other. Interestingly enough the direction of the Poynting interference contribution is solely determined by the relative phase $\Delta\varphi_{AS}$ of the two evanescent fields involved, regardless of their amplitude.

A careful consideration of this property reveals indeed counterintuitive consequences, in particular in the regime for which the Poynting interference dominates over the FTIR terms. Fig.3. illustrates the power flow across a $3\,\mu m$ long air gap separating two silicon ($n = 3.5$) half

spaces in a configuration similar to that of Fig.6., as a function of the auxiliary field power. Two electromagnetic waves of wavelength 1.5 μm are incident on the two interfaces at an angle of 20 degrees with respect to the normal, so as to be in total internal reflection mode. To demonstrate this effect, let us assume that the power density of the signal is kept at $1 W/m^2$ while the auxiliary field power density is varied over a broad range. The relative phase between the signal and the auxiliary field is optimally set at $\Delta\varphi_{AS} = \pi/2$. For the sake of comparison, in the absence of the auxiliary field the power density flux in the z direction that could tunnel across the structure by FTIR would be $1.28\times10^{-7} W/m^2$.

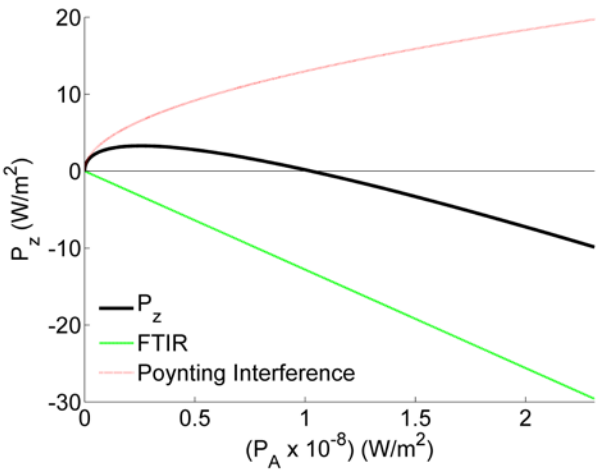

Figure 7 Power flow across a 3μm air gap between two Silicon half spaces.

Intuitively one would expect that if the auxiliary field is larger than the signal, power would flow in the negative z direction. Quite strikingly on the other hand Fig.7 shows that there is a whole

region where the auxiliary field is literally orders of magnitude larger than the signal and yet power flows across the gap in the positive z direction. Such anomaly is consequence of Poynting interference, shown in red in Fig.7. This effect indeed overcomes the auxiliary field FTIR contribution (shown in green in Fig.7) in the low intensity regime and enhances the tunneling of the signal.

It can be directly shown that maximum enhanced evanescent tunneling occurs when the amplitude of the auxiliary field is given by:

$$A_A = \frac{k_z^2 + \alpha^2}{2k_z\alpha}\sinh(\alpha d)\sin(\Delta\varphi_{AS})A_S \quad (3.8)$$

provided that $\Delta\varphi_{AS} = \pi/2$. Under the condition (2.8) the power flow across the gap attains a maximum value of:

$$P_{MAX} = \frac{k_z}{2k_0\eta_0}A_S^2 \qquad (3.9)$$

The power flow enhancement can be calculated by comparing the result of Eq. (2.9)with the corresponding quantity in the absence of the auxiliary field:

$$\frac{P_{MAX}}{P_z} = 1 + \frac{\left(k_z^2 + \alpha^2\right)^2 \sinh\left(\alpha d\right)^2}{4\left(k_z\alpha\right)^2} \qquad (3.10)$$

It is important to notice that a net increase in the total power transfer across the gap occurs if only if the signal and the auxiliary field are exactly phase matched, in other words, if they share the same transverse wave-vector. If such condition is not met the Poynting interference contribution averages to zero over the illuminated area. The question naturally arises as to whether the EET effect could be used to boost the evanescent spectrum of an illuminated object in order to resolve sub-diffraction features. A schematic of an EET imaging setup is shown in figure 8.

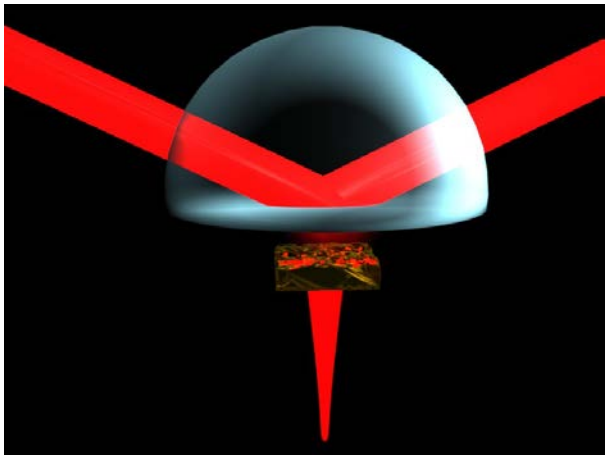

Figure 8 Enhanced evanescent tunneling in an imaging setup

This simple arrangement consists of a dielectric hemispherical dome of refractive index n brought in proximity of a back illuminated sample, whose scattered field $\mathbf{E}_S$ can be described in terms of the relations (2.1) and(2.2). The sub-diffraction features of the object would in this case be associated with evanescent waves in the region between the sample and the dielectric

hemisphere. In principle, if this gap were absent, i.e. if the sample could be placed in direct contact with the dome, a portion of the evanescent angular spectrum would tunnel into the dielectric region and be converted into propagating waves. Unfortunately in most experimental situations, depending on the structure of the sample, this might not be a viable option, and the fine features to be resolved could lie at some depth with respect to the dielectric interface.

In such instances the EET could effectively allow to measure amplitude and phase of a portion of the evanescent spectrum in order to improve the resolution of the optical instrument. In the configuration shown in figure 8 the auxiliary evanescent field is produced by the total internal reflection of a broad beam at the planar interface of the dielectric dome. In order to probe the evanescent spectrum scattered by the sample, different spatial harmonics have to be selectively enhanced. This can be achieved by scanning the auxiliary beam in azimuth and elevation, so as to phase-match the appropriate component. As a consequence upon tunneling the enhanced spatial harmonic will overlap with the reflected auxiliary beam. The resulting amplitude of the total Poynting vector can be expressed as:

$$I = \frac{nA_A^2}{2\eta} + \frac{2e^{-2\alpha d} n\alpha^2 A_S^2}{\left(k_z^2 + \alpha^2\right)\eta} + \frac{2e^{-\alpha d} n\alpha\left[k_z \sin\left(\Delta\varphi_{AS}\right) - \alpha\cos\left(\Delta\varphi_{AS}\right)\right]}{\left(k_z^2 + \alpha^2\right)\eta} A_A A_S \qquad (3.11)$$

Three components can be identified in the expression (2.11). The first term, quadratic in the auxiliary electric field amplitude A_A is the irradiance contribution due to the auxiliary wave reflection, and is clearly the dominant term. Nevertheless such unwanted background may be

eliminated by imposing a weak time harmonic modulation on the sample illumination and resorting to a heterodyne detection scheme. The second term in the expression (2.11) is quadratic in the spatial harmonic amplitude A_S and accounts for the "unaided" tunneling of the signal scattered by the sample. Such contribution is by far the smallest and decreases with the sample distance d as $\exp(-2\alpha d)$.

The effect of EET is described by the third term in equation(2.11), proportional to the product $A_A A_S$. Interestingly enough such contribution can be enhanced by merely increasing the amplitude A_A of the auxiliary field and by properly tuning the relative phase $\Delta\varphi_{AS}$ between the auxiliary field and the corresponding phase matched spatial harmonic of the signal. It is important to notice that the EET achieve a maximum when $\Delta\varphi_{AS} = \pi/2 + \arctan(k_z/\alpha)$. As a consequence, by scanning the phase of the auxiliary field until such maximum condition is reached, it is possible to determine the phase of the enhanced spatial harmonic of the sample. The corresponding amplitude follows by simple inversion of equation (2.12):

$$I_{EET} = \frac{4e^{-\alpha d}\alpha^2 k_z n}{\eta\left(\alpha^2 + k_z^2\right)^{3/2}} A_A A_S \qquad (3.12)$$

By scanning incidence angle of the auxiliary field it is in principle possible with this method to extend the collected angular spectrum up to maximum transverse wavevectors of amplitude $k_0 n$. This extra information could therefore allow to resolve details n times smaller than in a

conventional optical instrument. In conclusion the concept of enhanced evanescent tunneling has been introduced and possible applications for sub-diffraction imaging and optical gating have been proposed. Analogous phenomena in quantum mechanical scattering have been pointed out.

CHAPTER 4
GUIDED WAVES

Introduction

In this chapter we switch from surface bound modes to electromagnetic field confined in two dimensions: waveguide modes. In this case diffraction is compensated by the waveguide itself. The new geometrical constraints introduce a more complex dispersion relation. It is the purpose of this study to introduce specific structures supporting negative index modes.

The concept of negative index of refraction dates back to 1967, when Veselago [50] theoretically investigated the electrodynamics of a hypothetical medium having a negative dielectric permittivity and a negative magnetic permeability. In 2000, the first realization of a synthetic negative index medium was reported in the microwave regime [51]. This observation ushered a new area of intense research in both physics and engineering.

In the quest for the realization of negative index materials at ever higher frequencies, two main approaches emerged: one based on modifying the electromagnetic properties of a medium by means of distributed inclusions with appropriate electric and magnetic polarizabilities-such as split ring resonators [52], the other based on the anomalous dispersion of specific guiding configurations in which phase and group velocities are antiparallel [53]. While the first approach could in principle lead to isotropic negative index bulk media, the challenges in practically realizing such systems with current fabrication technologies are severe if not even prohibitive at shorter wavelengths. Indeed the only structures so far realized for the IR and the optical domains are based on few layers of inclusions [54].

On the other hand, while probably not providing the same degree of versatility, waveguide geometries supporting backward modes could represent a more practical avenue for the realization of local negative index environments. Negative index transmission lines were thoroughly investigated [55] and demonstrated in microwave strip line geometries [53] shortly after the first experiments on negative refraction in synthetic bulk media. Although extremely attractive for their ease of fabrication, the inductive loads necessary for the operation of such backward mode transmission lines pose severe challenges when extending these technologies to higher frequencies.

Interestingly, negative index behavior was in fact observed in waveguide configurations by Clarricoats and Waldron [56] in 1960, before the "official" introduction of the negative index concept. The microwave structure considered by Clarricoats and Waldron is built around two basic ingredients: (i) a cylindrical metallic waveguide (ii) coaxially loaded with a high permittivity rod. Even though is well known that backward wave propagation is possible in periodic waveguides [57], this inhomogeneous waveguide system is quite unique in that it may support backward modes, in spite of the fact that the structure is uniform in the propagation direction.

The geometrical conditions ensuring the existence of backward modes were originally studied by the same authors in [58, 59] for circular waveguides. A different perspective on these issues was more recently offered in 2004 by Ibanescu et al. in [60], in terms of degeneracy of the modes at cut-off. An extension to square geometries was considered by Tsandoulas [61].

In this work we exploit the principles of operation of the Clarricoats-Waldron arrangement to establish a negative index waveguide design suitable for the terahertz and far infrared spectral regions. The extreme simplicity of the proposed design, along with the non-conventional and counter intuitive electromagnetic properties of this family of waveguides, makes these structures excellent candidates for the practical realization of negative index devices with new and interesting functionalities for the far infrared and terahertz regimes. It is our further goal to provide an intuitive understanding of the mechanisms behind the emergence of the anomalous dispersion and ultimately of the negative index behavior. We will show in fact that the origin of the aforementioned effects lies in a local reversal of the Poynting vector due to the convective structure of the magnetic field.

Field analysis of the Clarricoats-Waldron waveguide

An idealized structure is presented here in order to isolate the physical mechanisms leading to the unusual electromagnetic properties of the Clarricoats-Waldron waveguide. Therefore in this specific example only lossless dielectrics and perfect electric conductors are considered to first order.

The cross section of a circular Clarricoats-Waldron waveguide is shown in the inset of Fig.1. A hollow perfect conductor (yellow cylindrical shell) with an internal radius of 31.7μm is loaded with a coaxial dielectric rod of permittivity ε^r=30 and radius 24.9μm (grey cylinder), surrounded by another (empty in this case) dielectric region. Such geometry is advantageous since all the fields can be computed analytically, in very much the same way as done for ordinary optical

fibers [57], with the sole difference that now the tangential electric fields have to vanish at the metallic boundary.

Following the prescriptions of [58, 59, 62], the structure was designed so as to induce degeneracy at cut-off of the first two modes. The dispersion curve shown in Fig.9 illustrates the frequency behavior of the propagation constant β. Under these design conditions the highlighted region of negative group velocity ($dk^0/d\beta$) emerges for the fundamental mode ($k^0=\omega/c$). As a consequence the power flow and the phase velocity become antiparallel, in other words the mode exhibits negative effective index.

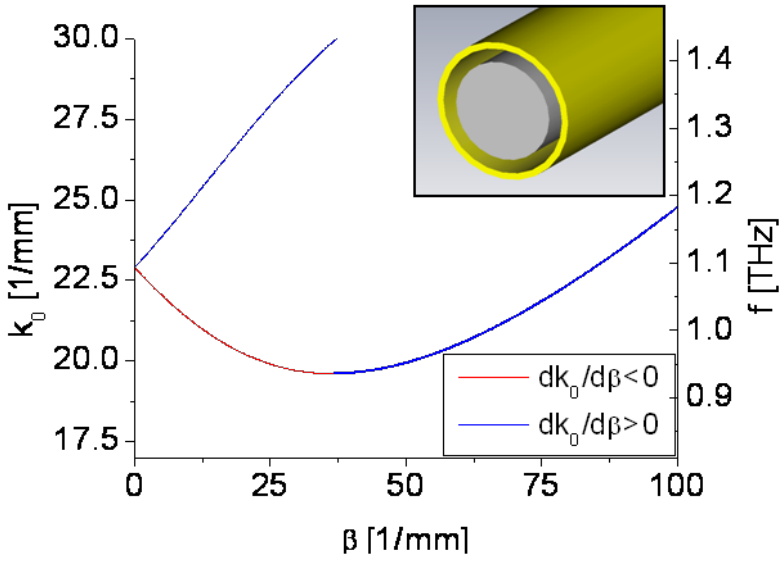

Figure 9 Dispersion curve of the circular Clarricoats-Waldron guide shown in the inset. The region of negative effective index is shown in red.

Physical insight about the operation of the Clarricoats-Waldron guide may be gained by analyzing in detail the field distributions leading to the anomalous behavior of this structure. Due to the dielectric discontinuity within the guide, the supported modes are necessarily hybrid. In particular, the fundamental mode is a mixture of the TE^{11} and TM^{11} modes of a circular metallic waveguide [63]. The electric and magnetic field distributions of the fundamental backward mode at 1THz are shown in Fig. 10. Interestingly enough, the electric field is reminiscent of the TE^{11} mode, while the magnetic field retains the symmetry of the TM^{11} mode.

The reversal of the magnetic lines of force around the two convective regions visible in the right panel of Fig.10 and Fig.11 causes the Poynting vector to change sign and become negative for radial positions external to the centers of the vortices. This, along with the enhancement of the normal component of the electric field in the low permittivity region (due to continuity of the electric displacement at the strong dielectric discontinuity), generates a large negative power flow that overcomes in magnitude the positive flow of the inner core.

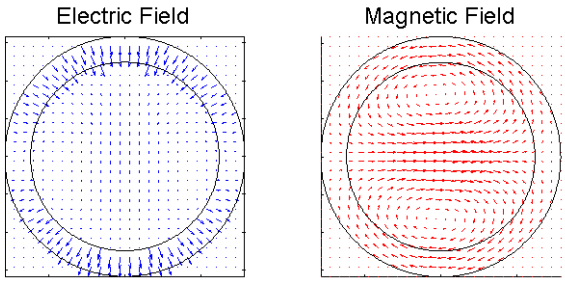

Figure 10 Electric and magnetic field distribution of the fundamental backward mode in a circular Clarricoats-Waldron guide with dielectric contrast 30, operating a 1THz.

The changing balance between positive and negative power flow induces the non-monotonic concave behavior of the frequency dispersion curve shown in Fig.9. When the negative power flow equals exactly the positive power flow, the dispersion curve attains an absolute minimum and the group velocity vanishes. Interestingly enough at any given frequency within the backward wave operation bandwidth, a degenerate orthogonal forward solution is always present ("blue" branch). The Poynting vector distributions of a backward mode ("red" branch) and the degenerate forward mode are shown in Fig. 11. along with the corresponding magnetic field lines. The regions of negative power flow are indicated in blue.

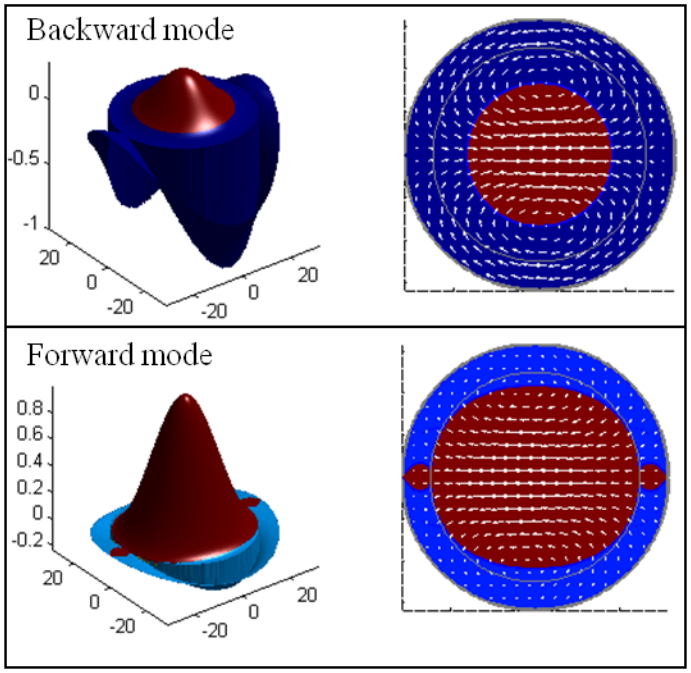

Figure 11 (left panel) Normalized Poynting vector distribution over a cross section of a Clarricoats-Waldron guide with dielectric contrast 30, operating at 1THz. The regions of positive power flow are indicated in red, while the regions of negative power flow are indicated in blue.

(right panel) the magnetic field is shown along with the regions of positive and negative flow. The dielectric interface is shown in gray.

We note that regions of such power flow reversal are also possible in high-contrast dielectric waveguides [64, 65]. The selective excitation of the two degenerate modes is discussed in the next section.

THz design of a Clarricoats-Waldron guide

In this section we present and analyze a design suitable for THz applications. Considering the fact that high permittivity low loss ceramic materials are nowadays available in the THz band [66], the original circular coaxial layout of the Clarricoats-Waldron waveguide could be in principle scaled down to operate in the THz regime. Nevertheless the practical realization of such circular geometry for THz applications, due to the small dimensions and the free standing central dielectric rod, could pose severe challenges from the fabrication point of view.

An important simplification of the original design may be achieved by considering the symmetry of the first backward mode. Due to the cosine azimuthal dependence of the electric field it is possible to replace half of the structure by an electric ground plane, while preserving all the boundary conditions and leaving the electromagnetic behavior unaffected. The resulting geometry in a half-square configuration is presented in Fig.12(a). The field distribution and the dispersion curve shown in Fig.12(b) were computed with the commercial finite elements software Comsol Multiphysics™.

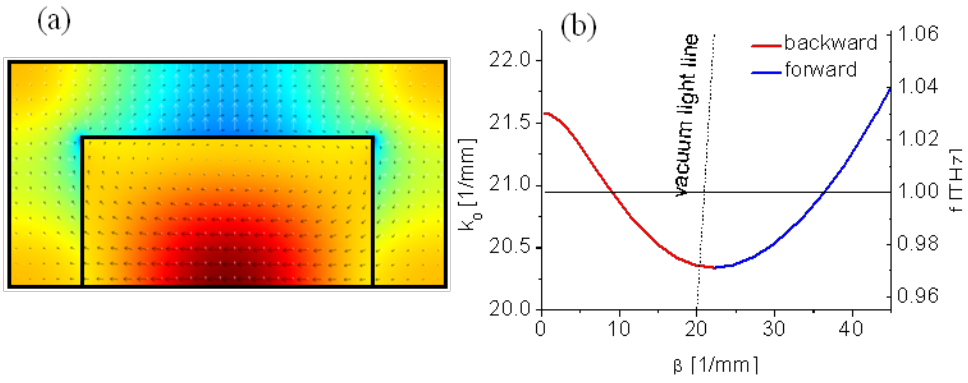

Figure 12 (a) Numerical simulation of power flow and field distribution in a Clarricoats-Waldron rectangular waveguide of dimensions 80μm x 40μm, loaded with a Germanium rod of dimensions 53μm x 26.5μm, operating at 1THz . (b) Dispersion relation.

For this specific design a rectangular hollow waveguide made of gold and loaded with a germanium rectangular rod is considered. The complex permittivity of Ge [67] at this frequency is 16.04+i*0.016. The skin depth of gold is estimated based on a Drude model [68] to be less than $2\text{x}10^{-5}$cm. The dimensions are chosen to be 80μm x 40μm for the metallic wall and 53μm x 26.5μm for the dielectric load, so as to achieve backward wave operation around 1THz. Based on these design parameters the field decay constant of the fundamental backward mode at 1THz is perturbatively estimated to be $\alpha = 0.37 cm^{-1}$.

A very important issue to be addressed is the selective excitation of only the backward mode. Given the orthogonality of the modes, one possibility is certainly the excitation at a waveguide cross-section with the exact field distribution matching the mode structure. A far more straightforward solution may be obtained by observing the dispersion curve in Fig. 12(b).

Even though the forward and backward solutions are degenerate in frequency, their wave-vectors are significantly different, so a properly phase matched field could effectively excite through a slit only one of the modes. Furthermore the vacuum light line in Fig.12(b) shows that the phase velocity of the backward mode is mostly superluminal, while the phase velocity of the forward mode is always subliminal. As a consequence the backward mode and the backward mode only could be excited through a slit by an external homogeneous plane wave. This can be done in a distributed manner from a standard waveguide-through an arrangement resembling that of a distributed feedback structure. As a further remark, this coupling approach could lead to the realization of waveguide couplers with non conventional routing properties.

Generalizations and extensions: Clarricoats-Waldron arrays

As pointed out in the previous paragraph, one of the obstacles towards the extension of the Clarricoats-Waldron design to higher frequencies is the need for an ideal metal to enclose the structure. A solution to this problem may be found by considering an array of identical square guides excited with the same mode. It is straightforward, by invoking the principle of images, to prove that all of the internal walls separating the single elements may be removed without affecting the field distribution. The numerical simulations of the field distribution for a single element and for a 2D array of 9 elements are shown in Fig. 13. As evident, each single element retains the field configuration of the structure in isolation.

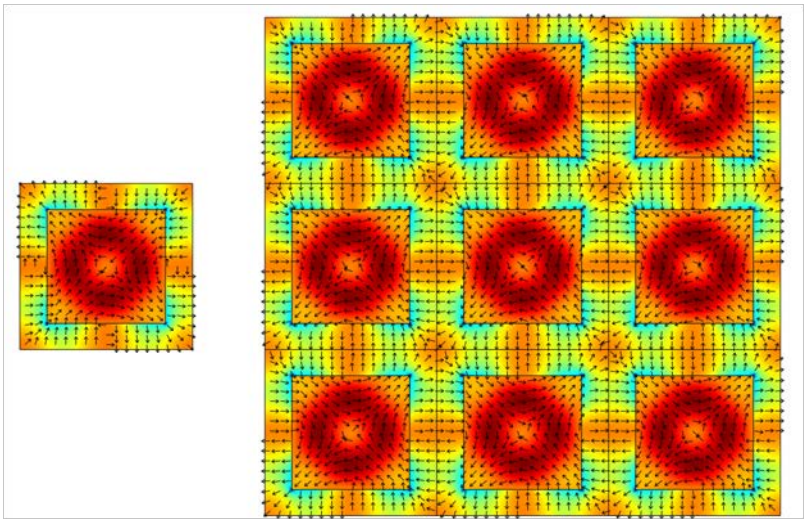

Figure 13. Power flow and electric field distribution in a single element and in a 2D Clarricoats-Waldron array.

The behavior shown in Fig. 13 is a consequence of the symmetry of both the structure and the excitation. The modal configuration of the isolated element is fully retained only by the super-mode with in-phase excitation of the elements. The more complex behavior of higher order super-modes will be the subject of further investigations.

Conclusions

A new class of THz and far infrared waveguides capable of supporting negative index modes was proposed. The working mechanisms were clarified in terms of their modal properties. A suitable design for THz operation was proposed and numerically analyzed. The simple geometry of the Clarricoats-Waldron waveguide makes these structures versatile tools for the study of phenomena related to negative index and backward-wave propagation in the THz domain. The

original design was generalized to array geometry as a possible avenue to extend the applicability of these components in the mid-IR regime.

CHAPTER 5
COUPLED WAVES

1. Introduction

Waveguide couplers are important elements in integrated optics and microwave circuits [69-72]. In its simplest realization, a directional coupler involves two evanescently coupled parallel waveguides in close proximity. In this arrangement, power is periodically exchanged among waveguides during propagation [70]. In general, the field evolution in such structures can be effectively described within the framework of coupled-mode theory and for basic configurations analytical solutions have been reported in the literature [71]. Evidently, for more involved coupled geometries, the field dynamics tend to become richer in behavior and typically not easily amenable to analytical approaches. One such class is that of adiabatic directional couplers where the local eigenstates remain instantaneously invariant under slowly acting perturbations [71].

In this chapter, we present a theoretical study of a new class of three-core adiabatic couplers. In this arrangement the intermediate waveguide is slanted with respect to an uncoupled pair of parallel channels (Fig.14). The power exchange and oscillations in this system is analytically described in terms of the adiabatic and coupling parameters. It is worth noting that this same configuration was recently studied [73-75] as an optical analogue of the stimulated Raman adiabatic passage (STIRAP) process [76]. The adiabatic evolution occurring in this particular type of three-core couplers can lead to a spatial switch over of local supermodes and to an irreversible power transfer.

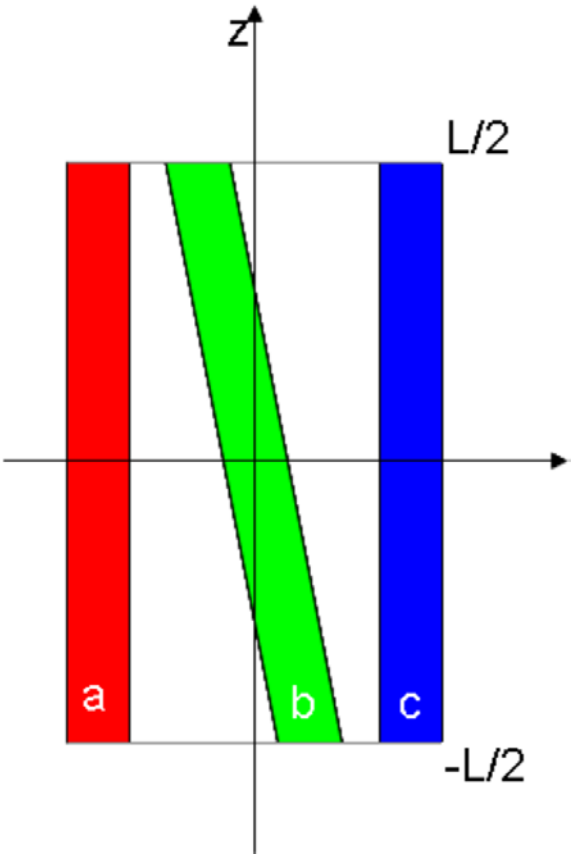

Figure 14 Layout of the structure.

2. Analysis and Results

To analyze this adiabatic three-core coupled waveguide system, we employ a coupled-mode formulation. All waveguide channels are assumed here to be identical with propagation constants β. The center of the coordinate system $z = 0$ is placed at the middle of this device, where the intermediate waveguide is equidistant from the other two. At this point the intermediate waveguide has the same coupling constant κ_0 with respect to both the left and right channels.

Given that the coupling coefficient varies exponentially with waveguide separation [77], then in this linearly slanted arrangement $\kappa(z)=\kappa_0\exp(\pm\hat{\gamma}\,z)$ where $\hat{\gamma}$ is proportional to the slant angle and is associated with the rate of increase/decrease of the coupling process. The total length of this structure is L, with its input at $z=-L/2$ and its output at $L/2$. By introducing a normalized propagation coordinate $\xi=\kappa_0 z$ and a small dimensionless perturbation parameter $\gamma=\hat{\gamma}/\kappa_0$, we then find that the modal field amplitudes a, b, c obey the following set of coupled differential equations:

$$\begin{aligned} i\frac{da}{d\xi}+\exp(\gamma\xi)b&=0\\ i\frac{db}{d\xi}+\exp(\gamma\xi)a+\exp(-\gamma\xi)c&=0\\ i\frac{dc}{d\xi}+\exp(-\gamma\xi)b&=0 \end{aligned} \qquad (5.1)$$

This three-core coupler will be studied under two different excitation conditions at $z=-L/2$: ($a_{in}=1, b_{in}=c_{in}=0$) and ($a_{in}=b_{in}=0, c_{in}=1$). In all cases the following conservation law (total power) applies during propagation, $|a|^2+|b|^2+|c|^2=1$. Equations (4.1)can be directly decoupled in the form:

$$\gamma^2\left(\frac{d^3a}{dt^3}-\frac{d^2a}{dt^2}\right)+2\cosh(2t)\frac{da}{dt}+2a\exp(2t)=0 \qquad (5.2)$$

$$\gamma^2\left(\frac{d^3c}{dt^3}+\frac{d^2c}{dt^2}\right)+2\cosh(2t)\frac{dc}{dt}-2c\exp(-2t)=0 \qquad (5.3)$$

where the new coordinate variable t is here defined as $t=\gamma\xi=\hat{\gamma}z$. Due to the symmetry of these two equations, once a general solution is obtained for any one of them, the other follows through t reversal. To solve Eq(4.2) we use the following WKB ansatz [78]:

$$a(t)=\exp\left[\frac{S_0(t)+\gamma S_1(t)}{\gamma}\right] \qquad (5.4)$$

By substituting (4.4)into Eq.(4.2) and by collecting terms γ^{-1},γ^0 of similar order in the adiabatic parameter γ, we find that:

$$\dot{S}_0\left[\dot{S}_0^2+2\cosh(2t)\right]=0 \qquad (5.5)$$

$$\dot{S}_0^2\left(3\dot{S}_1-1\right)+2\left[\exp(2t)+\cosh(2t)\dot{S}_1\right]+3\dot{S}_0\ddot{S}_0=0 \qquad (5.6)$$

where $\dot{S}_0=dS_0/dt$ etc. Equation (4.5) has three independent solutions, namely:

$$\begin{aligned} &S_0=A=const \\ &S_0(t)=\pm i\sqrt{2}\int_{-t_0}^{t}dx\sqrt{\cosh(2x)}=\pm i\gamma Q(t) \end{aligned} \qquad (5.7)$$

where $t_0=\gamma\kappa_0 L/2$. Note that the dimensionless distance t belongs to the range $-t_0\le t\le t_0$. From (4.6) one can obtain after integration the first order correction term

$S_1(t) = \tilde{c} - (1/2)\ln\left(1+\exp(\pm 4t)\right)$ corresponding to three branch solutions given in Eq.(4.7). Therefore, from Eq.(4.4), the general solution of Eq.(4.2) is given by:

$$a(t) = A_1 \frac{\sqrt{1+\exp(-4t_0)}}{\sqrt{1+\exp(4t)}} + A_2 \frac{\sqrt{1+\exp(4t_0)}}{\sqrt{1+\exp(-4t)}} \cos\left[Q(t)+\phi_a\right] \quad (5.8)$$

where the constants $A_{1,2}, \phi_a$ are to be determined from boundary conditions. A solution of a similar functional form can be obtained for $c(t)$ in Eq. (4.3)through space-reversal, i.e.,

$$c(t) = C_1 \frac{\sqrt{1+\exp(4t_0)}}{\sqrt{1+\exp(-4t)}} + C_2 \frac{\sqrt{1+\exp(-4t_0)}}{\sqrt{1+\exp(4t)}} \cos\left[Q(t)+\phi_c\right] \quad (5.9)$$

The phase function $Q(t)$ can be expressed in terms of elliptic integrals $F(u,k)$ and $E(u,k)$ of the first and second kind respectively [79], that is

$$\begin{aligned} Q(t) &= \gamma^{-1}\left[F\left(\alpha(t_0), 2^{-1/2}\right) - 2E\left(\alpha(t_0), 2^{-1/2}\right)\right] + 2^{1/2}\gamma^{-1}\sinh(2t_0)\left[\cosh(2t_0)\right]^{-1/2} \\ &+ \left(t/|t|\right)\left\{\gamma^{-1}\left[F\left(\alpha(t), 2^{-1/2}\right) - 2E\left(\alpha(t), 2^{-1/2}\right)\right] + 2^{1/2}\gamma^{-1}\sinh(2|t|)\left[\cosh(2t)\right]^{-1/2}\right\} \end{aligned} \quad (5.10)$$

where $\alpha(t) = \arcsin\left\{\left[\left(\cosh(2t)-1\right)/\cosh(2t)\right]^{1/2}\right\}$.

Under the first excitation condition, e.g. $a_{in}=1, b_{in}=c_{in}=0$, the following initial conditions hold true: $c(-t_0)=0, \dot{c}(-t_0)=0, \ddot{c}(-t_0)=-1/\gamma^2$. From here the constants involved in Eq.(7) can be directly evaluated:

$$C_1 = f_1(t_0,\gamma) = -\frac{1}{2\left[\gamma^2\tanh(2t_0)+2\gamma^2+\cosh(2t_0)\right]}$$
$$C_2 = f_2(t_0,\gamma) = \frac{\left[1+2\gamma^2\sec h(2t_0)\right]^{1/2}}{2\left[\gamma^2\tanh(2t_0)+2\gamma^2+\cosh(2t_0)\right]} \quad (5.11)$$
$$\phi_c = f_3(t_0,\gamma) = -\arctan\left[\frac{\gamma\sqrt{2}}{\left[\cosh(2t_0)\right]^{1/2}}\sqrt{\ }\right]$$

In this case the evolution of the optical field $c(t)$ in the waveguide c can be completely determined from Eqs.(4.9, 4.10, 4.11) and in turn $b(t)$ from Eq.(4.1). The power in the first channel $|a(t)|^2$ can then be obtained from the power conservation law. As an example let us consider a $L=2.5cm$ long three-core adiabatic AlGaAs structure similar to that examined in the experimental study of Ref. [73]. Let all three waveguides be $3\mu m$ wide and the edge to edge distance between the two parallel channels be $12\mu m$. The intermediate waveguide is slanted at 0.2 mrad with an edge to edge distance of $2\mu m$ from the third waveguide at the input $z=-L/2$. The coupling constant at the middle of the device is taken here to be $\kappa_0=7.9cm^{-1}$ with a growth rate of $\hat{\gamma}=0.9cm^{-1}$. In this case the resulting adiabatic parameter is $\gamma\cong 0.1$ and $t_0=1.15$. Figure

15(a) depicts the evolution of the power levels in this particular structure as a function of distance.

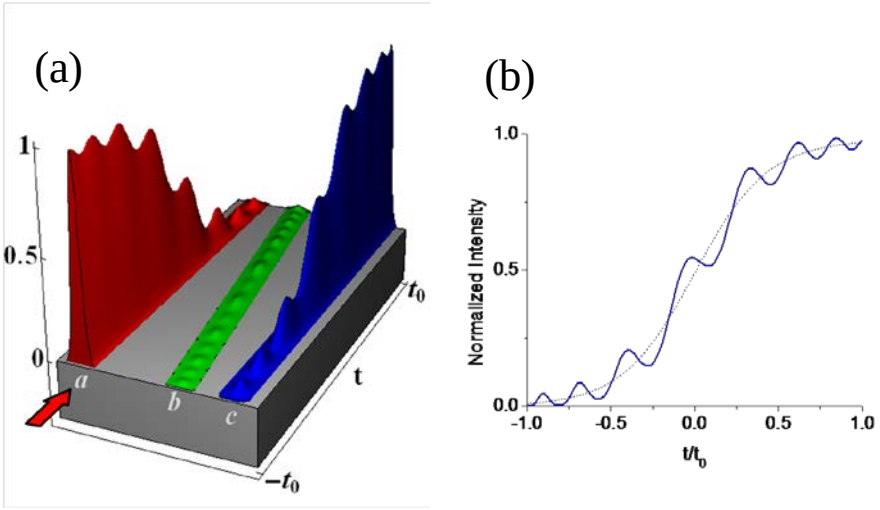

Figure 15. (a) Normalized power evolution in the adiabatic coupler under a [1,0,0] excitation. (b) Power in waveguide c. The dashed line represents the average monotonic increase of power in this waveguide.

The error resulting from the WKB approximation in this case is very small and for this reason is not shown here. In fact the error remains below 3% even for adiabatic parameters as high as $\gamma \approx 0.2$. As Fig.15(a) indicates, the power is adiabatically transferred from the initially excited waveguide a to c. Note that at all stages of propagation the intermediate channel b remains almost devoid of energy. In other words, the local supermode $[1,0,0]$ is switched over to $[0,0,1]$ in an irreversible fashion-the energy never returns back to channel a. We note that this almost 100% exchange is rather insensitive to any dependence the coupling may have on the wavelength

or the device length (provided the structure is long enough). In view of these properties this device may find applications as a broadband coupler that is robust to mechanical and thermal perturbations. The analytical solution found can also provide an accurate estimate of the rate at which the energy flows from a to c which is monotonically increasing as a function of distance. This monotonic increase can be obtained from the first term of Eq.(4.8), that is $|c(t)|^2 \approx C_1^2 \left[1+\exp(4t_0)\right]\left[1+\exp(-4t)\right]^{-1}$, as also shown by the dashed line in Fig. 15(b). The small decaying oscillations occurring during this process are determined from the second term in(4.8).

Similarly this structure can be analyzed for the second set of initial conditions, i.e., $a_{in} = b_{in} = 0, c_{in} = 1$, for which case one can show that $a(-t_0) = 0, \dot{a}(-t_0) = 0, \ddot{a}(-t_0) = -1/\gamma^2$. Under these excitation conditions, the optical field in waveguide a can be directly obtained from Eq.(6) where now the constants involved are given by Eq.(4.11) and are equal to: $A_j = f_j(-t_0, -\gamma)$ and $\phi_a = f_3(-t_0, -\gamma)$. From here $b(t), c(t)$ can be computed using Eqs. (4.1)

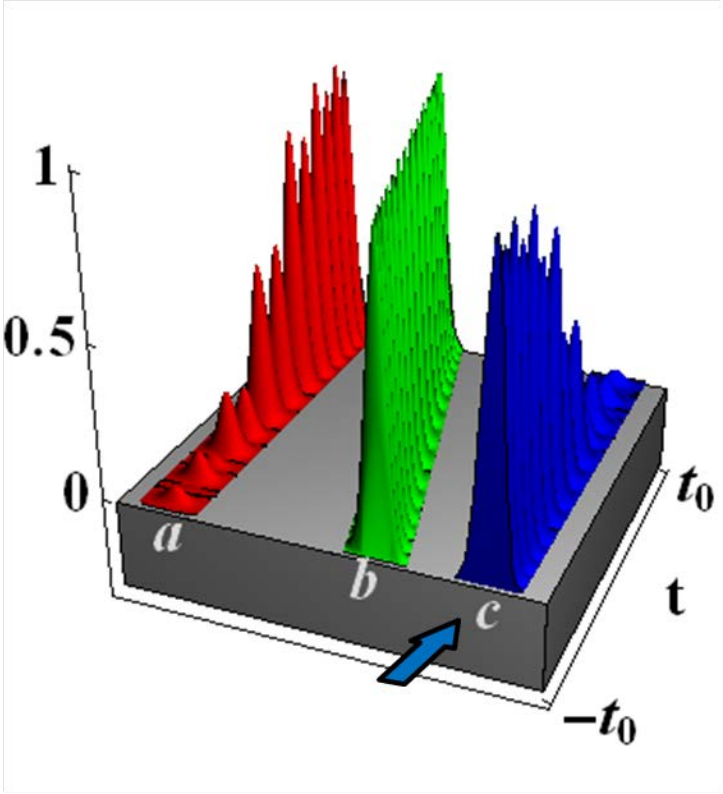

Figure 16 . Normalized power evolution in the adiabatic three-core waveguide coupler under a [0,0,1] excitation.

Figure 16 depicts the evolution of the intensity in these three waveguides when (as in the previous example) $\gamma \cong 0.1$ and $t_0 = 1.15$. As the figure indicates, the power in waveguide c, after a damped oscillation, is adiabatically transferred to both channels a and b. As opposed to the previous case, where only a small fraction of power was coupled to b, in this regime the energy is eventually shared (via oscillations) between a and b. This is because the two local approximate

supermodes $[0,1,\pm1]$ are both excited and adiabatically switched over in space at the output. Again, the process is irreversible, e.g. the energy never returns back to channel c.

3. Conclusion

In conclusion we have theoretically analyzed a new family of adiabatic three-core couplers. By using a multiple scale WKB approach we provided closed-form expressions describing the adiabatic energy exchange process. Some of the peculiar features of these structures have been highlighted and explained. Before closing we would like to note that our procedure is general and thus can be used to systematically study other classes of adiabatic coupled-wave devices.

CHAPTER 6
REVERSE OPTICAL FORCES IN NEGATIVE INDEX DIELECTRIC WAVEGUIDE ARRAYS

Non-conservative optical forces acting on dipolar particles are considered in longitudinally invariant optical fields. We demonstrate that the orientation of these forces is strictly dictated by the propagation vector associated with such field configurations. As a direct consequence of this, it is impossible to achieve a reversal of optical forces in homogeneous media. We show instead that translation invariant optical tractor fields can in fact be generated in the negative index environment produced in a special class of fully dielectric waveguide arrays.

One of the most intriguing properties of light-matter interaction is the ability of an electromagnetic field to exert mechanical forces upon polarizable objects. Such phenomenon is a direct consequence of the process of light scattering, and is dictated by a principle as fundamental as the momentum conservation itself.

The first experimental observations of opto-mechanical interactions date back to the beginning of the past century with the seminal experiments conducted by Lebedev [80] and by Nichols and Hull [81]. The idea of harnessing optical forces culminated in the celebrated work of Ashkin [82-88] on optical tweezers, which endowed the most diverse fields of science with a new and powerful tool for the remote manipulation of microscopic objects.

The amount of momentum transferred to a scattering and/or absorbing body immersed in electromagnetic radiation can, at least in principle, be exactly calculated by evaluating the flux of the Maxwell's stress tensor through any arbitrary surface enclosing the object. This in general requires the exact knowledge, not only of the incident field, but also of the field scattered by the object itself. The formulation becomes substantially simpler when light interacts with particles of dimensions much smaller than the wavelength of the incident radiation. Under such circumstances the scattered field is essentially dipolar. The expression of the total force acting on the particle is then amenable to the following simpler expression [89] in terms of the particle complex polarizability $\alpha = \alpha_r + i\,\alpha_i$ and the electromagnetic field at the interaction site:

$$\langle \mathbf{F} \rangle = \frac{1}{4}\alpha_r \nabla |\mathbf{E}|^2 + \frac{k_0 \alpha_i}{\varepsilon_0}\left[\frac{\langle \mathbf{S} \rangle}{c} + c\nabla \times \langle \mathbf{L}_S \rangle\right] \qquad (6.1)$$

Equation (6.1) represents the average force exerted by a monochromatic field of frequency $\omega = k_0 c$ on a dipolar scatterer. Notice that the imaginary part of the particle polarizability is simply related to the total cross section σ through $\sigma = k_0 \alpha_i / \varepsilon_0$. The first term in the force of Eq. (6.1) is a conservative field contribution derived from the scalar potential $|\mathbf{E}|^2$, and is commonly referred to as the gradient force. The second term, proportional to the average

Poynting vector $\mathbf{S}$, represents the so called radiation pressure. Finally the last contribution is directly related to a non uniform spin angular momentum density of the electromagnetic field $\langle \mathbf{L}_S \rangle = (\varepsilon_0 / 4\omega i)\mathbf{E} \times \mathbf{E}^*$. We will refer to this contribution as the spin force throughout this chapter. The second and the third components of the optical force are often designated in the literature as non-conservative.

The gradient force offers high degree of versatility in trapping or manipulating particles, based on the simple fact that it will in general push or pull a polarizable object towards the regions of highest modulus of $|\mathbf{E}|^2$ [87, 90]. More subtle is harnessing the behavior of the other two components in (1). The very fact that radiation pressure is proportional to the Poynting vector intuitively suggests that the effect on a dipolar particle would be to push it away from the radiation source. Yet, this is not always the case, due to the complex interplay between radiation pressure and spin force, as recently shown by Sukhov and Dogariu [91] using a combination of Bessel beams. Other possibilities include the use of active particles [92].

In this chapter we would like to address the following question: is it possible to devise a translation invariant field distribution capable of uniformly attracting a dipolar object towards the source of radiation? Requiring a translation invariant field, say along z, has important conceptual and practical implications, most notably the fact that such a tractor field would exert the same force on a particle regardless of its axial z position.

From an electromagnetic point of view, any electric or magnetic component of a z translation-invariant field is constrained to have a general functional dependence of the form $f(x,y)\exp(i\beta z)$. Such requirement is in general satisfied by waveguide modes, but also by free space diffraction-free beams like for example those of the Bessel family [20]. Based on these assumptions it is straightforward to show that the Maxwell set decouples into TE(z) and TM(z) modes, expressible solely in terms of the longitudinal electric and magnetic fields $E_z(x,y)e^{i\beta z}$ and $H_z(x,y)e^{i\beta z}$ as follows:

$$\begin{aligned}\overline{\mathbf{E}} &= \left[i\frac{\beta \nabla_T E_z - \omega\mu_0 \hat{\mathbf{z}}\times\nabla_T H_z}{k_0^2\varepsilon - \beta^2} + \hat{\mathbf{z}}\, E_z \right] e^{i\beta z} \\ \overline{\mathbf{H}} &= \left[i\frac{\omega\varepsilon_0\varepsilon \hat{\mathbf{z}}\times\nabla_T E_z + \beta\nabla_T H_z}{k_0^2\varepsilon - \beta^2} + \hat{\mathbf{z}}\, H_z \right] e^{i\beta z}\end{aligned} \qquad (6.2)$$

where ∇_T stands for the transverse gradient operator and ε is the dielectric constant of the host medium. Using Eqs. (6.2)in the general expression (6.1) leads to the first conclusion of this work regarding longitudinal forces in translation invariant fields:

$$\left\langle F_z \right\rangle = \frac{\alpha_i \left[\left(k_0^2\varepsilon - \beta^2\right)^2 \left|E_z\right|^2 + \left|\beta\nabla_T E_z + k_0\varepsilon\eta\nabla_T H_z \times \hat{\mathbf{z}}\right|^2 \right]}{2\left(k_0^2\varepsilon - \beta^2\right)^2}\beta \qquad (6.3)$$

where η is the vacuum characteristic impedance. For passive particles $\alpha_i > 0$, therefore the longitudinal force is the product of a definite positive prefactor and the field propagation constant β. Based on the result (6.3) the possibility of translation invariant tractor beams in homogeneous dielectric media is ruled out, since $\beta > 0$. The present formulation applies to particles with isotropic polarizability such as nanospheres. The extension to other geometries such as ellipsoids [93] or more complex composite nanostructures [94] is straightforward and leads to similar conclusions.

At this point a question naturally arises as to whether and under what conditions a translation invariant tractor field could be obtained. The easiest answer in principle, but most elusive in practice, would be considering a background material with a negative index of refraction. In that case power could flow away from the source while $\beta < 0$, reversing therefore the direction of F_z. Unfortunately though, the current realizations of bulk optical negative [95] index metamaterials involve complex and densely packed inclusions which would in fact impede the motion of a test particle. A more careful consideration of this problem indicates that the requirement of a negative index medium is far too stringent, and that indeed it can be relaxed by considering instead negative index modes.

Backward-wave propagation is generally achieved in waveguide configurations by periodic perturbations of the guiding structure [57]. In these instances the mode propagation constant β is defined, and is to be understood, as the “crystal momentum” is intended in solid-state physics

[96]. The “modes” of a periodic waveguide are hence invariant only under discrete translations, as opposed to case of longitudinally uniform structures where the modes display continuous translational symmetry. This marks also a departure from negative index bands in photonic crystals [97]. Based on this, longitudinally modulated structures cannot provide the translation invariance that we are seeking.

Radically different is the case of longitudinally uniform backward-wave waveguides. To the best of our knowledge the only non plasmonic configuration falling in this category is given by the Clarricoats-Waldron waveguides [56], sketched in Fig.17. The structure is constituted by a hollow metallic waveguide coaxially loaded with a high permittivity rod.

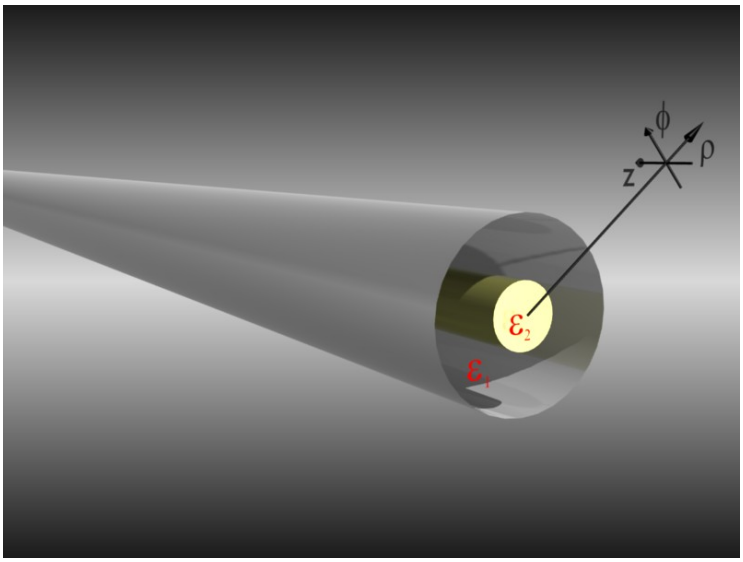

Figure 17 Layout of a circular Clarricoats-Waldron waveguide. Different cross-sections are also possible.

Introduced for the first time in 1960 by Clarricoats and Waldron in the microwave domain, these waveguides have the unique property of supporting modes with negative phase velocity without resorting in any longitudinal perturbation or negative index material loading. As an example, in Fig.18 we show the dispersion curve of the backward mode in a square Clarricoats-Waldron waveguide loaded with a germanium rod and operating around $2\mu m$.

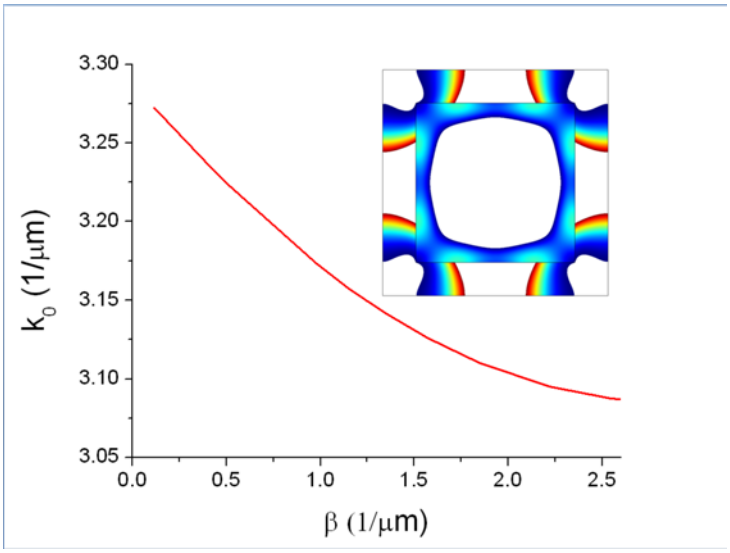

Figure 18. Dispersion a Ge loaded square Clarricoats-Waldron waveguide. (inset) Regions of negative Poynting vector.

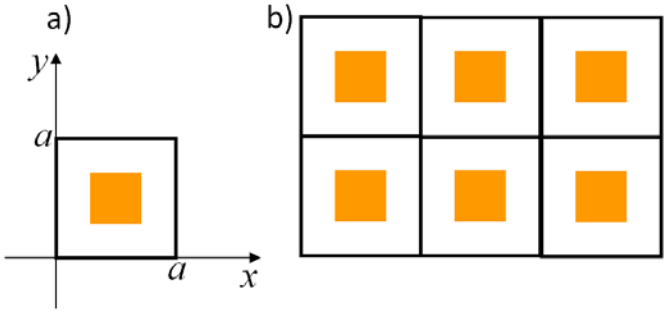

Figure 19. a) Single square element. b) Two dimensional array of isolated elements.

A field analysis of such configurations [98] reveals extended regions of reverse Poynting vector in every transverse cross-section. The origin of such phenomenon lies in the vorticity of the magnetic lines of force induced by the strong dielectric discontinuity in the waveguide interior.

The extension of such interesting configurations to the optical domain is made difficult by the need for low loss metallic walls and high permittivity materials for the waveguide core. Moreover the fact that such structures are fully enclosed in metal renders the access to the internal region virtually impossible from outside.

Of interest will be to devise a new class of structures that could support backward-wave propagation as in a Clarricoats-Waldron waveguide, without the need for metallic walls or any other reflective enclosures that could prevent the access to the internal regions. In other words, is there any way to remove the metallic boundaries without affecting the field distribution of a Clarricoats-Waldron waveguide?

As a consequence of the uniqueness theorem in electrodynamics, a necessary and sufficient condition in order to remove the metallic walls without affecting the internal field is that the tangential components of both the electric and the magnetic fields at the waveguide boundary remain unaltered. To this end we consider an array of Clarricoats-Waldron waveguides with square cross-section, as shown in Fig.19b. In this case there is no interaction between adjacent elements since each waveguide is fully shielded by a metallic boundary and independently operates in the backward-wave regime. We further make the assumption that neighboring waveguides are excited π out of phase. These field configurations correspond to Floquet-Bloch modes at the Brillouin zone boundaries.

Given the fact that the tangential electric field vanishes at each of the metallic boundaries it is easy to understand that removing them would not affect the continuity of the transverse field. Concerning the magnetic field, eliminating the waveguide walls suppresses the surface currents which ordinarily extinguish the external field. With reference to Fig.19a, a necessary and sufficient condition to ensure the continuity of the tangential magnetic fields in the absence of the metallic boundary is that the mode under consideration is endowed with the following symmetry:

$$\begin{aligned} H_x\big|_{y=0} &= H_x\big|_{y=a} \\ H_y\big|_{x=0} &= H_y\big|_{x=a} \end{aligned} \qquad (6.4)$$

If condition (6.4) holds, all the walls separating adjacent elements can be removed without affecting the modal fields. Notice that in principle the external wall enclosing the whole array is still necessary, except for infinite arrays. Nevertheless if one considers the elements far from the periphery of a large array they will be affected only marginally by the absence of the external enclosure. The full-wave finite element simulation presented in Fig.20 confirms this expected behavior in the dielectric array obtained removing the internal walls from the structure of Fig.18b. In this specific example we considered an array of germanium $(\varepsilon = 16)$ square rods in air, of side length $600nm$ operating at $\lambda = 2\mu m$. The center to center distance between elements is $850nm$. The propagation constant associated to such mode is $\beta = -85.6 \cdot 10^4 m^{-1}$, corresponding to an effective mode index of $n_e = -0.27$.

As a consequence of equation (6.3) a particle placed in the empty regions between the dielectric rods would be propelled backward, against the power flow and the radiation pressure. As previously pointed out such optical force is uniform along the longitudinal direction. This is of course due to the translation invariance of the modal field. To the best of our knowledge this is currently the only configuration allowing a translation invariant reversal of the non-conservative optical forces.

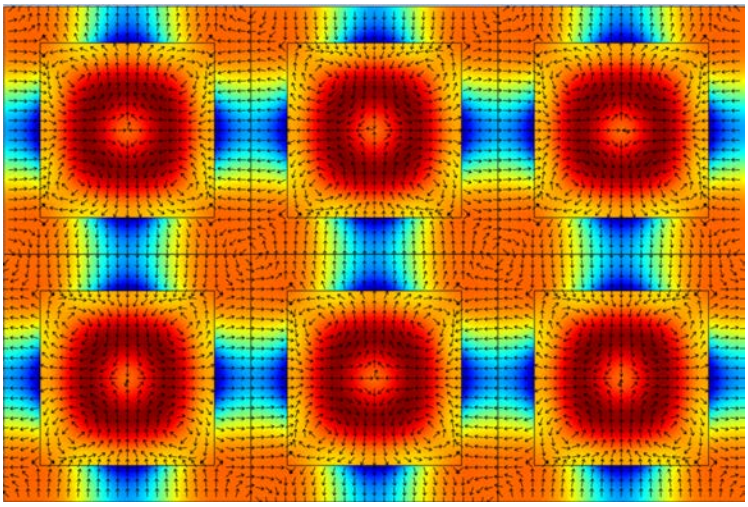

Figure 20. Electric field and intensity distribution in a 6 element array of square dielectric rods of permittivity 16.

In conclusion we have shown that a translation invariant tractor beam cannot be generated in a homogeneous medium like free space. Instead we showed that a negative index environment can be created in a properly designed dielectric array. A particle immersed in the modal field of such optical array would be propelled upstream, against the power flow and the radiation pressure of the incident mode. A tractor force uniform with respect to the longitudinal coordinate is ensured by longitudinal translation invariance of such an electromagnetic field distribution.

CHAPTER 7
GENERALIZED MIE THEORY OF OPTICAL FORCES

In this chapter we introduce a general theory of the optical forces experienced by a sphere of arbitrary radius a and permittivity ε_c, immersed in a medium of permittivity ε_m, under general excitation conditions. The problem of the optical forces on a sphere under plane wave illumination was addressed for the first time by Debye [93, 99] in 1909. Approximate treatments of the general problem exist for the limiting cases of spheres much larger or much smaller than the incident wavelength [93]. When the electrical dimensions of the object are much smaller than the incident wavelength the scattering is approximated by sole electric dipole contribution. On the other hand, when the dimensions of the object are much larger than the incident wavelength a ray optics approach gives satisfactory results.

In what follows we are going to consider a general incident electromagnetic field, expressed in terms of vector spherical harmonics. Vector spherical harmonics are the general solution of the vectorial Helmholtz problem in spherical coordinates:

$$\nabla \times \nabla \times \mathbf{E} - k^2 \mathbf{E} = 0 \tag{7.1}$$

The solutions to the equation (7.1) can be found in terms of the following generating potentials:

$$\begin{aligned} \psi_{emn} &= \cos(m\varphi) P_n^m(\cos\theta) z_n(k r) \\ \psi_{omn} &= \sin(m\varphi) P_n^m(\cos\theta) z_n(k r) \end{aligned} \tag{7.2}$$

The expressions (7.2) are solutions of the scalar Helmholtz equation. The subscripts “e” and “m” stand for even and odd and they refer to the azimuthal dependence of the solutions. The angular dependence in (7.2) is given in terms of trigonometric functions and associated Legendre functions of integer degree n and integer order m. The radial dependence in (7.2) is given in terms of the appropriate spherical Bessel functions j_n or spherical Hankel functions of first kind $h_n^{(1)}$ or second kind $h_n^{(2)}$,of integer order n. The vector spherical harmonics are obtained by differentiation of (7.2) as follows:

$$\begin{aligned}
\mathbf{M}_{emn} &= \nabla \times \left(\hat{\mathbf{r}}\, r\, \psi_{emn} \right) \\
\mathbf{M}_{omn} &= \nabla \times \left(\hat{\mathbf{r}}\, r\, \psi_{omn} \right) \\
\mathbf{N}_{emn} &= \frac{\nabla \times \mathbf{M}_{emn}}{k} \\
\mathbf{N}_{omn} &= \frac{\nabla \times \mathbf{M}_{omn}}{k}
\end{aligned} \tag{7.3}$$

In (7.3) $\hat{\mathbf{r}}$ is the radial unit vector. The explicit expressions of the vector spherical harmonics are the following:

$$\mathbf{M}_{emn} = -\frac{m}{\sin\theta} \sin\left(m\phi\right) P_n^m\left(\cos\theta\right) z_n\left(\rho\right) \hat{\theta} - \cos\left(m\phi\right) \frac{dP_n^m\left(\cos\theta\right)}{d\theta} z_n\left(\rho\right) \hat{\phi} \tag{7.4}$$

$$\mathbf{M}_{omn} = \frac{m}{\sin\theta} \cos\left(m\phi\right) P_n^m\left(\cos\theta\right) z_n\left(\rho\right) \hat{\theta} - \sin\left(m\phi\right) \frac{dP_n^m\left(\cos\theta\right)}{d\theta} z_n\left(\rho\right) \hat{\phi} \tag{7.5}$$

$$\mathbf{N}_{emn} = \frac{z_n(\rho)}{\rho}\cos(m\phi)\,n(n+1)\,P_n^m(\cos\theta)\,\hat{r} + \cos(m\phi)\frac{dP_n^m(\cos\theta)}{d\theta}\frac{1}{\rho}\frac{d}{d\rho}\left[\rho\, z_n(\rho)\right]\hat{\theta} +$$
$$-m\sin(m\phi)\frac{P_n^m(\cos\theta)}{\sin\theta}\frac{1}{\rho}\frac{d}{d\rho}\left[\rho\, z_n(\rho)\right]\hat{\phi} \tag{7.6}$$

$$\mathbf{N}_{omn} = \frac{z_n(\rho)}{\rho}\sin(m\phi)\,n(n+1)\,P_n^m(\cos\theta)\,\hat{r} + \sin(m\phi)\frac{dP_n^m(\cos\theta)}{d\theta}\frac{1}{\rho}\frac{d}{d\rho}\left[\rho\, z_n(\rho)\right]\hat{\theta} +$$
$$+m\cos(m\phi)\frac{P_n^m(\cos\theta)}{\sin\theta}\frac{1}{\rho}\frac{d}{d\rho}\left[\rho\, z_n(\rho)\right]\hat{\phi} \tag{7.7}$$

In what follows we are going to adopt the following symbol convention to identify the radial functional dependence:

$$\begin{aligned} &if \quad z_n(kr) = j_n(kr) \quad \Rightarrow \ \mathbf{M}_{emn} \\ &if \quad z_n(kr) = h_n^{(1,2)}(kr) \ \Rightarrow \ \mathbf{M}_{emn}^{(1,2)} \end{aligned} \tag{7.8}$$

The vector spherical harmonics (7.3) form a complete set over an unbound isotropic region and can be therefore used to expand any incident field as follows:

$$\mathbf{E}_i = \sum_{n=1}^{\infty}\sum_{m=0}^{n} a_{enm}\mathbf{N}_{enm} + a_{onm}\mathbf{N}_{onm} + b_{enm}\mathbf{M}_{enm} + b_{onm}\mathbf{M}_{onm} \tag{7.9}$$

The corresponding magnetic field is given by:

$$\mathbf{H}_i = \frac{\nabla \times \mathbf{E}_i}{i\omega\mu_0} = \frac{1}{ik_0\eta_0}\sum_{n=1}^{\infty}\sum_{m=0}^{n} a_{enm}\nabla\times\mathbf{N}_{enm} + a_{onm}\nabla\times\mathbf{N}_{onm} + b_{enm}\nabla\times\mathbf{M}_{enm} + b_{onm}\nabla\times\mathbf{M}_{onm} =$$

$$= \frac{\sqrt{\varepsilon_m}}{i\eta_0}\sum_{n=1}^{\infty}\sum_{m=0}^{n} a_{enm}\mathbf{M}_{enm} + a_{onm}\mathbf{M}_{onm} + b_{enm}\mathbf{N}_{enm} + b_{onm}\mathbf{N}_{onm}$$

(7.10)

The quantity η_0 is the vacuum characteristic impedance. In the expansions (7.9) and (7.10) the spherical Bessel functions j_n have to be used in order to ensure that the fields are finite at the origin. As a consequence of the interaction of the incident electromagnetic field with the dielectric sphere, polarization charges are induced which sustain an internal field within the object and a scattered field outside of it. The internal fields can be expressed similarly to the incident field as a superposition of vector spherical harmonics with radial dependence in terms of spherical Bessel functions:

$$\mathbf{E}_c = \sum_{n=1}^{\infty}\sum_{m=0}^{n} a^c_{enm}\mathbf{N}_{enm} + a^c_{onm}\mathbf{N}_{onm} + b^c_{enm}\mathbf{M}_{enm} + b^c_{onm}\mathbf{M}_{onm} \qquad (7.11)$$

$$\mathbf{H}_c = \frac{\sqrt{\varepsilon_c}}{i\eta_0}\sum_{n=1}^{\infty}\sum_{m=0}^{n} a^c_{enm}\mathbf{M}_{enm} + a^c_{onm}\mathbf{M}_{onm} + b^c_{enm}\mathbf{N}_{enm} + b^c_{onm}\mathbf{N}_{onm} \qquad (7.12)$$

The scattered fields are defined for $r > a$ and have the nature of propagating spherical waves and can be therefore expressed as:

$$\mathbf{E}_s = \sum_{n=1}^{\infty}\sum_{m=0}^{n} a_{enm}^{s}\mathbf{N}_{enm}^{(1)} + a_{onm}^{s}\mathbf{N}_{onm}^{(1)} + b_{enm}^{s}\mathbf{M}_{enm}^{(1)} + b_{onm}^{s}\mathbf{M}_{onm}^{(1)} \tag{7.13}$$

$$\mathbf{H}_s = \frac{\sqrt{\varepsilon_m}}{i\eta_0}\sum_{n=1}^{\infty}\sum_{m=0}^{n} a_{enm}^{s}\mathbf{M}_{emn}^{(1)} + a_{onm}^{s}\mathbf{M}_{omn}^{(1)} + b_{enm}^{s}\mathbf{N}_{emn}^{(1)} + b_{onm}^{s}\mathbf{N}_{omn}^{(1)} \tag{7.14}$$

The radial dependence of the vector spherical harmonics in this case is in terms of spherical Hankel function of the first kind. Notice that the singularity at the origin is excluded from the domain of existence of the scattered field $(r > a)$. The unknown coefficients in the expansion of the internal and the scattered fields can be determined by imposing the continuity of the tangential electric and magnetic field at the interface surface $r = a$:

$$\begin{aligned}
&\left(\mathbf{E}_i + \mathbf{E}_s - \mathbf{E}_c\right)\Big|_{r=a} \cdot \hat{\theta} = 0 \\
&\left(\mathbf{E}_i + \mathbf{E}_s - \mathbf{E}_c\right)\Big|_{r=a} \cdot \hat{\phi} = 0 \\
&\left(\mathbf{H}_i + \mathbf{H}_s - \mathbf{H}_c\right)\Big|_{r=a} \cdot \hat{\theta} = 0 \\
&\left(\mathbf{H}_i + \mathbf{H}_s - \mathbf{H}_c\right)\Big|_{r=a} \cdot \hat{\phi} = 0
\end{aligned} \tag{7.15}$$

Once the scattered field is determined the optical forces on the sphere can be calculated using the Maxwell stress tensor. The average force experienced by a scattering and/or absorbing body immersed in a monochromatic field can be computed by evaluating the flux of the Maxwell stress tensor $\overline{\mathbf{T}}$ through any surface S enclosing the object:

$$\langle \mathbf{F} \rangle = \frac{1}{2} \mathrm{Re} \oint_S \overline{\mathbf{T}} \cdot \hat{\mathbf{n}} dS \tag{7.16}$$

In expression (7.16) $\hat{\mathbf{n}}$ is the unit vector normal to the surface S and pointing outward. Given the spherical symmetry of the functions (7.3) we choose S to be a sphere centered at the origin of a spherical reference system, with an outward normal unit vector given by $\hat{\mathbf{r}}$.

The expression of the Maxwell stress tensor is given by:

$$\overline{\mathbf{T}} = \varepsilon_0 \mathbf{E}\mathbf{E}^* + \mu_0 \mathbf{H}\mathbf{H}^* - \frac{1}{2}\left(\varepsilon_0 \mathbf{E}\cdot\mathbf{E}^* + \mu_0 \mathbf{H}\cdot\mathbf{H}^*\right)\overline{\mathbf{I}} \tag{7.17}$$

where $\overline{\mathbf{I}}$ is the 3 by 3 identity matrix. In terms of incident and scattered field we can write:

$$\begin{aligned}
\overline{\mathbf{T}} = & \left\{ \varepsilon_0 \mathbf{E}_i \mathbf{E}_i^* + \mu_0 \mathbf{H}_i \mathbf{H}_i^* - \frac{1}{2}\overline{\mathbf{I}}\left[\varepsilon_0 \mathbf{E}_i \cdot \mathbf{E}_i^* + \mu_0 \mathbf{H}_i \cdot \mathbf{H}_i^* \right] \right\} + \\
& + \left\{ \varepsilon_0 \mathbf{E}_s \mathbf{E}_s^* + \mu_0 \mathbf{H}_s \mathbf{H}_s^* - \frac{1}{2}\overline{\mathbf{I}}\left[\varepsilon_0 \mathbf{E}_s \cdot \mathbf{E}_s^* + \mu_0 \mathbf{H}_s \cdot \mathbf{H}_s^* \right] \right\} + \\
& + \left\{ \varepsilon_0 \mathbf{E}_i \mathbf{E}_s^* + \mu_0 \mathbf{H}_i \mathbf{H}_s^* - \frac{1}{2}\overline{\mathbf{I}}\left[\varepsilon_0 \mathbf{E}_i \cdot \mathbf{E}_s^* + \mu_0 \mathbf{H}_i \cdot \mathbf{H}_s^* \right] \right\} + \\
& + \left\{ \varepsilon_0 \mathbf{E}_s \mathbf{E}_i^* + \mu_0 \mathbf{H}_s \mathbf{H}_i^* - \frac{1}{2}\overline{\mathbf{I}}\left[\varepsilon_0 \mathbf{E}_s \cdot \mathbf{E}_i^* + \mu_0 \mathbf{H}_s \cdot \mathbf{H}_i^* \right] \right\}
\end{aligned} \tag{7.18}$$

In the expression (7.18) different terms may be identified. The first term depends only on the incident fields and represents the Maxwell stress tensor in the absence of the scattering object. Clearly this term does not lead to any net force. The second term depends on the scattered fields only and can lead to a force contribution, due to the interaction between multipoles of different order and degree. Notice that this term does not depend on the way the scattered field is excited. In other words, as far as this contribution is concerned the scattered field may be even generated by a process with the dielectric body, such as lasing. From a heuristic point of view one may see this force contribution as arising from the asymmetry in the radiation pattern. An asymmetric radiation pattern implies in fact an uneven redistribution of electromagnetic momentum that has to be compensated by a net mechanical momentum acquired by the anisotropic radiator. It is worth stressing the fact that, as it will be shown rigorously later, the contribution to the force from this term arises from the "mixing" of different multipoles: if the scattered field contains one single multipole, say the electric dipole, the resulting force would be zero. The last term finally involves products of the incident fields and the scattered fields.

The expression of the average optical force reduces to:

$$\langle \mathbf{F} \rangle = \langle \mathbf{F}_{ss} \rangle + \langle \mathbf{F}_{is} \rangle \tag{7.19}$$

$$\langle \mathbf{F}_{ss} \rangle = \frac{1}{2} \mathrm{Re} \oint_S \left[\left(\varepsilon_0 \mathbf{E}_s \mathbf{E}_s^* + \mu_0 \mathbf{H}_s \mathbf{H}_s^* \right) \cdot \hat{\mathbf{r}} - \frac{1}{2} \left(\varepsilon_0 \mathbf{E}_s \cdot \mathbf{E}_s^* + \mu_0 \mathbf{H}_s \cdot \mathbf{H}_s^* \right) \hat{\mathbf{r}} \right] dS \tag{7.20}$$

$$\left\langle \mathbf{F}_{is} \right\rangle = \frac{1}{2}\mathrm{Re}\oint_S \left[\left(\varepsilon_0 \mathbf{E}_i \mathbf{E}_s^* + \mu_0 \mathbf{H}_i \mathbf{H}_s^* \right) \cdot \hat{\mathbf{r}} - \frac{1}{2}\left(\varepsilon_0 \mathbf{E}_i \cdot \mathbf{E}_s^* + \mu_0 \mathbf{H}_i \cdot \mathbf{H}_s^* \right) \hat{\mathbf{r}} \right] dS \quad (7.21)$$

$$\left\langle \mathbf{F}_{si} \right\rangle = \frac{1}{2}\mathrm{Re}\oint_S \left[\left(\varepsilon_0 \mathbf{E}_s \mathbf{E}_i^* + \mu_0 \mathbf{H}_s \mathbf{H}_i^* \right) \cdot \hat{\mathbf{r}} - \frac{1}{2}\left(\varepsilon_0 \mathbf{E}_s \cdot \mathbf{E}_i^* + \mu_0 \mathbf{H}_s \cdot \mathbf{H}_i^* \right) \hat{\mathbf{r}} \right] dS \quad (7.22)$$

Using the expressions (7.13),(7.14) and (7.9),(7.10) we can write (7.20) as:

$$\left\langle \mathbf{F}_{ss} \right\rangle = \frac{1}{4}\mathrm{Re}\sum_{n_1=1}^{\infty}\sum_{m_1=0}^{n_1}\sum_{n_2=1}^{\infty}\sum_{m_2=0}^{n_2} \varepsilon_0$$

$$\left[\begin{array}{l}
2\oint_S \left[\left(a^s_{en_1m_1}\mathbf{N}^{(1)}_{en_1m_1} + a^s_{on_1m_1}\mathbf{N}^{(1)}_{on_1m_1} + b^s_{en_1m_1}\mathbf{M}^{(1)}_{en_1m_1} + b^s_{on_1m_1}\mathbf{M}^{(1)}_{on_1m_1} \right) \left(a^{s*}_{en_2m_2}\mathbf{N}^{(1)*}_{en_2m_2} \cdot \hat{\mathbf{r}} + a^{s*}_{on_2m_2}\mathbf{N}^{(1)*}_{on_2m_2} \cdot \hat{\mathbf{r}} \right) \right] dS + \\
+2\oint_S \left[\left(a^s_{en_1m_1}\mathbf{M}^{(1)}_{en_1m_1} + a^s_{on_1m_1}\mathbf{M}^{(1)}_{on_1m_1} + b^s_{en_1m_1}\mathbf{N}^{(1)}_{en_1m_1} + b^s_{on_1m_1}\mathbf{N}^{(1)}_{on_1m_1} \right) \left(b^{s*}_{en_2m_2}\mathbf{N}^{(1)*}_{en_2m_2} \cdot \hat{\mathbf{r}} + b^{s*}_{on_2m_2}\mathbf{N}^{(1)*}_{on_2m_2} \cdot \hat{\mathbf{r}} \right) \right] dS + \\
-\oint_S \left[\begin{array}{l} \left(a^s_{en_1m_1}\mathbf{N}^{(1)}_{en_1m_1} + a^s_{on_1m_1}\mathbf{N}^{(1)}_{on_1m_1} + b^s_{en_1m_1}\mathbf{M}^{(1)}_{en_1m_1} + b^s_{on_1m_1}\mathbf{M}^{(1)}_{on_1m_1} \right) \cdot \\ \cdot \left(a^{s*}_{en_2m_2}\mathbf{N}^{(1)*}_{en_2m_2} + a^{s*}_{on_2m_2}\mathbf{N}^{(1)*}_{on_2m_2} + b^{s*}_{en_2m_2}\mathbf{M}^{(1)*}_{en_2m_2} + b^{s*}_{on_2m_2}\mathbf{M}^{(1)*}_{on_2m_2} \right) \hat{\mathbf{r}} \end{array} \right] dS + \\
-\oint_S \left[\begin{array}{l} \left(a^s_{en_1m_1}\mathbf{M}^{(1)}_{en_1m_1} + a^s_{on_1m_1}\mathbf{M}^{(1)}_{on_1m_1} + b^s_{en_1m_1}\mathbf{N}^{(1)}_{en_1m_1} + b^s_{on_1m_1}\mathbf{N}^{(1)}_{on_1m_1} \right) \cdot \\ \cdot \left(a^{s*}_{en_2m_2}\mathbf{M}^{(1)*}_{en_2m_2} + a^{s*}_{on_2m_2}\mathbf{M}^{(1)*}_{on_2m_2} + b^{s*}_{en_2m_2}\mathbf{N}^{(1)*}_{en_2m_2} + b^{s*}_{on_2m_2}\mathbf{N}^{(1)*}_{on_2m_2} \right) \hat{\mathbf{r}} \end{array} \right] dS +
\end{array} \right]$$

(7.23)

Similarly for (7.21) we have:

$$\left\langle \mathbf{F}_{si} \right\rangle = \frac{1}{4}\mathrm{Re}\sum_{n_1=1}^{\infty}\sum_{m_1=0}^{n_1}\sum_{n_2=1}^{\infty}\sum_{m_2=0}^{n_2}\varepsilon_0$$

$$\left[\begin{array}{l}
2\oint\limits_S\left[\left(a^s_{en_1m_1}\mathbf{N}^{(1)}_{en_1m_1}+a^s_{on_1m_1}\mathbf{N}^{(1)}_{on_1m_1}+b^s_{en_1m_1}\mathbf{M}^{(1)}_{en_1m_1}+b^s_{on_1m_1}\mathbf{M}^{(1)}_{on_1m_1}\right)\left(a^*_{en_2m_2}\mathbf{N}^*_{en_2m_2}\cdot\hat{\mathbf{r}}+a^*_{on_2m_2}\mathbf{N}^*_{on_2m_2}\cdot\hat{\mathbf{r}}\right)\right]dS+\\
+2\oint\limits_S\left[\left(a^s_{en_1m_1}\mathbf{M}^{(1)}_{en_1m_1}+a^s_{on_1m_1}\mathbf{M}^{(1)}_{on_1m_1}+b^s_{en_1m_1}\mathbf{N}^{(1)}_{en_1m_1}+b^s_{on_1m_1}\mathbf{N}^{(1)}_{on_1m_1}\right)\left(b^*_{en_2m_2}\mathbf{N}^*_{en_2m_2}\cdot\hat{\mathbf{r}}+b^*_{on_2m_2}\mathbf{N}^*_{on_2m_2}\cdot\hat{\mathbf{r}}\right)\right]dS+\\
-\oint\limits_S\left[\begin{array}{l}\left(a^s_{en_1m_1}\mathbf{N}^{(1)}_{en_1m_1}+a^s_{on_1m_1}\mathbf{N}^{(1)}_{on_1m_1}+b^s_{en_1m_1}\mathbf{M}^{(1)}_{en_1m_1}+b^s_{on_1m_1}\mathbf{M}^{(1)}_{on_1m_1}\right)\cdot\\ \cdot\left(a^*_{en_2m_2}\mathbf{N}^*_{en_2m_2}+a^*_{on_2m_2}\mathbf{N}^*_{on_2m_2}+b^*_{en_2m_2}\mathbf{M}^*_{en_2m_2}+b^*_{on_2m_2}\mathbf{M}^*_{on_2m_2}\right)\hat{\mathbf{r}}\end{array}\right]dS+\\
-\oint\limits_S\left[\begin{array}{l}\left(a^s_{en_1m_1}\mathbf{M}^{(1)}_{en_1m_1}+a^s_{on_1m_1}\mathbf{M}^{(1)}_{on_1m_1}+b^s_{en_1m_1}\mathbf{N}^{(1)}_{en_1m_1}+b^s_{on_1m_1}\mathbf{N}^{(1)}_{on_1m_1}\right)\cdot\\ \cdot\left(a^*_{en_2m_2}\mathbf{M}^*_{en_2m_2}+a^*_{on_2m_2}\mathbf{M}^*_{on_2m_2}+b^*_{en_2m_2}\mathbf{N}^*_{en_2m_2}+b^*_{on_2m_2}\mathbf{N}^*_{on_2m_2}\right)\hat{\mathbf{r}}\end{array}\right]dS+
\end{array}\right]$$

(7.24)

For (7.22) we have:

$$\left\langle \mathbf{F}_{is} \right\rangle = \frac{1}{4}\mathrm{Re}\sum_{n_1=1}^{\infty}\sum_{m_1=0}^{n_1}\sum_{n_2=1}^{\infty}\sum_{m_2=0}^{n_2}\varepsilon_0$$

$$\left[\begin{array}{l}
2\oint\limits_S\left[\left(a_{en_1m_1}\mathbf{N}_{en_1m_1}+a_{on_1m_1}\mathbf{N}_{on_1m_1}+b_{en_1m_1}\mathbf{M}_{en_1m_1}+b_{on_1m_1}\mathbf{M}_{on_1m_1}\right)\left(a^{s*}_{en_2m_2}\mathbf{N}^{(1)*}_{en_2m_2}\cdot\hat{\mathbf{r}}+a^{s*}_{on_2m_2}\mathbf{N}^{(1)*}_{on_2m_2}\cdot\hat{\mathbf{r}}\right)\right]dS+\\
+2\oint\limits_S\left[\left(a_{en_1m_1}\mathbf{M}_{en_1m_1}+a_{on_1m_1}\mathbf{M}_{on_1m_1}+b_{on_1m_1}\mathbf{N}_{en_1m_1}+b_{on_1m_1}\mathbf{N}_{on_1m_1}\right)\left(b^{s*}_{en_2m_2}\mathbf{N}^{(1)*}_{en_2m_2}\cdot\hat{\mathbf{r}}+b^{s*}_{on_2m_2}\mathbf{N}^{(1)*}_{on_2m_2}\cdot\hat{\mathbf{r}}\right)\right]dS+\\
-\oint\limits_S\left[\begin{array}{l}\left(a_{en_1m_1}\mathbf{N}_{en_1m_1}+a_{on_1m_1}\mathbf{N}_{on_1m_1}+b_{en_1m_1}\mathbf{M}_{en_1m_1}+b_{on_1m_1}\mathbf{M}_{on_1m_1}\right)\cdot\\ \cdot\left(a^{s*}_{en_2m_2}\mathbf{N}^{(1)*}_{en_2m_2}+a^{s*}_{on_2m_2}\mathbf{N}^{(1)*}_{on_2m_2}+b^{s*}_{en_2m_2}\mathbf{M}^{(1)*}_{en_2m_2}+b^{s*}_{on_2m_2}\mathbf{M}^{(1)*}_{on_2m_2}\right)\hat{\mathbf{r}}\end{array}\right]dS+\\
-\oint\limits_S\left[\begin{array}{l}\left(a_{en_1m_1}\mathbf{M}_{en_1m_1}+a_{on_1m_1}\mathbf{M}_{on_1m_1}+b_{en_1m_1}\mathbf{N}_{en_1m_1}+b_{on_1m_1}\mathbf{N}_{on_1m_1}\right)\cdot\\ \cdot\left(a^{s*}_{en_2m_2}\mathbf{M}^{(1)*}_{en_2m_2}+a^{s*}_{on_2m_2}\mathbf{M}^{(1)*}_{on_2m_2}+b^{s*}_{en_2m_2}\mathbf{N}^{(1)*}_{en_2m_2}+b^{s*}_{on_2m_2}\mathbf{N}^{(1)*}_{on_2m_2}\right)\hat{\mathbf{r}}\end{array}\right]dS+
\end{array}\right]$$

(7.25)

In (7.23),(7.24) and (7.25)we have used the fact that $\mathbf{M}\cdot\hat{\mathbf{r}}=0$ and $\mu_0/\eta_0^2=\varepsilon_0$.

The previous expressions can be rearranged so as to highlight a series of recurring integrals.

The expression (7.23) can be rearranged as follows:

$$\left\langle \mathbf{F}_{ss}\right\rangle =\frac{1}{4}\mathrm{Re}\sum_{n_1=1}^{\infty}\sum_{m_1=0}^{n_1}\sum_{n_2=1}^{\infty}\sum_{m_2=0}^{n_2}\varepsilon_0$$

$$\times\left[\begin{array}{l}
\left(a^s_{en_1m_1}a^{s^*}_{en_2m_2}+b^s_{en_1m_1}b^{s^*}_{en_2m_2}\right)\left[2\oint_S\mathbf{N}^{(1)}_{en_1m_1}\mathbf{N}^{(1)*}_{en_2m_2}\cdot\hat{\mathbf{r}}dS-\oint_S\left(\mathbf{N}^{(1)}_{en_1m_1}\cdot\mathbf{N}^{(1)*}_{en_2m_2}\right)\hat{\mathbf{r}}dS-\oint_S\left(\mathbf{M}^{(1)}_{en_1m_1}\cdot\mathbf{M}^{(1)*}_{en_2m_2}\right)\hat{\mathbf{r}}dS\right]+\\
+\left(a^s_{on_1m_1}a^{s^*}_{on_2m_2}+b^s_{on_1m_1}b^{s^*}_{on_2m_2}\right)\left[2\oint_S\mathbf{N}^{(1)}_{on_1m_1}\mathbf{N}^{(1)*}_{on_2m_2}\cdot\hat{\mathbf{r}}dS-\oint_S\left(\mathbf{N}^{(1)}_{on_1m_1}\cdot\mathbf{N}^{(1)*}_{on_2m_2}\right)\hat{\mathbf{r}}dS-\oint_S\left(\mathbf{M}^{(1)}_{on_1m_1}\cdot\mathbf{M}^{(1)*}_{on_2m_2}\right)\hat{\mathbf{r}}dS\right]+\\
+\left(a^s_{en_1m_1}a^{s^*}_{on_2m_2}+b^s_{en_1m_1}b^{s^*}_{on_2m_2}\right)\left[2\oint_S\mathbf{N}^{(1)}_{en_1m_1}\mathbf{N}^{(1)*}_{on_2m_2}\cdot\hat{\mathbf{r}}dS-\oint_S\left(\mathbf{N}^{(1)}_{en_1m_1}\cdot\mathbf{N}^{(1)*}_{on_2m_2}\right)\hat{\mathbf{r}}dS-\oint_S\left(\mathbf{M}^{(1)}_{en_1m_1}\cdot\mathbf{M}^{(1)*}_{on_2m_2}\right)\hat{\mathbf{r}}dS\right]+\\
+\left(a^s_{on_1m_1}a^{s^*}_{en_2m_2}+b^s_{on_1m_1}b^{s^*}_{en_2m_2}\right)\left[2\oint_S\mathbf{N}^{(1)}_{on_1m_1}\mathbf{N}^{(1)*}_{en_2m_2}\cdot\hat{\mathbf{r}}dS-\oint_S\left(\mathbf{N}^{(1)}_{on_1m_1}\cdot\mathbf{N}^{(1)*}_{en_2m_2}\right)\hat{\mathbf{r}}dS-\oint_S\left(\mathbf{M}^{(1)}_{on_1m_1}\cdot\mathbf{M}^{(1)*}_{en_2m_2}\right)\hat{\mathbf{r}}dS\right]+\\
+\left(b^s_{en_1m_1}a^{s^*}_{en_2m_2}+a^s_{en_1m_1}b^{s^*}_{en_2m_2}\right)\left[2\oint_S\mathbf{M}^{(1)}_{en_1m_1}\mathbf{N}^{(1)*}_{en_2m_2}\cdot\hat{\mathbf{r}}dS-\oint_S\left(\mathbf{M}^{(1)}_{en_1m_1}\cdot\mathbf{N}^{(1)*}_{en_2m_2}\right)\hat{\mathbf{r}}dS-\oint_S\left(\mathbf{N}^{(1)}_{en_1m_1}\cdot\mathbf{M}^{(1)*}_{en_2m_2}\right)\hat{\mathbf{r}}dS\right]+\\
+\left(b^s_{en_1m_1}a^{s^*}_{on_2m_2}+a^s_{en_1m_1}b^{s^*}_{on_2m_2}\right)\left[2\oint_S\mathbf{M}^{(1)}_{en_1m_1}\mathbf{N}^{(1)*}_{on_2m_2}\cdot\hat{\mathbf{r}}dS-\oint_S\left(\mathbf{M}^{(1)}_{en_1m_1}\cdot\mathbf{N}^{(1)*}_{on_2m_2}\right)\hat{\mathbf{r}}dS\right]+\\
+\left(b^s_{on_1m_1}a^{s^*}_{en_2m_2}+a^s_{on_1m_1}b^{s^*}_{en_2m_2}\right)\left[2\oint_S\mathbf{M}^{(1)}_{on_1m_1}\mathbf{N}^{(1)*}_{en_2m_2}\cdot\hat{\mathbf{r}}dS-\oint_S\left(\mathbf{M}^{(1)}_{on_1m_1}\cdot\mathbf{N}^{(1)*}_{en_2m_2}\right)\hat{\mathbf{r}}dS\right]+\\
+\left(b^s_{on_1m_1}a^{s^*}_{on_2m_2}+a^s_{on_1m_1}b^{s^*}_{on_2m_2}\right)\left[2\oint_S\mathbf{M}^{(1)}_{on_1m_1}\mathbf{N}^{(1)*}_{on_2m_2}\cdot\hat{\mathbf{r}}dS-\oint_S\left(\mathbf{M}^{(1)}_{on_1m_1}\cdot\mathbf{N}^{(1)*}_{on_2m_2}\right)\hat{\mathbf{r}}dS-\oint_S\left(\mathbf{N}^{(1)}_{on_1m_1}\cdot\mathbf{M}^{(1)*}_{on_2m_2}\right)\hat{\mathbf{r}}dS\right]+\\
-\left(a^s_{on_1m_1}b^{s^*}_{en_2m_2}+b^s_{on_1m_1}a^{s^*}_{en_2m_2}\right)\oint_S\left(\mathbf{N}^{(1)}_{on_1m_1}\cdot\mathbf{M}^{(1)*}_{en_2m_2}\right)\hat{\mathbf{r}}dS-\left(a^s_{en_1m_1}b^{s^*}_{on_2m_2}+b^s_{en_1m_1}a^{s^*}_{on_2m_2}\right)\oint_S\left(\mathbf{N}^{(1)}_{en_1m_1}\cdot\mathbf{M}^{(1)*}_{on_2m_2}\right)\hat{\mathbf{r}}dS
\end{array}\right]$$

(7.26)

The expression (7.24) can be rearranged as follows:

$$\left\langle \mathbf{F}_{si} \right\rangle = \frac{1}{4}\mathrm{Re}\sum_{n_1=1}^{\infty}\sum_{m_1=0}^{n_1}\sum_{n_2=1}^{\infty}\sum_{m_2=0}^{n_2}\varepsilon_0$$

$$\times\left[\begin{array}{l}
\left(a^s_{en_1m_1}a^*_{en_2m_2}+b^s_{en_1m_1}b^*_{en_2m_2}\right)\left[2\oint_S \mathbf{N}^{(1)}_{en_1m_1}\mathbf{N}^*_{en_2m_2}\cdot\hat{\mathbf{r}}dS-\oint_S\left(\mathbf{N}^{(1)}_{en_1m_1}\cdot\mathbf{N}^*_{en_2m_2}\right)\hat{\mathbf{r}}dS-\oint_S\left(\mathbf{M}^{(1)}_{en_1m_1}\cdot\mathbf{M}^*_{en_2m_2}\right)\hat{\mathbf{r}}dS\right]+\\
+\left(a^s_{on_1m_1}a^*_{on_2m_2}+b^s_{on_1m_1}b^*_{on_2m_2}\right)\left[2\oint_S \mathbf{N}^{(1)}_{on_1m_1}\mathbf{N}^*_{on_2m_2}\cdot\hat{\mathbf{r}}dS-\oint_S\left(\mathbf{N}^{(1)}_{on_1m_1}\cdot\mathbf{N}^*_{on_2m_2}\right)\hat{\mathbf{r}}dS-\oint_S\left(\mathbf{M}^{(1)}_{on_1m_1}\cdot\mathbf{M}^*_{on_2m_2}\right)\hat{\mathbf{r}}dS\right]+\\
+\left(a^s_{en_1m_1}a^*_{on_2m_2}+b^s_{en_1m_1}b^*_{on_2m_2}\right)\left[2\oint_S \mathbf{N}^{(1)}_{en_1m_1}\mathbf{N}^*_{on_2m_2}\cdot\hat{\mathbf{r}}dS-\oint_S\left(\mathbf{N}^{(1)}_{en_1m_1}\cdot\mathbf{N}^*_{on_2m_2}\right)\hat{\mathbf{r}}dS-\oint_S\left(\mathbf{M}^{(1)}_{en_1m_1}\cdot\mathbf{M}^*_{on_2m_2}\right)\hat{\mathbf{r}}dS\right]+\\
+\left(a^s_{on_1m_1}a^*_{en_2m_2}+b^s_{on_1m_1}b^*_{en_2m_2}\right)\left[2\oint_S \mathbf{N}^{(1)}_{on_1m_1}\mathbf{N}^*_{en_2m_2}\cdot\hat{\mathbf{r}}dS-\oint_S\left(\mathbf{N}^{(1)}_{on_1m_1}\cdot\mathbf{N}^*_{en_2m_2}\right)\hat{\mathbf{r}}dS-\oint_S\left(\mathbf{M}^{(1)}_{on_1m_1}\cdot\mathbf{M}^*_{en_2m_2}\right)\hat{\mathbf{r}}dS\right]+\\
+\left(b^s_{en_1m_1}a^*_{en_2m_2}+a^s_{en_1m_1}b^*_{en_2m_2}\right)\left[2\oint_S \mathbf{M}^{(1)}_{en_1m_1}\mathbf{N}^*_{en_2m_2}\cdot\hat{\mathbf{r}}dS-\oint_S\left(\mathbf{M}^{(1)}_{en_1m_1}\cdot\mathbf{N}^*_{en_2m_2}\right)\hat{\mathbf{r}}dS-\oint_S\left(\mathbf{N}^{(1)}_{en_1m_1}\cdot\mathbf{M}^*_{en_2m_2}\right)\hat{\mathbf{r}}dS\right]+\\
+\left(b^s_{en_1m_1}a^*_{on_2m_2}+a^s_{en_1m_1}b^*_{on_2m_2}\right)\left[2\oint_S \mathbf{M}^{(1)}_{en_1m_1}\mathbf{N}^*_{on_2m_2}\cdot\hat{\mathbf{r}}dS-\oint_S\left(\mathbf{M}^{(1)}_{en_1m_1}\cdot\mathbf{N}^*_{on_2m_2}\right)\hat{\mathbf{r}}dS\right]+\\
+\left(b^s_{on_1m_1}a^*_{en_2m_2}+a^s_{on_1m_1}b^*_{en_2m_2}\right)\left[2\oint_S \mathbf{M}^{(1)}_{on_1m_1}\mathbf{N}^*_{en_2m_2}\cdot\hat{\mathbf{r}}dS-\oint_S\left(\mathbf{M}^{(1)}_{on_1m_1}\cdot\mathbf{N}^*_{en_2m_2}\right)\hat{\mathbf{r}}dS\right]+\\
+\left(b^s_{on_1m_1}a^*_{on_2m_2}+a^s_{on_1m_1}b^*_{on_2m_2}\right)\left[2\oint_S \mathbf{M}^{(1)}_{on_1m_1}\mathbf{N}^*_{on_2m_2}\cdot\hat{\mathbf{r}}dS-\oint_S\left(\mathbf{M}^{(1)}_{on_1m_1}\cdot\mathbf{N}^*_{on_2m_2}\right)\hat{\mathbf{r}}dS-\oint_S\left(\mathbf{N}^{(1)}_{on_1m_1}\cdot\mathbf{M}^*_{on_2m_2}\right)\hat{\mathbf{r}}dS\right]+\\
-\left(a^s_{on_1m_1}b^*_{en_2m_2}+b^s_{on_1m_1}a^*_{en_2m_2}\right)\oint_S\left(\mathbf{N}^{(1)}_{on_1m_1}\cdot\mathbf{M}^*_{en_2m_2}\right)\hat{\mathbf{r}}dS-\left(a^s_{en_1m_1}b^*_{on_2m_2}+b^s_{en_1m_1}a^*_{on_2m_2}\right)\oint_S\left(\mathbf{N}^{(1)}_{en_1m_1}\cdot\mathbf{M}^*_{on_2m_2}\right)\hat{\mathbf{r}}dS
\end{array}\right] \tag{7.27}$$

The expression (7.25) can be rearranged as follows:

$$\left\langle \mathbf{F}_{is} \right\rangle = \frac{1}{4}\mathrm{Re}\sum_{n_1=1}^{\infty}\sum_{m_1=0}^{n_1}\sum_{n_2=1}^{\infty}\sum_{m_2=0}^{n_2}\varepsilon_0$$

$$\times\left[\begin{array}{l}
\left(a_{en_1m_1}a_{en_2m_2}^{s*}+b_{en_1m_1}b_{en_2m_2}^{s*}\right)\left[2\oint_S \mathbf{N}_{en_1m_1}\mathbf{N}_{en_2m_2}^{(1)*}\cdot\hat{\mathbf{r}}dS-\oint_S\left(\mathbf{N}_{en_1m_1}\cdot\mathbf{N}_{en_2m_2}^{(1)*}\right)\hat{\mathbf{r}}dS-\oint_S\left(\mathbf{M}_{en_1m_1}\cdot\mathbf{M}_{en_2m_2}^{(1)*}\right)\hat{\mathbf{r}}dS\right]+\\
+\left(a_{on_1m_1}a_{on_2m_2}^{s*}+b_{on_1m_1}b_{on_2m_2}^{s*}\right)\left[2\oint_S \mathbf{N}_{on_1m_1}\mathbf{N}_{on_2m_2}^{(1)*}\cdot\hat{\mathbf{r}}dS-\oint_S\left(\mathbf{N}_{on_1m_1}\cdot\mathbf{N}_{on_2m_2}^{(1)*}\right)\hat{\mathbf{r}}dS-\oint_S\left(\mathbf{M}_{on_1m_1}\cdot\mathbf{M}_{on_2m_2}^{(1)*}\right)\hat{\mathbf{r}}dS\right]+\\
+\left(a_{en_1m_1}a_{on_2m_2}^{s*}+b_{en_1m_1}b_{on_2m_2}^{s*}\right)\left[2\oint_S \mathbf{N}_{en_1m_1}\mathbf{N}_{on_2m_2}^{(1)*}\cdot\hat{\mathbf{r}}dS-\oint_S\left(\mathbf{N}_{en_1m_1}\cdot\mathbf{N}_{on_2m_2}^{(1)*}\right)\hat{\mathbf{r}}dS-\oint_S\left(\mathbf{M}_{en_1m_1}\cdot\mathbf{M}_{on_2m_2}^{(1)*}\right)\hat{\mathbf{r}}dS\right]+\\
+\left(a_{on_1m_1}a_{en_2m_2}^{s*}+b_{on_1m_1}b_{en_2m_2}^{s*}\right)\left[2\oint_S \mathbf{N}_{on_1m_1}\mathbf{N}_{en_2m_2}^{(1)*}\cdot\hat{\mathbf{r}}dS-\oint_S\left(\mathbf{N}_{on_1m_1}\cdot\mathbf{N}_{en_2m_2}^{(1)*}\right)\hat{\mathbf{r}}dS-\oint_S\left(\mathbf{M}_{on_1m_1}\cdot\mathbf{M}_{en_2m_2}^{(1)*}\right)\hat{\mathbf{r}}dS\right]+\\
+\left(b_{en_1m_1}a_{en_2m_2}^{s*}+a_{en_1m_1}b_{en_2m_2}^{s*}\right)\left[2\oint_S \mathbf{M}_{en_1m_1}\mathbf{N}_{en_2m_2}^{(1)*}\cdot\hat{\mathbf{r}}dS-\oint_S\left(\mathbf{M}_{en_1m_1}\cdot\mathbf{N}_{en_2m_2}^{(1)*}\right)\hat{\mathbf{r}}dS-\oint_S\left(\mathbf{N}_{en_1m_1}\cdot\mathbf{M}_{en_2m_2}^{(1)*}\right)\hat{\mathbf{r}}dS\right]+\\
+\left(b_{en_1m_1}a_{on_2m_2}^{s*}+a_{en_1m_1}b_{on_2m_2}^{s*}\right)\left[2\oint_S \mathbf{M}_{en_1m_1}\mathbf{N}_{on_2m_2}^{(1)*}\cdot\hat{\mathbf{r}}dS-\oint_S\left(\mathbf{M}_{en_1m_1}\cdot\mathbf{N}_{on_2m_2}^{(1)*}\right)\hat{\mathbf{r}}dS\right]+\\
+\left(b_{on_1m_1}a_{en_2m_2}^{s*}+a_{on_1m_1}b_{en_2m_2}^{s*}\right)\left[2\oint_S \mathbf{M}_{on_1m_1}\mathbf{N}_{en_2m_2}^{(1)*}\cdot\hat{\mathbf{r}}dS-\oint_S\left(\mathbf{M}_{on_1m_1}\cdot\mathbf{N}_{en_2m_2}^{(1)*}\right)\hat{\mathbf{r}}dS\right]+\\
+\left(b_{on_1m_1}a_{on_2m_2}^{s*}+a_{on_1m_1}b_{on_2m_2}^{s*}\right)\left[2\oint_S \mathbf{M}_{on_1m_1}\mathbf{N}_{on_2m_2}^{(1)*}\cdot\hat{\mathbf{r}}dS-\oint_S\left(\mathbf{M}_{on_1m_1}\cdot\mathbf{N}_{on_2m_2}^{(1)*}\right)\hat{\mathbf{r}}dS-\oint_S\left(\mathbf{N}_{on_1m_1}\cdot\mathbf{M}_{on_2m_2}^{(1)*}\right)\hat{\mathbf{r}}dS\right]+\\
-\left(a_{on_1m_1}b_{en_2m_2}^{s*}+b_{on_1m_1}a_{en_2m_2}^{s*}\right)\oint_S\left(\mathbf{N}_{on_1m_1}\cdot\mathbf{M}_{en_2m_2}^{(1)*}\right)\hat{\mathbf{r}}dS-\left(a_{en_1m_1}b_{on_2m_2}^{s*}+b_{en_1m_1}a_{on_2m_2}^{s*}\right)\oint_S\left(\mathbf{N}_{en_1m_1}\cdot\mathbf{M}_{on_2m_2}^{(1)*}\right)\hat{\mathbf{r}}dS
\end{array}\right]$$

(7.28)

The expressions of the surface integrals appearing in (7.26), (7.27) and (7.28) are reported in Appendix D. Using these results, equation (7.26) reduces to:

$$\left\langle \mathbf{F}_{ss}\cdot\hat{\mathbf{z}}\right\rangle = \frac{\pi\varepsilon_0}{k_0^2}\sum_{n_1=1}^{\infty}\sum_{m_1=0}^{n_1}\left(1+\delta_{m_1,0}\right)\frac{2n_1\left(n_1+2\right)\left(n_1+m_1+1\right)}{\left(2n_1+3\right)\left(2n_1+1\right)}\frac{\left(n_1+m_1\right)!}{\left(n_1-m_1\right)!}\mathrm{Im}\left[a^{s}_{en_1m_1}a^{s*}_{e(n_1+1)m_1}+b^{s}_{en_1m_1}b^{s*}_{e(n_1+1)m_1}\right]+$$
$$+\frac{\pi\varepsilon_0}{k_0^2}\sum_{n_1=1}^{\infty}\sum_{m_1=0}^{n_1}\left(1-\delta_{m_1,0}\right)\frac{2n_1\left(n_1+2\right)\left(n_1+m_1+1\right)}{\left(2n_1+3\right)\left(2n_1+1\right)}\frac{\left(n_1+m_1\right)!}{\left(n_1-m_1\right)!}\mathrm{Im}\left[a^{s}_{on_1m_1}a^{s*}_{o(n_1+1)m_1}+b^{s}_{on_1m_1}b^{s*}_{o(n_1+1)m_1}\right]+$$
$$+\frac{\pi\varepsilon_0}{k_0^2}\sum_{n_1=1}^{\infty}\sum_{m_1=0}^{n_1}\frac{2m_1}{\left(2n_1+1\right)}\frac{\left(n_1+m_1\right)!}{\left(n_1-m_1\right)!}\mathrm{Im}\left[a^{s}_{en_1m_1}b^{s*}_{on_1m_1}+b^{s}_{en_1m_1}a^{s*}_{on_1m_1}\right] \tag{7.29}$$

$$\left\langle\left(\mathbf{F}_{is}+\mathbf{F}_{si}\right)\cdot\hat{\mathbf{z}}\right\rangle =$$
$$=\frac{\pi\varepsilon_0}{2k_0^2}\sum_{n_1=1}^{\infty}\sum_{m_1=0}^{n_1}\left(1+\delta_{m_1,0}\right)\frac{2n_1\left(n_1+2\right)\left(n_1+m_1+1\right)}{\left(2n_1+3\right)\left(2n_1+1\right)}\frac{\left(n_1+m_1\right)!}{\left(n_1-m_1\right)!}\mathrm{Im}\left[a_{en_1m_1}a^{s*}_{e(n_1+1)m_1}+a^{s}_{en_1m_1}a^{*}_{e(n_1+1)m_1}\right]$$
$$+\frac{\pi\varepsilon_0}{2k_0^2}\sum_{n_1=1}^{\infty}\sum_{m_1=0}^{n_1}\left(1+\delta_{m_1,0}\right)\frac{2n_1\left(n_1+2\right)\left(n_1+m_1+1\right)}{\left(2n_1+3\right)\left(2n_1+1\right)}\frac{\left(n_1+m_1\right)!}{\left(n_1-m_1\right)!}\mathrm{Im}\left[b_{en_1m_1}b^{s*}_{e(n_1+1)m_1}+b^{s}_{en_1m_1}b^{*}_{e(n_1+1)m_1}\right]+$$
$$+\frac{\pi\varepsilon_0}{2k_0^2}\sum_{n_1=1}^{\infty}\sum_{m_1=0}^{n_1}\left(1-\delta_{m_1,0}\right)\frac{2n_1\left(n_1+2\right)\left(n_1+m_1+1\right)}{\left(2n_1+3\right)\left(2n_1+1\right)}\frac{\left(n_1+m_1\right)!}{\left(n_1-m_1\right)!}\mathrm{Im}\left[a_{on_1m_1}a^{s*}_{o(n_1+1)m_1}+a^{s}_{on_1m_1}a^{*}_{o(n_1+1)m_1}\right]+$$
$$+\frac{\pi\varepsilon_0}{2k_0^2}\sum_{n_1=1}^{\infty}\sum_{m_1=0}^{n_1}\left(1-\delta_{m_1,0}\right)\frac{2n_1\left(n_1+2\right)\left(n_1+m_1+1\right)}{\left(2n_1+3\right)\left(2n_1+1\right)}\frac{\left(n_1+m_1\right)!}{\left(n_1-m_1\right)!}\mathrm{Im}\left[b_{on_1m_1}b^{s*}_{o(n_1+1)m_1}+b^{s}_{on_1m_1}b^{*}_{o(n_1+1)m_1}\right]+$$
$$+\frac{\pi\varepsilon_0}{k_0^2}\sum_{n_1=1}^{\infty}\sum_{m_1=0}^{n_1}\frac{2m_1}{\left(2n_1+1\right)}\frac{\left(n_1+m_1\right)!}{\left(n_1-m_1\right)!}\mathrm{Im}\left[a^{s}_{en_1m_1}b^{*}_{on_1m_1}+a_{en_1m_1}b^{s*}_{on_1m_1}+b^{s}_{en_1m_1}a^{*}_{on_1m_1}+b_{en_1m_1}a^{s*}_{on_1m_1}\right] \tag{7.30}$$

So the total force in the $\hat{\mathbf{z}}$ direction is given by:

$$\left\langle \mathbf{F}\cdot\hat{\mathbf{z}}\right\rangle = \frac{\pi\varepsilon_0}{k_0^2}\sum_{n_1=1}^{\infty}\sum_{m_1=0}^{n_1}\frac{2n_1\left(n_1+2\right)\left(n_1+m_1+1\right)}{\left(2n_1+3\right)\left(2n_1+1\right)}\frac{\left(n_1+m_1\right)!}{\left(n_1-m_1\right)!}\times$$

$$\times\left\{\begin{array}{l}\left(1+\delta_{m_1,0}\right)\mathrm{Im}\left[\begin{array}{l}a^{s}_{en_1m_1}a^{s*}_{e(n_1+1)m_1}+b^{s}_{en_1m_1}b^{s*}_{e(n_1+1)m_1}+\\+\dfrac{a_{en_1m_1}a^{s*}_{e(n_1+1)m_1}+a^{s}_{en_1m_1}a^{*}_{e(n_1+1)m_1}}{2}+\dfrac{b_{en_1m_1}b^{s*}_{e(n_1+1)m_1}+b^{s}_{en_1m_1}b^{*}_{e(n_1+1)m_1}}{2}\end{array}\right]+\\+\left(1-\delta_{m_1,0}\right)\mathrm{Im}\left[\begin{array}{l}a^{s}_{on_1m_1}a^{s*}_{o(n_1+1)m_1}+b^{s}_{on_1m_1}b^{s*}_{o(n_1+1)m_1}+\\+\dfrac{a_{on_1m_1}a^{s*}_{o(n_1+1)m_1}+a^{s}_{on_1m_1}a^{*}_{o(n_1+1)m_1}}{2}+\dfrac{b_{on_1m_1}b^{s*}_{o(n_1+1)m_1}+b^{s}_{on_1m_1}b^{*}_{o(n_1+1)m_1}}{2}\end{array}\right]\end{array}\right\} \quad (7.31)$$

$$+\frac{\pi\varepsilon_0}{k_0^2}\sum_{n_1=1}^{\infty}\sum_{m_1=0}^{n_1}\frac{2m_1}{\left(2n_1+1\right)}\frac{\left(n_1+m_1\right)!}{\left(n_1-m_1\right)!}\mathrm{Im}\left[\begin{array}{l}a^{s}_{en_1m_1}b^{s*}_{on_1m_1}+b^{s}_{en_1m_1}a^{s*}_{on_1m_1}+a^{s}_{en_1m_1}b^{*}_{on_1m_1}+\\+a_{en_1m_1}b^{s*}_{on_1m_1}+b^{s}_{en_1m_1}a^{*}_{on_1m_1}+b_{en_1m_1}a^{s*}_{on_1m_1}\end{array}\right]$$

Similarly we can calculate the force along $\hat{\mathbf{x}}$:

$$\left\langle \mathbf{F}\cdot\hat{\mathbf{x}}\right\rangle = \left\langle \mathbf{F}_{ss}\cdot\hat{\mathbf{x}}\right\rangle + \left\langle \left(\mathbf{F}_{is}+\mathbf{F}_{si}\right)\cdot\hat{\mathbf{x}}\right\rangle \quad (7.32)$$

with the following components:

$$\left\langle \mathbf{F}_{ss}\cdot\hat{\mathbf{x}}\right\rangle =$$
$$=-\frac{\pi\varepsilon_0}{k_0^2}\sum_{n_1=1}^{\infty}\sum_{m_1=0}^{n_1}\left(1+\delta_{m_1,0}\right)\frac{2n_1\left(n_1+2\right)}{\left(2n_1+3\right)\left(2n_1+1\right)}\frac{\left(n_1+2+m_1\right)!}{2\left(n_1-m_1\right)!}\mathrm{Im}\left[a^{s}_{en_1m_1}a^{s*}_{e(n_1+1)(m_1+1)}+b^{s}_{en_1m_1}b^{s*}_{e(n_1+1)(m_1+1)}\right]+$$
$$+\frac{\pi\varepsilon_0}{k_0^2}\sum_{n_1=1}^{\infty}\sum_{m_1=0}^{n_1-1}\left(1+\delta_{m_1,0}\right)\frac{2n_1\left(n_1+2\right)}{\left(2n_1+3\right)\left(2n_1+1\right)}\frac{\left(n_1+1+m_1\right)!}{2\left(n_1-1-m_1\right)!}\mathrm{Im}\left[a^{s}_{en_1(m_1+1)}a^{s*}_{e(n_1+1)m_1}+b^{s}_{e(m_1+1)m_1}b^{s*}_{e(n_1+1)m_1}\right]+$$
$$-\frac{\pi\varepsilon_0}{k_0^2}\sum_{n_1=1}^{\infty}\sum_{m_1=0}^{n_1}\left(1-\delta_{m_1,0}\right)\frac{2n_1\left(n_1+2\right)}{\left(2n_1+3\right)\left(2n_1+1\right)}\frac{\left(n_1+2+m_1\right)!}{2\left(n_1-m_1\right)!}\mathrm{Im}\left[a^{s}_{on_1m_1}a^{s*}_{o(n_1+1)(m_1+1)}+b^{s}_{on_1m_1}b^{s*}_{o(n_1+1)(m_1+1)}\right]+$$
$$+\frac{\pi\varepsilon_0}{k_0^2}\sum_{n_1=1}^{\infty}\sum_{m_1=0}^{n_1-1}\left(1-\delta_{m_1,0}\right)\frac{2n_1\left(n_1+2\right)}{\left(2n_1+3\right)\left(2n_1+1\right)}\frac{\left(n_1+1+m_1\right)!}{2\left(n_1-1-m_1\right)!}\mathrm{Im}\left[a^{s}_{on_1(m_1+1)}a^{s*}_{o(n_1+1)m_1}+b^{s}_{o(m_1+1)m_1}b^{s*}_{o(n_1+1)m_1}\right]$$
$$-\frac{\pi\varepsilon_0}{k_0^2}\sum_{n_1=1}^{\infty}\sum_{m_1=0}^{n_1}\frac{1}{\left(2n_1+1\right)}\frac{\left(n_1+m_1+1\right)!}{\left(n_1-m_1-1\right)!}\mathrm{Im}\left[a^{s}_{en_1(m_1+1)}b^{s*}_{on_1m_1}+a^{s}_{en_1m_1}b^{s*}_{on_1(m_1+1)}+b^{s}_{en_1(m_1+1)}a^{s*}_{on_1m_1}+b^{s}_{en_1m_1}a^{s*}_{on_1(m_1+1)}\right]$$

(7.33)

$$\left\langle \left(\mathbf{F}_{is}+\mathbf{F}_{si}\right)\cdot\hat{\mathbf{x}}\right\rangle =$$
$$=-\frac{\pi\varepsilon_0}{2k_0^2}\sum_{n_1=1}^{\infty}\sum_{m_1=0}^{n_1}\left(1+\delta_{m_1,0}\right)\frac{2n_1\left(n_1+2\right)}{\left(2n_1+3\right)\left(2n_1+1\right)}\frac{\left(n_1+2+m_1\right)!}{2\left(n_1-m_1\right)!}\mathrm{Im}\left[\begin{matrix}a_{en_1m_1}a^{s*}_{e(n_1+1)(m_1+1)}+b_{en_1m_1}b^{s*}_{e(n_1+1)(m_1+1)}+\\+a^{s}_{en_1m_1}a^{*}_{e(n_1+1)(m_1+1)}+b^{s}_{en_1m_1}b^{*}_{e(n_1+1)(m_1+1)}\end{matrix}\right]+$$
$$+\frac{\pi\varepsilon_0}{2k_0^2}\sum_{n_1=1}^{\infty}\sum_{m_1=0}^{n_1-1}\left(1+\delta_{m_1,0}\right)\frac{2n_1\left(n_1+2\right)}{\left(2n_1+3\right)\left(2n_1+1\right)}\frac{\left(n_1+1+m_1\right)!}{2\left(n_1-1-m_1\right)!}\mathrm{Im}\left[\begin{matrix}a_{en_1(m_1+1)}a^{s*}_{e(n_1+1)m_1}+b_{en_1(m_1+1)}b^{s*}_{e(n_1+1)m_1}+\\+a^{s}_{en_1(m_1+1)}a^{*}_{e(n_1+1)m_1}+b^{s}_{e(m_1+1)m_1}b^{*}_{e(n_1+1)m_1}\end{matrix}\right]+$$
$$-\frac{\pi\varepsilon_0}{2k_0^2}\sum_{n_1=1}^{\infty}\sum_{m_1=0}^{n_1}\left(1-\delta_{m_1,0}\right)\frac{2n_1\left(n_1+2\right)}{\left(2n_1+3\right)\left(2n_1+1\right)}\frac{\left(n_1+2+m_1\right)!}{2\left(n_1-m_1\right)!}\mathrm{Im}\left[\begin{matrix}a_{on_1m_1}a^{s*}_{o(n_1+1)(m_1+1)}+b_{on_1m_1}b^{s*}_{o(n_1+1)(m_1+1)}+\\+a^{s}_{on_1m_1}a^{*}_{o(n_1+1)(m_1+1)}+b^{s}_{on_1m_1}b^{*}_{o(n_1+1)(m_1+1)}\end{matrix}\right]+$$
$$+\frac{\pi\varepsilon_0}{2k_0^2}\sum_{n_1=1}^{\infty}\sum_{m_1=0}^{n_1-1}\left(1-\delta_{m_1,0}\right)\frac{2n_1\left(n_1+2\right)}{\left(2n_1+3\right)\left(2n_1+1\right)}\frac{\left(n_1+1+m_1\right)!}{2\left(n_1-1-m_1\right)!}\mathrm{Im}\left[\begin{matrix}a_{on_1(m_1+1)}a^{s*}_{o(n_1+1)m_1}+b_{on_1(m_1+1)}b^{s*}_{o(n_1+1)m_1}+\\+a^{s}_{on_1(m_1+1)}a^{*}_{o(n_1+1)m_1}+b^{s}_{o(m_1+1)m_1}b^{*}_{o(n_1+1)m_1}\end{matrix}\right]+$$
$$-\frac{\pi\varepsilon_0}{2k_0^2}\sum_{n_1=1}^{\infty}\sum_{m_1=0}^{n_1}\frac{1}{\left(2n_1+1\right)}\frac{\left(n_1+m_1+1\right)!}{\left(n_1-m_1-1\right)!}\mathrm{Im}\left[\begin{matrix}a_{en_1(m_1+1)}b^{s*}_{on_1m_1}+a_{en_1m_1}b^{s*}_{on_1(m_1+1)}+b_{en_1(m_1+1)}a^{s*}_{on_1m_1}+b_{en_1m_1}a^{s*}_{on_1(m_1+1)}+\\+a^{s}_{en_1(m_1+1)}b^{*}_{on_1m_1}+a^{s}_{en_1m_1}b^{*}_{on_1(m_1+1)}+b^{s}_{en_1(m_1+1)}a^{*}_{on_1m_1}+b^{s}_{en_1m_1}a^{*}_{on_1(m_1+1)}\end{matrix}\right]$$

(7.34)

We finally evaluate the $\hat{\mathbf{y}}$ component of the force:

$$\left\langle \mathbf{F}\cdot\hat{\mathbf{y}}\right\rangle = \left\langle \mathbf{F}_{ss}\cdot\hat{\mathbf{y}}\right\rangle + \left\langle \left(\mathbf{F}_{is}+\mathbf{F}_{si}\right)\cdot\hat{\mathbf{y}}\right\rangle \tag{7.35}$$

$$\begin{aligned}
&\left\langle \mathbf{F}_{ss}\cdot\hat{\mathbf{y}}\right\rangle = \\
&= -\frac{\pi\varepsilon_0}{k_0^2}\sum_{n_1=1}^{\infty}\sum_{m_1=0}^{n_1}\left(1+\delta_{m_1,0}\right)\frac{2n_1\left(n_1+2\right)}{\left(2n_1+3\right)\left(2n_1+1\right)}\frac{\left(n_1+2+m_1\right)!}{2\left(n_1-m_1\right)!}\operatorname{Im}\left[a^{s}_{en_1m_1}a^{s*}_{o(n_1+1)(m_1+1)}+b^{s}_{en_1m_1}b^{s*}_{o(n_1+1)(m_1+1)}\right]+\\
&+\frac{\pi\varepsilon_0}{k_0^2}\sum_{n_1=1}^{\infty}\sum_{m_1=0}^{n_1-1}\left(1+\delta_{m_1,0}\right)\frac{2n_1\left(n_1+2\right)}{\left(2n_1+3\right)\left(2n_1+1\right)}\frac{\left(n_1+1+m_1\right)!}{2\left(n_1-1-m_1\right)!}\operatorname{Im}\left[a^{s}_{on_1(m_1+1)}a^{s*}_{e(n_1+1)m_1}+b^{s}_{o(m_1+1)m_1}b^{s*}_{e(n_1+1)m_1}\right]+\\
&+\frac{\pi\varepsilon_0}{k_0^2}\sum_{n_1=1}^{\infty}\sum_{m_1=0}^{n_1}\left(1-\delta_{m_1,0}\right)\frac{2n_1\left(n_1+2\right)}{\left(2n_1+3\right)\left(2n_1+1\right)}\frac{\left(n_1+2+m_1\right)!}{2\left(n_1-m_1\right)!}\operatorname{Im}\left[a^{s}_{on_1m_1}a^{s*}_{e(n_1+1)(m_1+1)}+b^{s}_{on_1m_1}b^{s*}_{e(n_1+1)(m_1+1)}\right]+\\
&-\frac{\pi\varepsilon_0}{k_0^2}\sum_{n_1=1}^{\infty}\sum_{m_1=0}^{n_1-1}\left(1-\delta_{m_1,0}\right)\frac{2n_1\left(n_1+2\right)}{\left(2n_1+3\right)\left(2n_1+1\right)}\frac{\left(n_1+1+m_1\right)!}{2\left(n_1-1-m_1\right)!}\operatorname{Im}\left[a^{s}_{en_1(m_1+1)}a^{s*}_{o(n_1+1)m_1}+b^{s}_{e(m_1+1)m_1}b^{s*}_{o(n_1+1)m_1}\right]\\
&+\frac{\pi\varepsilon_0}{k_0^2}\sum_{n_1=1}^{\infty}\sum_{m_1=0}^{n_1}\left(1+\delta_{m_1,0}\right)\frac{1}{\left(2n_1+1\right)}\frac{\left(n_1+m_1+1\right)!}{\left(n_1-m_1-1\right)!}\operatorname{Im}\left[a^{s}_{en_1(m_1+1)}b^{s*}_{en_1m_1}+b^{s}_{en_1(m_1+1)}a^{s*}_{en_1m_1}\right]+\\
&-\frac{\pi\varepsilon_0}{k_0^2}\sum_{n_1=1}^{\infty}\sum_{m_1=0}^{n_1}\left(1-\delta_{m_1,0}\right)\frac{1}{\left(2n_1+1\right)}\frac{\left(n_1+m_1+1\right)!}{\left(n_1-m_1-1\right)!}\operatorname{Im}\left[a^{s}_{on_1m_1}b^{s*}_{on_1(m_1+1)}+b^{s}_{on_1m_1}a^{s*}_{on_1(m_1+1)}\right]
\end{aligned} \tag{7.36}$$

$$\left\langle \left(\mathbf{F}_{is}+\mathbf{F}_{si}\right)\cdot\hat{\mathbf{y}}\right\rangle =$$

$$=-\frac{\pi\varepsilon_0}{k_0^2}\sum_{n_1=1}^{\infty}\sum_{m_1=0}^{n_1}\left(1+\delta_{m_1,0}\right)\frac{2n_1\left(n_1+2\right)}{\left(2n_1+3\right)\left(2n_1+1\right)}\frac{\left(n_1+2+m_1\right)!}{2\left(n_1-m_1\right)!}\mathrm{Im}\left[\begin{array}{l}a_{en_1m_1}a^{s*}_{o(n_1+1)(m_1+1)}+b_{en_1m_1}b^{s*}_{o(n_1+1)(m_1+1)}+\\+a^{s}_{en_1m_1}a^{*}_{o(n_1+1)(m_1+1)}+b^{s}_{en_1m_1}b^{*}_{o(n_1+1)(m_1+1)}\end{array}\right]+$$

$$+\frac{\pi\varepsilon_0}{k_0^2}\sum_{n_1=1}^{\infty}\sum_{m_1=0}^{n_1-1}\left(1+\delta_{m_1,0}\right)\frac{2n_1\left(n_1+2\right)}{\left(2n_1+3\right)\left(2n_1+1\right)}\frac{\left(n_1+1+m_1\right)!}{2\left(n_1-1-m_1\right)!}\mathrm{Im}\left[\begin{array}{l}a_{on_1(m_1+1)}a^{s*}_{e(n_1+1)m_1}+b_{on_1(m_1+1)}b^{s*}_{e(n_1+1)m_1}+\\+a^{s}_{on_1(m_1+1)}a^{*}_{e(n_1+1)m_1}+b^{s}_{o(m_1+1)m_1}b^{*}_{e(n_1+1)m_1}\end{array}\right]+$$

$$+\frac{\pi\varepsilon_0}{k_0^2}\sum_{n_1=1}^{\infty}\sum_{m_1=0}^{n_1}\left(1-\delta_{m_1,0}\right)\frac{2n_1\left(n_1+2\right)}{\left(2n_1+3\right)\left(2n_1+1\right)}\frac{\left(n_1+2+m_1\right)!}{2\left(n_1-m_1\right)!}\mathrm{Im}\left[\begin{array}{l}a_{on_1m_1}a^{s*}_{e(n_1+1)(m_1+1)}+b_{on_1m_1}b^{s*}_{e(n_1+1)(m_1+1)}+\\+a^{s}_{on_1m_1}a^{*}_{e(n_1+1)(m_1+1)}+b^{s}_{on_1m_1}b^{*}_{e(n_1+1)(m_1+1)}\end{array}\right]+$$

$$-\frac{\pi\varepsilon_0}{k_0^2}\sum_{n_1=1}^{\infty}\sum_{m_1=0}^{n_1-1}\left(1-\delta_{m_1,0}\right)\frac{2n_1\left(n_1+2\right)}{\left(2n_1+3\right)\left(2n_1+1\right)}\frac{\left(n_1+1+m_1\right)!}{2\left(n_1-1-m_1\right)!}\mathrm{Im}\left[\begin{array}{l}a_{en_1(m_1+1)}a^{s*}_{o(n_1+1)m_1}+b_{en_1(m_1+1)}b^{s*}_{o(n_1+1)m_1}+\\+a^{s}_{en_1(m_1+1)}a^{*}_{o(n_1+1)m_1}+b^{s}_{e(m_1+1)m_1}b^{*}_{o(n_1+1)m_1}\end{array}\right]$$

$$+\frac{\pi\varepsilon_0}{k_0^2}\sum_{n_1=1}^{\infty}\sum_{m_1=0}^{n_1}\left(1+\delta_{m_1,0}\right)\frac{1}{\left(2n_1+1\right)}\frac{\left(n_1+m_1+1\right)!}{\left(n_1-m_1-1\right)!}\mathrm{Im}\left[\begin{array}{l}a_{en_1(m_1+1)}b^{s*}_{en_1m_1}+b_{en_1(m_1+1)}a^{s*}_{en_1m_1}+\\+a^{s}_{en_1(m_1+1)}b^{*}_{en_1m_1}+b^{s}_{en_1(m_1+1)}a^{*}_{en_1m_1}\end{array}\right]+$$

$$-\frac{\pi\varepsilon_0}{k_0^2}\sum_{n_1=1}^{\infty}\sum_{m_1=0}^{n_1}\left(1-\delta_{m_1,0}\right)\frac{1}{\left(2n_1+1\right)}\frac{\left(n_1+m_1+1\right)!}{\left(n_1-m_1-1\right)!}\mathrm{Im}\left[\begin{array}{l}a_{on_1m_1}b^{s*}_{on_1(m_1+1)}+b_{on_1m_1}a^{s*}_{on_1(m_1+1)}+\\+a^{s}_{on_1m_1}b^{*}_{on_1(m_1+1)}+b^{s}_{on_1m_1}a^{*}_{on_1(m_1+1)}\end{array}\right]$$

(7.37)

From the expressions (7.29) - (7.37) we can infer the following set of general rules that apply to force calculations in terms of spherical multipoles. For the force along $\hat{\mathbf{z}}$ we have non-vanishing contributions from the interaction of:

- Electric multipoles of degree n and order m with electric multipoles of degree $n\pm1$ and the same order m and the same azimuthal parity
- Magnetic multipoles of degree n and order m with magnetic multipoles of degree $n\pm1$ and the same order m and the same azimuthal parity

- Electric multipoles of degree n and order m with magnetic multipoles of the same degree n and the same order m and opposite azimuthal parity

For the force along $\hat{\mathbf{x}}$ we have non-vanishing contributions from the interaction of:

- Electric multipoles of degree n and order m with electric multipoles of degree $n \pm 1$ and the order $m \pm 1$, and the same azimuthal parity
- Magnetic multipoles of degree n and order m with magnetic multipoles of degree $n \pm 1$ and the same order $m \pm 1$, and the same azimuthal parity
- Electric multipoles of degree n and order m with magnetic multipoles of the same degree n and the order $m \pm 1$, and opposite azimuthal parity

For the force along $\hat{\mathbf{y}}$ we have non-vanishing contributions from the interaction of:

- Electric multipoles of degree n and order m with electric multipoles of degree $n \pm 1$ and the order $m \pm 1$, and opposite azimuthal parity
- Magnetic multipoles of degree n and order m with magnetic multipoles of degree $n \pm 1$ and the same order $m \pm 1$, and opposite azimuthal parity
- Electric multipoles of degree n and order m with magnetic multipoles of the same degree n and the order $m \pm 1$, and the same azimuthal parity

CHAPTER 8:
OPTICAL FORCES ON A MIE-PARTICLE IN A TRANSVERSE POYNTING FLOW

In this chapter we would like to use the theory developed in chapter 7 to some counterintuitive effects related to the force experienced by a dielectric sphere illuminated by two electromagnetic plane waves of different polarization.

The momentum transferred by an electromagnetic field to a scattering and/or absorbing body is given by the flux of the Maxwell's stress tensor through any arbitrary surface enclosing the object [93]. This in general requires the exact knowledge of the incident field as well as of the field scattered by the object. Such demanding task is somehow alleviated when the characteristic dimensions of the scatterer are either much larger or much smaller of the wavelength of the impinging radiation.

In the former case, an accurate account of the momentum redistribution and transfer can be obtained using ray-tracing methods. On the other hand, when light interacts with Rayleigh scatterers, i.e. particles of dimensions much smaller than the wavelength of the incident radiation, a major simplification derives from the fact that the scattered field is essentially dipolar. The expression of the total force exerted on the particle is in this case amenable to the expression [89] given by:

$$\langle \mathbf{F} \rangle = \frac{1}{4}\alpha_r \nabla |\mathbf{E}|^2 + \frac{k_0 \alpha_i}{\varepsilon_0}\left[\frac{\langle \mathbf{S} \rangle}{c} + c\nabla \times \langle \mathbf{L}_S \rangle\right] \qquad (8.1)$$

Equation(8.1) represents the average force exerted by a monochromatic field of frequency $\omega = k_0 c$ on a dipolar scatterer of complex polarizability $\alpha = \alpha_r + i\,\alpha_i$. The imaginary part of the particle polarizability is simply related to the total cross section σ through $\sigma = k_0 \alpha_i / \varepsilon_0$. Notice that the expression of the force in the small particle limit depends only on the incident electromagnetic field at the interaction site. The first term in the force of Eq. (8.1)is commonly referred to as the gradient force. The second term, proportional to the average Poynting vector $\mathbf{S}$, represents the so called radiation pressure. Finally the last contribution is directly related to a non uniform spin angular momentum density of the electromagnetic field $\langle \mathbf{L}_S \rangle = (\varepsilon_0 / 4\omega i)\mathbf{E} \times \mathbf{E}^*$. We will refer to this term as spin force.

Structured illumination and polarization control offer important degrees of freedom in tailoring the behavior of optical forces which results in new and interesting phenomenology. In this chapter we would like to show that a combination of plane waves of appropriate polarization and coplanar propagation vectors can, quite surprisingly, lead to non conservative optical forces which are orthogonal to the power flow associated with each plane wave component.

To this end, let us consider the superposition of two plane waves with propagation vectors lying on the *xz* plane and forming an angle 2θ of as shown in Figure 21(a).

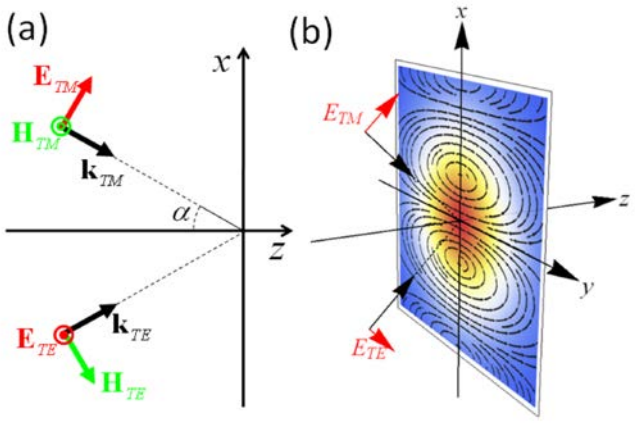

Figure 21. Plane wave superposition

With respect to this plane of incidence, the first plane wave is assumed to have its electric field along y (TE wave), while the other will have its magnetic field along y (TM wave). The TE electric field and the TM magnetic field are given respectively by:

$$\begin{aligned}\mathbf{E}_{TE} &= E_0 \exp\left[ik_0 \sin(\theta) x\right]\exp\left[ik_0 \cos(\theta) z\right]\hat{\mathbf{y}} \\ \mathbf{H}_{TM} &= H_0 \exp\left[-ik_0 \sin(\theta) x\right]\exp\left[ik_0 \cos(\theta) z\right]\hat{\mathbf{y}}\end{aligned} \qquad (8.2)$$

We further assume that $H_0 = E_0 / \eta$, where η is the vacuum characteristic impedance. Under these conditions both waves carry the same amount of power.

It is straightforward to show that such superposition of TE and TM waves, because of their orthogonal polarizations, does not lead to any interference when observed on a plane defined by a normal vector $\hat{\mathbf{n}}$ contained in the xz plane. The total power flow density is trivially given by the

superposition of the Poynting vectors associated with the two waves. A net power flow along z is therefore expected. Nevertheless such overly simple field distribution hides some rather counterintuitive characteristics which can be highlighted by considering the Poynting vector distribution:

$$\mathbf{S} = \left(\left| E_0 \right|^2 / \eta_0 \right) \left\{ \hat{\mathbf{z}} \cos(\theta) - \hat{\mathbf{y}} \sin(2\theta) \cos\left[2k_0 \sin(\theta) x \right] / 2 \right\} \quad (8.3)$$

As clear from (3) there is in fact a component of the Poynting vector directed along the transverse direction $\hat{\mathbf{y}}$ which arises from the mixing of the TE and the TM waves. If on one hand the interpretation of the z component of the Poynting vector as power flow is immediate and unambiguous, the meaning of the y component is less intuitive because of its anomalous features. There is in fact no wave propagation or phase accumulation in the y direction. Moreover, as equation (8.3) indicates, this transverse component of the Poynting vector is characterized by periodic reversals depending on the x coordinate. Notice that the same phenomenon occurs for finite size beams of appropriate polarization, as shown in Figure 1b for the case of two Gaussian beams. As the simulation clearly indicates the Poynting vector lines circulate in the transverse plane xy. For the ideal case of plane waves one can assume that the turning points of these lines of force occur at $|y| \to \infty$.

The first issue that we would like to address here is whether or not such transverse Poynting vector flow could be detected at all, by means of an optical force measurement for instance. To

this end we start by considering the optical forces exerted on a Rayleigh particle of polarizability $\alpha = \alpha_r + i\,\alpha_i$ illuminated by the fields(8.2). Since the superposition of these two plane waves does not lead to any interference, the gradient force is zero. Considering on the other hand the radiation force contribution one finds that:

$$\mathbf{F}_{RP} = \frac{k_0 \alpha_i}{\varepsilon_0} \frac{\langle \mathbf{S} \rangle}{c} = \hat{\mathbf{z}}\, \alpha_i E_0^2 k_0 \cos(\theta) + \\ -\hat{\mathbf{y}}\, \alpha_i \frac{E_0^2}{2} k_0 \sin(2\theta) \cos\left[2k_0 \sin(\theta)\, x\right] \qquad (8.4)$$

The spin force is given by:

$$\mathbf{F}_S = \hat{\mathbf{y}}\, \alpha_i \frac{E_0^2}{2} k_0 \sin(2\theta) \cos\left[2k_0 \sin(\theta)\, x\right] \qquad (8.5)$$

By comparing equations (8.4) and(8.5), it is apparent that for a Rayleigh particle the transverse radiation pressure is exactly compensated by the spin force. As a consequence the total force experienced by the particle is simply the superposition of the longitudinal components of the radiation pressure due to each incident plane wave. In other words, an electric dipole cannot detect the transverse Poynting vector associated with the plane wave combination(8.2). This is consistent with the symmetry with respect to y of the scattered radiation pattern shown in figure 22(a).

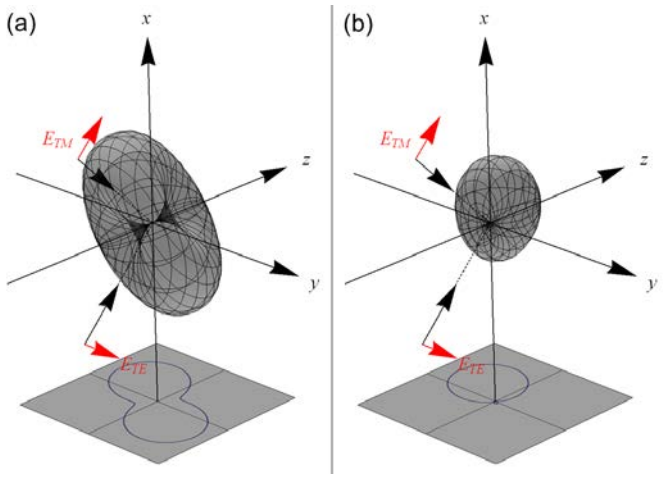

Figure 22. (a) Raileigh particle scattering. (b) Mie particle scattering.

From a heuristic point of view it is intuitive that if the scattered radiation pattern breaks the dipolar symmetry shown in figure 22(a), then the electromagnetic momentum redistribution would be uneven and could lead to a net mechanical momentum transfer along y. We will show that a sufficient condition to meet such requirement is that the scatterer is endowed with a magnetic polarizability γ in addition to an electric polarizability α.

Based On the results of chapter 8 it is straightforward to show that regardless of the number of scattering orders excited, neither the TE plane wave by itself, nor the TM wave by itself can exert an optical force in the y direction. When the waves are applied separately the optical force simply propels the particle along the direction of the corresponding wave-vector. The situation is completely different when both waves are applied as show in figure 21. In this case the force along the x direction assumes the following functional form:

$$F_x = E_{TE}^2 \sigma \sin\theta - E_{TM}^2 \sigma \sin\theta$$

Where E_{TE} and E_{TM} represent the amplitude of the electric fields associated with the TE and the TM wave respectively. The parameter σ depends in general on the size and permittivity of the sphere. Notice that when $E_{TE} = \pm E_{TM}$ the force along x vanishes as intuitively expected. The force along the z direction assumes the following form:

$$F_z = E_{TE}^2 \sigma \cos\theta + E_{TM}^2 \sigma \cos\theta$$

So as in the x case the two contributions add up "incoherently".

Completely different and counterintuitive is the behavior along y. when the particle shows both an electric and a magnetic polarizability. In this case the cooperative effects of the TE and TM wave lead to a non-vanishing contribution of the force along y, which depends only on the product $E_{TE} \times E_{TM} \sin(2\theta)$. The direction of the force is opposite to the y component of the Poynting vector. In other words, two otherwise non-interfering waves show a cooperative action as a consequence of their interaction with a scatterer displaying electric and magnetic polarizabilities.

APPENDIX A:
PUBLICATIONS

Chapter 2:

Alessandro Salandrino and Demetrios N. Christodoulides, "Airy plasmon: a nondiffracting surface wave," Opt. Lett. 35, 2082-2084 (2010).

A. Salandrino and D. N. Christodoulides, "Airy Plasmon: A Non-Diffracting Surface Wave," in Quantum Electronics and Laser Science Conference, OSA Technical Digest (CD) (Optical Society of America, 2010), paper QMD2.

Chapter 3:

Alessandro Salandrino and Demetrios N. Christodoulides, "Superresolution via enhanced evanescent tunneling," Opt. Lett. 36, 487-489 (2011)

Chapter 4:

Alessandro Salandrino and Demetrios N. Christodoulides, "Negative index Clarricoats-Waldron waveguides for terahertz and far infrared applications," Opt. Express 18, 3626-3631 (2010)

Chapter 5:

A.Salandrino, K. Makris, D.N. Christodoulides, Y. Lahini, Y. Silberberg, R. Morandotti, ” Analysis of a three-core adiabatic directional coupler ” , Optics Communications, 282 (23), p.4524-4526, Dec 2009

APPENDIX B:
SPHERICAL HARMONICS AND VECTOR SPHERICAL HARMONICS

Spherical harmonics are defined as:

$$Y_{n,m}(\theta,\phi)=\left(\frac{2n+1}{4\pi}\frac{(n-m)!}{(n+m)!}\right)^{\frac{1}{2}}\ P_n^m(\cos\theta)e^{im\phi}$$

Using the notation from Jackson, the vector spherical harmonics are defined as:

$$\mathbf{M}_{nm}(r,\theta,\phi)=z_n(kr)\mathbf{X}_{nm}(\theta,\phi)=\frac{z_n(kr)}{\sqrt{n(n+1)}}\mathbf{L}Y_{nm}(\theta,\phi)=\frac{z_n(kr)}{i\sqrt{n(n+1)}}\left[\mathbf{r}\times\nabla Y_{nm}(\theta,\phi)\right]=$$

$$=z_n(kr)\frac{1}{i}\sqrt{\frac{1}{4\pi}\ \frac{2n+1}{n(n+1)}\ \frac{(n-m)!}{(n+m)!}}\ \ \mathbf{r}\times\nabla\left[P_n^m(\cos\theta)e^{im\phi}\right]=$$

$$=\frac{1}{i}\sqrt{\frac{1}{4\pi}\ \frac{2n+1}{n(n+1)}\ \frac{(n-m)!}{(n+m)!}}\ \left[-\hat{\theta}\,z_n(kr)\frac{P_n^m(\cos\theta)}{\sin\theta}im+\hat{\boldsymbol{\varphi}}\,z_n(kr)\frac{dP_n^m(\cos\theta)}{d\theta}\right]e^{im\phi}=$$

$$=\sqrt{\frac{1}{4\pi}\ \frac{2n+1}{n(n+1)}\ \frac{(n-m)!}{(n+m)!}}\ \left[-\frac{m}{\sin\theta}\cos(m\phi)P_n^m(\cos\theta)z_n(kr)\hat{\theta}+\sin(m\phi)\frac{dP_n^m(\cos\theta)}{d\theta}z_n(kr)\hat{\boldsymbol{\varphi}}\right]+$$

$$i\sqrt{\frac{1}{4\pi}\ \frac{2n+1}{n(n+1)}\ \frac{(n-m)!}{(n+m)!}}\ \left[-\frac{m}{\sin\theta}\sin(m\phi)P_n^m(\cos\theta)z_n(kr)\hat{\theta}-\cos(m\phi)\frac{dP_n^m(\cos\theta)}{d\theta}z_n(kr)\hat{\boldsymbol{\varphi}}\right]=$$

$$=i\sqrt{\frac{1}{4\pi}\ \frac{2n+1}{n(n+1)}\ \frac{(n-m)!}{(n+m)!}}\left[\mathbf{M}_{emn}(r,\theta,\phi)+i\mathbf{M}_{omn}(r,\theta,\phi)\right]$$

$$\mathbf{N}_{nm}(r,\theta,\phi)=\frac{i}{k}\nabla\times\left[z_n(kr)\mathbf{X}_{nm}(\theta,\phi)\right]=$$
$$=-\left[\frac{1}{4\pi}\frac{2n+1}{n(n+1)}\frac{(n-m)!}{(n+m)!}\right]^{1/2}\left[\frac{\nabla\times\mathbf{M}_{emn}(r,\theta,\phi)}{k}+i\frac{\nabla\times\mathbf{M}_{omn}(r,\theta,\phi)}{k}\right]=$$
$$=-\left[\frac{1}{4\pi}\frac{2n+1}{n(n+1)}\frac{(n-m)!}{(n+m)!}\right]^{1/2}\left[\mathbf{N}_{emn}(r,\theta,\phi)+i\,\mathbf{N}_{omn}(r,\theta,\phi)\right]$$

These functions are related to the vector spherical harmonics from Bohren and Huffman:

$$\mathbf{M}_{emn}=-\frac{m}{\sin\theta}\sin(m\phi)P_n^m(\cos\theta)z_n(kr)\hat{\theta}-\cos(m\phi)\frac{dP_n^m(\cos\theta)}{d\theta}z_n(kr)\hat{\phi}$$
$$\mathbf{M}_{omn}=\frac{m}{\sin\theta}\cos(m\phi)P_n^m(\cos\theta)z_n(kr)\hat{\theta}-\sin(m\phi)\frac{dP_n^m(\cos\theta)}{d\theta}z_n(kr)\hat{\phi}$$
$$\mathbf{N}_{emn}=\frac{z_n(kr)}{kr}\cos(m\phi)n(n+1)P_n^m(\cos\theta)\hat{r}+\cos(m\phi)\frac{dP_n^m(\cos\theta)}{d\theta}\frac{1}{kr}\frac{d}{d(kr)}\left[kr\,z_n(kr)\right]\hat{\theta}+$$
$$-m\sin(m\phi)\frac{P_n^m(\cos\theta)}{\sin\theta}\frac{1}{kr}\frac{d}{d(kr)}\left[kr\,z_n(kr)\right]\hat{\phi}$$
$$\mathbf{N}_{omn}=\frac{z_n(\rho)}{\rho}\sin(m\phi)n(n+1)P_n^m(\cos\theta)\hat{r}+\sin(m\phi)\frac{dP_n^m(\cos\theta)}{d\theta}\frac{1}{kr}\frac{d}{d(kr)}\left[kr\,z_n(kr)\right]\hat{\theta}+$$
$$+m\cos(m\phi)\frac{P_n^m(\cos\theta)}{\sin\theta}\frac{1}{kr}\frac{d}{d(kr)}\left[kr\,z_n(kr)\right]\hat{\phi}$$

The electromagnetic field can be in general expanded as follows:

$$\mathbf{E} = E_0 \sum_{n=1}^{\infty} \sum_{m=-n}^{n} \left\{ a_E(n,m) \frac{i}{k} \nabla \times \left[z_n(kr) \mathbf{X}_{nm}(\theta,\phi) \right] + a_M(n,m) z_n(kr) \mathbf{X}_{nm}(\theta,\phi) \right\}$$

$$\mathbf{H} = \frac{E_0}{\eta_0} \sum_{n=1}^{\infty} \sum_{m=-n}^{n} \left\{ a_E(n,m) z_n(kr) \mathbf{X}_{nm}(\theta,\phi) - a_M(n,m) \frac{i}{k} \nabla \times \left[z_n(kr) \mathbf{X}_{nm}(\theta,\phi) \right] \right\}$$

APPENDIX C:
GENERAL PLANE-WAVE EXPANSION

We consider an electric field given by:

$$\begin{aligned}
&\mathbf{E} = \mathbf{E}_0 e^{i\mathbf{k}\cdot\mathbf{r}} = \hat{\mathbf{e}}\, E_0\, e^{i\mathbf{k}\cdot\mathbf{r}} \\
&\mathbf{k} = k_0\hat{\mathbf{k}} = k_0\left(\hat{\mathbf{x}}\sin\theta_i\cos\phi_i + \hat{\mathbf{y}}\sin\theta_i\sin\phi_i + \hat{\mathbf{z}}\cos\theta_i\right) \\
&\hat{\mathbf{k}}\cdot\hat{\mathbf{e}} = 0 \\
&\hat{\mathbf{e}} = \hat{\mathbf{x}}\, e_x + \hat{\mathbf{y}}\, e_y + \hat{\mathbf{z}}\left[1-\left(e_x^2 + e_y^2\right)\right]^{1/2}
\end{aligned} \qquad \text{(C.1)}$$

where $\hat{\mathbf{e}}$ is the unit vector parallel to the electric field. The corresponding magnetic field is given by:

$$\begin{aligned}
&\mathbf{H} = \mathbf{H}_0 e^{i\mathbf{k}\cdot\mathbf{r}} = \hat{\mathbf{h}}\frac{E_0}{\eta_0} e^{i\mathbf{k}\cdot\mathbf{r}} \\
&\hat{\mathbf{h}} = \hat{\mathbf{k}}\times\hat{\mathbf{e}} \\
&h_x = \left(\sin\theta_i\sin\phi_i\right)e_z - \left(\cos\theta_i\right)e_y \qquad \text{(C.2)} \\
&h_y = -\left(\sin\theta_i\cos\phi_i\right)e_z + \left(\cos\theta_i\right)e_x \\
&h_x = \left(\sin\theta_i\cos\phi_i\right)e_y - \left(\sin\theta_i\sin\phi_i\right)e_x
\end{aligned}$$

The exponential can be expanded as follows:

$$\begin{aligned}
&e^{i\mathbf{k}\cdot\mathbf{r}} = e^{ik\sin(\theta_i)\cos(\phi_i)r\sin(\theta)\cos(\phi)+ik\sin(\theta_i)\sin(\phi_i)r\sin(\theta)\sin(\phi)+ik\cos(\theta_i)r\cos(\theta)} = \\
&= 4\pi\sum_{n=0}^{\infty}\sum_{m=-n}^{n} i^n j_n\left(k\,r\right)Y_{nm}^{*}\left(\theta,\phi\right)Y_{nm}\left(\theta_i,\phi_i\right)
\end{aligned} \qquad \text{(C.3)}$$

Using (B.10), (C.1) and (C.3) we can write:

$$\hat{\mathbf{e}}\,4\pi\sum_{n=0}^{\infty}\sum_{m=-n}^{n} i^n j_n\left(k\,r\right)Y_{nm}^{*}\left(\theta,\phi\right)Y_{nm}\left(\theta_i,\phi_i\right)=$$
$$\sum_{n=1}^{\infty}\sum_{m=-n}^{n}\left\{a_E\left(n,m\right)\frac{i}{k}\nabla\times\left[z_n\left(k\,r\right)\mathbf{X}_{nm}\left(\theta,\phi\right)\right]+a_M\left(n,m\right)z_n\left(k\,r\right)\mathbf{X}_{nm}\left(\theta,\phi\right)\right\} \tag{C.4}$$

And using (B.10), (C.2) and (C.3) we have:

$$\hat{\mathbf{h}}\,4\pi\sum_{n=0}^{\infty}\sum_{m=-n}^{n} i^n j_n\left(k\,r\right)Y_{nm}^{*}\left(\theta,\phi\right)Y_{nm}\left(\theta_i,\phi_i\right)=$$
$$=\sum_{n=1}^{\infty}\sum_{m=-n}^{n}\left\{a_E\left(n,m\right)z_n\left(k\,r\right)\mathbf{X}_{nm}\left(\theta,\phi\right)-a_M\left(n,m\right)\frac{i}{k}\nabla\times\left[z_n\left(k\,r\right)\mathbf{X}_{nm}\left(\theta,\phi\right)\right]\right\} \tag{C.5}$$

The expansion coefficients can be found by using the orthogonality properties of the vector spherical harmonics:

$$a_M\left(n_1,m_1\right)z_{n_1}\left(k\,r\right)=4\pi\int_0^{2\pi}\int_0^{\pi}\left[\mathbf{X}_{n_1m_1}^{*}\left(\theta,\phi\right)\cdot\hat{\mathbf{e}}\sum_{n=0}^{\infty}\sum_{m=-n}^{n} i^n j_n\left(k\,r\right)Y_{nm}^{*}\left(\theta,\phi\right)Y_{nm}\left(\theta_i,\phi_i\right)\right]\sin\left(\theta\right)d\theta d\phi \tag{C.6}$$

$$a_E\left(n_1,m_1\right)z_{n_1}\left(k\,r\right)=4\pi\int_0^{\pi}\int_0^{2\pi}\left[\mathbf{X}_{n_1m_1}^{*}\left(\theta,\phi\right)\cdot\hat{\mathbf{h}}\sum_{n=0}^{\infty}\sum_{m=-n}^{n} i^n j_n\left(k\,r\right)Y_{nm}^{*}\left(\theta,\phi\right)Y_{nm}\left(\theta_i,\phi_i\right)\right]\sin\left(\theta\right)d\phi\,d\theta \tag{C.7}$$

We use now the definition (B.7) to write:

$$\mathbf{X}^*_{n_1 m_1}(\theta,\phi) = \frac{\mathbf{L}^* Y^*_{n_1 m_1}(\theta,\phi)}{\sqrt{n_1(n_1+1)}} \qquad \text{(C.8)}$$

The angular momentum operator is written in terms of its components:

$$\begin{aligned}
\mathbf{L} &= \frac{1}{i}(\mathbf{r}\times\nabla) = \hat{\mathbf{x}}L_x + \hat{\mathbf{y}}L_y + \hat{\mathbf{z}}L_z = \hat{\mathbf{x}}\left(\frac{L_+ + L_-}{2}\right) + \hat{\mathbf{y}}\left(\frac{L_+ - L_-}{2i}\right) + \hat{\mathbf{z}}L_z \\
\mathbf{L}^* &= -\frac{1}{i}(\mathbf{r}\times\nabla) = \hat{\mathbf{x}}L^*_x + \hat{\mathbf{y}}L^*_y + \hat{\mathbf{z}}L^*_z = \hat{\mathbf{x}}\left(\frac{L^*_+ + L^*_-}{2}\right) + \hat{\mathbf{y}}\left(\frac{L^*_- - L^*_+}{2i}\right) + \hat{\mathbf{z}}L^*_z
\end{aligned} \qquad \text{(C.9)}$$

With the following definitions:

$$\begin{cases}
L_+ = e^{i\phi}\left(\dfrac{\partial}{\partial\theta} + i\cot\theta\dfrac{\partial}{\partial\phi}\right) \\
L_- = e^{-i\phi}\left(-\dfrac{\partial}{\partial\theta} + i\cot\theta\dfrac{\partial}{\partial\phi}\right) \\
L_z = -i\dfrac{\partial}{\partial\phi}
\end{cases}
\quad
\begin{cases}
L^*_+ = e^{-i\phi}\left(\dfrac{\partial}{\partial\theta} - i\cot\theta\dfrac{\partial}{\partial\phi}\right) = -L_- \\
L^*_- = e^{i\phi}\left(-\dfrac{\partial}{\partial\theta} - i\cot\theta\dfrac{\partial}{\partial\phi}\right) = -L_+ \\
L^*_z = i\dfrac{\partial}{\partial\phi} = -L_z
\end{cases} \qquad \text{(C.10)}$$

The operators (C.10) act on the spherical harmonics as follows:

$$\begin{cases}
L_+ Y_{nm} = \sqrt{(n-m)(n+m+1)}\,Y_{n,m+1} \\
L_- Y_{nm} = \sqrt{(n+m)(n-m+1)}\,Y_{n,m-1} \\
L_z Y_{nm} = mY_{nm}
\end{cases} \qquad \text{(C.11)}$$

$$\begin{cases} L_+^* Y_{nm}^* = (-1)^m L_+^* Y_{n,-m} = -(-1)^m L_- Y_{n,-m} = \\ = (-1)^{m+1} (n-m)^{\frac{1}{2}} (n+m+1)^{\frac{1}{2}} Y_{n,-(m+1)} = (n-m)^{\frac{1}{2}} (n+m+1)^{\frac{1}{2}} Y_{n,(m+1)}^* \\ L_-^* Y_{nm}^* = (-1)^m L_-^* Y_{n,-m} = -(-1)^m L_+ Y_{n,-m} = \\ = (-1)^{m-1} (n+m)^{\frac{1}{2}} (n-m+1)^{\frac{1}{2}} Y_{n,-(m-1)} = (n+m)^{\frac{1}{2}} (n-m+1)^{\frac{1}{2}} Y_{n,(m-1)}^* \\ L_z^* Y_{nm}^* = (-1)^m L_z^* Y_{n,-m} = -(-1)^m L_z Y_{n,-m} = m(-1)^m Y_{n,-m} = m Y_{nm}^* \end{cases} \quad \text{(C.12)}$$

Using the definition (C.8), we write (C.6) as follows:

$$\begin{aligned} & a_M(n_1, m_1) z_{n_1}(kr) = \\ & = 4\pi \int_0^{2\pi} \int_0^{\pi} \left[\mathbf{X}_{n_1 m_1}^*(\theta,\phi) \cdot \hat{\mathbf{e}} \sum_{n=0}^{\infty} \sum_{m=-n}^{n} i^n j_n(kr) Y_{nm}(\theta,\phi) Y_{nm}^*(\theta_i,\phi_i) \right] \sin(\theta)\, d\theta d\phi = \\ & = 4\pi \int_0^{2\pi} \int_0^{\pi} \left[\frac{\mathbf{L}^* Y_{n_1 m_1}^*(\theta,\phi)}{\sqrt{n_1(n_1+1)}} \cdot \hat{\mathbf{e}} \sum_{n=0}^{\infty} \sum_{m=-n}^{n} i^n j_n(kr) Y_{nm}(\theta,\phi) Y_{nm}^*(\theta_i,\phi_i) \right] \sin(\theta)\, d\theta d\phi = \\ & = 4\pi \sum_{n=0}^{\infty} \sum_{m=-n}^{n} i^n j_n(kr) Y_{nm}^*(\theta_i,\phi_i) \frac{e_x}{2} \int_0^{2\pi} \int_0^{\pi} \frac{\left(L_+^* + L_-^*\right) Y_{n_1 m_1}^*(\theta,\phi)}{\sqrt{n_1(n_1+1)}} Y_{nm}(\theta,\phi) \sin(\theta)\, d\theta d\phi + \\ & + 4\pi \sum_{n=0}^{\infty} \sum_{m=-n}^{n} i^n j_n(kr) Y_{nm}^*(\theta_i,\phi_i) \frac{e_y}{2i} \int_0^{2\pi} \int_0^{\pi} \frac{\left(L_-^* - L_+^*\right) Y_{n_1 m_1}^*(\theta,\phi)}{\sqrt{n_1(n_1+1)}} Y_{nm}(\theta,\phi) \sin(\theta)\, d\theta d\phi + \\ & + 4\pi \sum_{n=0}^{\infty} \sum_{m=-n}^{n} i^n j_n(kr) Y_{nm}^*(\theta_i,\phi_i) e_z \int_0^{2\pi} \int_0^{\pi} \frac{L_z^* Y_{n_1 m_1}^*(\theta,\phi)}{\sqrt{n_1(n_1+1)}} Y_{nm}(\theta,\phi) \sin(\theta)\, d\theta d\phi \end{aligned}$$

(C.13)

Using the properties (C.12) we obtain:

$$
\begin{aligned}
&a_M\left(n_1,m_1\right)z_{n_1}\left(k\,r\right)=\\
&=-4\pi\sum_{n=0}^{\infty}\sum_{m=-n}^{n}i^n\,j_n\left(k\,r\right)Y_{nm}^{*}\left(\theta_i,\phi_i\right)\frac{e_x}{2\sqrt{n_1\left(n_1+1\right)}}\times\\
&\times\int_0^{2\pi}\int_0^{\pi}\left(\sqrt{\left(n_1-m_1\right)\left(n_1+m_1+1\right)}\,Y_{n_1,\left(m_1+1\right)}^{*}\left(\theta,\phi\right)+\sqrt{\left(n_1+m_1\right)\left(n_1-m_1+1\right)}\,Y_{n_1,\left(m_1-1\right)}^{*}\left(\theta,\phi\right)\right)Y_{nm}\left(\theta,\phi\right)\sin\left(\theta\right)d\theta d\phi+\\
&-4\pi\sum_{n=0}^{\infty}\sum_{m=-n}^{n}i^n\,j_n\left(k\,r\right)Y_{nm}^{*}\left(\theta_i,\phi_i\right)\frac{e_y}{2i\sqrt{n_1\left(n_1+1\right)}}\times\\
&\times\int_0^{2\pi}\int_0^{\pi}\left(\sqrt{\left(n_1+m_1\right)\left(n_1-m_1+1\right)}\,Y_{n_1,\left(m_1-1\right)}^{*}\left(\theta,\phi\right)-\sqrt{\left(n_1-m_1\right)\left(n_1+m_1+1\right)}\,Y_{n_1,\left(m_1+1\right)}^{*}\left(\theta,\phi\right)\right)Y_{nm}\left(\theta,\phi\right)\sin\left(\theta\right)d\theta d\phi\\
&-4\pi\sum_{n=0}^{\infty}\sum_{m=-n}^{n}i^n\,j_n\left(k\,r\right)Y_{nm}^{*}\left(\theta_i,\phi_i\right)\frac{e_z}{\sqrt{n_1\left(n_1+1\right)}}m_1\int_0^{2\pi}\int_0^{\pi}Y_{n_1,m_1}^{*}\left(\theta,\phi\right)Y_{nm}\left(\theta,\phi\right)\sin\left(\theta\right)d\theta d\phi
\end{aligned}
\tag{C.14}
$$

And finally using the orthogonality relations of spherical harmonics we can write (C.14) as:

$$
\begin{aligned}
&a_M\left(n_1,m_1\right)=\\
&=4\pi i^{n_1}Y_{n_1,m_1+1}^{*}\left(\theta_i,\phi_i\right)\sqrt{\frac{\left(n_1-m_1\right)\left(n_1+m_1+1\right)}{n_1\left(n_1+1\right)}}\left(\frac{e_x+ie_y}{2}\right)+\\
&+4\pi i^{n_1}Y_{n_1,m_1-1}^{*}\left(\theta_i,\phi_i\right)\sqrt{\frac{\left(n_1+m_1\right)\left(n_1-m_1+1\right)}{n_1\left(n_1+1\right)}}\left(\frac{e_x-ie_y}{2}\right)+\\
&+4\pi\frac{i^{n_1}m_1Y_{n_1m_1}^{*}\left(\theta_i,\phi_i\right)}{\sqrt{n_1\left(n_1+1\right)}}e_z
\end{aligned}
\tag{C.15}
$$

In a similar fashion we obtain:

$$
\begin{aligned}
&a_E\left(n_1,m_1\right)= \\
&=4\pi i^{n_1}Y^*_{n_1,m_1+1}\left(\theta_i,\phi_i\right)\left[\frac{\left(n_1-m_1\right)\left(n_1+m_1+1\right)}{n_1\left(n_1+1\right)}\right]^{1/2}\left(\frac{h_x+ih_y}{2}\right)+ \\
&+4\pi i^{n_1}Y^*_{n_1,m_1-1}\left(\theta_i,\phi_i\right)\left[\frac{\left(n_1+m_1\right)\left(n_1-m_1+1\right)}{n_1\left(n_1+1\right)}\right]^{1/2}\left(\frac{h_x-ih_y}{2}\right)+ \\
&+4\pi\frac{i^{n_1}m_1Y^*_{n_1m_1}\left(\theta_i,\phi_i\right)}{\left[n_1\left(n_1+1\right)\right]^{1/2}}h_z
\end{aligned}
\qquad \text{(C.16)}
$$

And the complete expression for the plane wave is:

$$
\begin{aligned}
\mathbf{E}&=E_0\sum_{n=1}^{\infty}\sum_{m=-n}^{n}\left\{a_E\left(n,m\right)\frac{i}{k}\nabla\times\left[j_n\left(kr\right)\mathbf{X}_{nm}\left(\theta,\phi\right)\right]+a_M\left(n,m\right)j_n\left(kr\right)\mathbf{X}_{nm}\left(\theta,\phi\right)\right\} \\
\mathbf{H}&=\frac{E_0}{\eta_0}\sum_{n=1}^{\infty}\sum_{m=-n}^{n}\left\{a_E\left(n,m\right)j_n\left(kr\right)\mathbf{X}_{nm}\left(\theta,\phi\right)-a_M\left(n,m\right)\frac{i}{k}\nabla\times\left[j_n\left(kr\right)\mathbf{X}_{nm}\left(\theta,\phi\right)\right]\right\}
\end{aligned}
\qquad \text{(C.17)}
$$

In terms of the functions $\mathbf{M}$ and $\mathbf{N}$ we have:

$$
\begin{aligned}
\mathbf{E}&=E_0\sum_{n=1}^{\infty}\sum_{m=-n}^{n}\sqrt{\frac{1}{4\pi}\frac{2n+1}{n\left(n+1\right)}\frac{\left(n-m\right)!}{\left(n+m\right)!}}\left[-a_E\left(n,m\right)\left(\mathbf{N}_{emn}+i\,\mathbf{N}_{omn}\right)+a_M\left(n,m\right)\left(i\mathbf{M}_{emn}-\mathbf{M}_{omn}\right)\right] \\
\mathbf{H}&=\frac{E_0}{\eta_0}\sum_{n=1}^{\infty}\sum_{m=-n}^{n}\sqrt{\frac{1}{4\pi}\frac{2n+1}{n\left(n+1\right)}\frac{\left(n-m\right)!}{\left(n+m\right)!}}\left[a_E\left(n,m\right)\left(i\mathbf{M}_{emn}-\mathbf{M}_{omn}\right)+a_M\left(n,m\right)\left(\mathbf{N}_{emn}+i\,\mathbf{N}_{omn}\right)\right]
\end{aligned}
\qquad \text{(C.18)}
$$

The expression (C.18) can be put in the following form containing only positive values of the order m:

$$\mathbf{E} = E_0 \sum_{n=1}^{\infty} \sum_{m=-n}^{n} \sqrt{\frac{1}{4\pi} \frac{2n+1}{n(n+1)} \frac{(n-m)!}{(n+m)!}} \left[-a_E(n,m)\left(\mathbf{N}_{emn} + i\,\mathbf{N}_{omn}\right) + a_M(n,m)\left(i\mathbf{M}_{emn} - \mathbf{M}_{omn}\right) \right] =$$

$$= E_0 \sum_{n=1}^{\infty} \sqrt{\frac{1}{4\pi} \frac{2n+1}{n(n+1)}} \left[-a_E(n,0)\left(\mathbf{N}_{e0n} + i\,\mathbf{N}_{o0n}\right) + a_M(n,0)\left(i\mathbf{M}_{e0n} - \mathbf{M}_{o0n}\right) \right] +$$

$$+ E_0 \sum_{n=1}^{\infty} \sum_{m=0}^{n} \sqrt{\frac{1}{4\pi} \frac{2n+1}{n(n+1)} \frac{(n-m)!}{(n+m)!}} \left[-a_E(n,m)\left(\mathbf{N}_{emn} + i\,\mathbf{N}_{omn}\right) + a_M(n,m)\left(i\mathbf{M}_{emn} - \mathbf{M}_{omn}\right) \right] +$$

$$E_0 \sum_{n=1}^{\infty} \sum_{m=1}^{n} \sqrt{\frac{1}{4\pi} \frac{2n+1}{n(n+1)} \frac{(n+m)!}{(n-m)!}} \left[-a_E(n,-m)\left(\mathbf{N}_{e(-m)n} + i\,\mathbf{N}_{o(-m)n}\right) + a_M(n,-m)\left(i\mathbf{M}_{e(-m)n} - \mathbf{M}_{o(-m)n}\right) \right]$$

(C.19)

Using the parity properties of the spherical harmonics with respect to the order, the expression (C.19) becomes:

$$\mathbf{E} = E_0 \sum_{n=1}^{\infty}\sum_{m=1}^{n} \sqrt{\frac{1}{4\pi}\,\frac{2n+1}{n(n+1)}\,\frac{(n-m)!}{(n+m)!}} \Big[-a_E(n,m)\left(\mathbf{N}_{emn} + i\,\mathbf{N}_{omn}\right) + a_M(n,m)\left(i\mathbf{M}_{emn} - \mathbf{M}_{omn}\right)\Big] +$$

$$E_0 \sum_{n=1}^{\infty}\sum_{m=1}^{n} \sqrt{\frac{1}{4\pi}\,\frac{2n+1}{n(n+1)}\,\frac{(n+m)!}{(n-m)!}} \Big[-a_E(n,-m)\left(\mathbf{N}_{e(-m)n} + i\,\mathbf{N}_{o(-m)n}\right) + a_M(n,-m)\left(i\mathbf{M}_{e(-m)n} - \mathbf{M}_{o(-m)n}\right)\Big]$$

$$= E_0 \sum_{n=1}^{\infty}\sum_{m=1}^{n} \sqrt{\frac{1}{4\pi}\,\frac{2n+1}{n(n+1)}\,\frac{(n-m)!}{(n+m)!}} \Big[-a_E(n,m)\left(\mathbf{N}_{emn} + i\,\mathbf{N}_{omn}\right) + a_M(n,m)\left(i\mathbf{M}_{emn} - \mathbf{M}_{omn}\right)\Big] +$$

$$E_0 \sum_{n=1}^{\infty}\sum_{m=1}^{n} \sqrt{\frac{1}{4\pi}\,\frac{2n+1}{n(n+1)}\,\frac{(n-m)!}{(n+m)!}} \Big[-a_E^*(n,m)\left(\mathbf{N}_{emn} - i\,\mathbf{N}_{omn}\right) + a_M^*(n,m)\left(i\mathbf{M}_{emn} + \mathbf{M}_{omn}\right)\Big] =$$

$$= E_0 \sum_{n=1}^{\infty}\sum_{m=1}^{n} \sqrt{\frac{1}{4\pi}\,\frac{2n+1}{n(n+1)}\,\frac{(n-m)!}{(n+m)!}} \times$$

$$\times \left[\begin{Bmatrix} -\left[a_E(n,m) - (-1)^n a_E^*(n,m)\right]\mathbf{N}_{emn} - \left[a_M(n,m) + (-1)^n a_M^*(n,m)\right]\mathbf{M}_{omn} + \\ -i\left[a_E(n,m) + (-1)^n a_E^*(n,m)\right]\mathbf{N}_{omn} + i\left[a_M(n,m) - (-1)^n a_M^*(n,m)\right]\mathbf{M}_{emn} \end{Bmatrix} \right] \tag{C.20}$$

In order to match the Bohren & Huffman notation we define the following coefficients:

$$\begin{aligned}
A_e(n,m) &= -\left[\frac{1}{4\pi}\,\frac{2n+1}{n(n+1)}\,\frac{(n-m)!}{(n+m)!}\right]^{1/2}\left[a_E(n,m) - (-1)^n a_E^*(n,m)\right] \\
B_o(n,m) &= -\left[\frac{1}{4\pi}\,\frac{2n+1}{n(n+1)}\,\frac{(n-m)!}{(n+m)!}\right]^{1/2}\left[a_M(n,m) + (-1)^n a_M^*(n,m)\right] \\
A_o(n,m) &= -\left[\frac{1}{4\pi}\,\frac{2n+1}{n(n+1)}\,\frac{(n-m)!}{(n+m)!}\right]^{1/2} i\left[a_E(n,m) + (-1)^n a_E^*(n,m)\right] \\
B_e(n,m) &= i\left[\frac{1}{4\pi}\,\frac{2n+1}{n(n+1)}\,\frac{(n-m)!}{(n+m)!}\right]^{1/2}\left[a_M(n,m) - (-1)^n a_M^*(n,m)\right]
\end{aligned} \tag{C.21}$$

So eventually we obtain the expansion:

$$\begin{aligned}\mathbf{E} &= E_0 \sum_{n=1}^{\infty} \sum_{m=1}^{n} \left[A_e(n,m)\mathbf{N}_{emn} + B_o(n,m)\mathbf{M}_{omn} + A_o(n,m)\mathbf{N}_{omn} + B_e(n,m)\mathbf{M}_{emn} \right] \\ \mathbf{H} &= \frac{E_0}{i\eta_0} \sum_{n=1}^{\infty} \sum_{m=1}^{n} \left[A_e(n,m)\mathbf{M}_{emn} + B_o(n,m)\mathbf{N}_{omn} + A_o(n,m)\mathbf{M}_{omn} + B_e(n,m)\mathbf{N}_{emn} \right]\end{aligned} \tag{C.22}$$

APPENDIX D: STRESS TENSOR INTEGRALS

In the following we report the analytical expressions of the integrals involved in the computation of optical forces.

Integrals of the dot product $\mathbf{N}_{em_1n_1} \cdot \mathbf{N}^*_{em_2n_2}$:

$$\oint_S \left(\mathbf{N}_{em_1n_1} \cdot \mathbf{N}^*_{em_2n_2}\right)\left(\hat{\mathbf{r}} \cdot \hat{\mathbf{x}}\right) dS =$$
$$= \left(1+\delta_{m_1 0}+\delta_{0m_2}\right)\left[\begin{array}{l} -\delta_{n_1(n_2+1)}\delta_{m_1(m_2+1)}\dfrac{(n_1+m_1)!}{4n_1(n_1-m_1)!}+\delta_{n_1(n_2+1)}\delta_{m_1(m_2-1)}\dfrac{(n_2+m_2)!}{4n_1(n_2-m_2)!}+ \\ +\delta_{n_2(n_1+1)}\delta_{m_1(m_2+1)}\dfrac{(n_1+m_1)!}{4n_2(n_1-m_1)!}-\delta_{n_2(n_1+1)}\delta_{m_1(m_2-1)}\dfrac{(n_2+m_2)!}{4n_1(n_2-m_2)!} \end{array}\right]\times$$
$$\times \oint_S \left(\mathbf{N}_{e0n_1} \cdot \mathbf{N}^*_{e0n_2}\right)\left(\hat{\mathbf{r}} \cdot \hat{\mathbf{z}}\right) dS =$$

$$\oint_S \left(\mathbf{N}_{em_1n_1} \cdot \mathbf{N}^*_{em_2n_2}\right)\left(\hat{\mathbf{r}} \cdot \hat{\mathbf{y}}\right) dS = 0$$

$$\oint_S \left(\mathbf{N}_{em_1n_1} \cdot \mathbf{N}^*_{em_2n_2}\right)\left(\hat{\mathbf{r}} \cdot \hat{\mathbf{z}}\right) dS =$$
$$= \frac{\pi\,\delta_{m_1m_2}}{k_0^2} z_{n_1}\left(k_0 r\right) z^*_{n_2}\left(k_0 r\right)\times\left(\delta_{m_1m_2}+\delta_{m_1 0}\delta_{0m_2}\right)\times$$
$$\times\left[\frac{2n_1\left(1+n_1\right)^2\left(n_1+2\right)\left(n_1+m_1+1\right)}{\left(2n_1+1\right)\left(2n_1+3\right)}\frac{(n_1+m_1)!}{(n_1-m_1)!}\delta_{(n_1+1)n_2}+\frac{2n_1^2\left(n_1^2-1\right)\left(n_1-m_1\right)}{\left(2n_1+1\right)\left(2n_1-1\right)}\frac{(n_1+m_1)!}{(n_1-m_1)!}\delta_{(n_1-1)n_2}\right]+$$
$$+\frac{\pi\,\delta_{m_1m_2}}{k_0^2}\frac{d}{d\left(k_0 r\right)}\left[k_0 r\, z_{n_1}\left(k_0 r\right)\right]\frac{d}{d\left(k_0 r\right)}\left[k_0 r\, z^*_{n_2}\left(k_0 r\right)\right]\times\left(\delta_{m_1m_2}+\delta_{m_1 0}\delta_{0m_2}\right)\times$$
$$\times\left[\frac{2n_1\left(n_1+2\right)\left(n_1+m_1+1\right)}{\left(2n_1+3\right)\left(2n_1+1\right)}\frac{(n_1+m_1)!}{(n_1-m_1)!}\delta_{(n_1+1)n_2}+\frac{2\left(n_1^2-1\right)\left(n_1-m_1\right)}{\left(2n_1+1\right)\left(2n_1-1\right)}\frac{(n_1+m_1)!}{(n_1-m_1)!}\delta_{(n_1-1)n_2}\right]$$

Integrals of the dot product $\mathbf{N}_{om_1n_1} \cdot \mathbf{N}^*_{om_2n_2}$:

$$\oint_S \left(\mathbf{N}_{om_1n_1} \cdot \mathbf{N}^*_{om_2n_2}\right)\left(\hat{\mathbf{r}} \cdot \hat{\mathbf{x}}\right) dS =$$

$$= \left(1 - \delta_{m_1 0} - \delta_{0 m_2}\right) \left[\begin{array}{l} -\delta_{n_1(n_2+1)}\delta_{m_1(m_2+1)} \dfrac{(n_1+m_1)!}{4n_1(n_1-m_1)!} + \delta_{n_1(n_2+1)}\delta_{m_1(m_2-1)} \dfrac{(n_2+m_2)!}{4n_1(n_2-m_2)!} + \\ +\delta_{n_2(n_1+1)}\delta_{m_1(m_2+1)} \dfrac{(n_1+m_1)!}{4n_2(n_1-m_1)!} - \delta_{n_2(n_1+1)}\delta_{m_1(m_2-1)} \dfrac{(n_2+m_2)!}{4n_1(n_2-m_2)!} \end{array}\right] \times$$

$$\times \oint_S \left(\mathbf{N}_{e0n_1} \cdot \mathbf{N}^*_{e0n_2}\right)\left(\hat{\mathbf{r}} \cdot \hat{\mathbf{z}}\right) dS =$$

$$\oint_S \left(\mathbf{N}_{om_1n_1} \cdot \mathbf{N}^*_{om_2n_2}\right)\left(\hat{\mathbf{r}} \cdot \hat{\mathbf{y}}\right) dS = 0$$

$$\oint_S \left(\mathbf{N}_{om_1n_1} \cdot \mathbf{N}^*_{om_2n_2}\right)\left(\hat{\mathbf{r}} \cdot \hat{\mathbf{z}}\right) dS =$$

$$= \frac{\pi \delta_{m_1 m_2}}{k_0^2} z_{n_1}\left(k_0 r\right) z^*_{n_2}\left(k_0 r\right) \times \left(\delta_{m_1 m_2} - \delta_{m_1 0}\delta_{0 m_2}\right) \times$$

$$\times \left[\frac{2n_1(1+n_1)^2(n_1+2)(n_1+m_1+1)}{(2n_1+1)(2n_1+3)} \frac{(n_1+m_1)!}{(n_1-m_1)!} \delta_{(n_1+1)n_2} + \frac{2n_1^2(n_1^2-1)(n_1-m_1)}{(2n_1+1)(2n_1-1)} \frac{(n_1+m_1)!}{(n_1-m_1)!} \delta_{(n_1-1)n_2}\right] +$$

$$+ \frac{\pi \delta_{m_1 m_2}}{k_0^2} \frac{d}{d\left(k_0 r\right)}\left[k_0 r\, z_{n_1}\left(k_0 r\right)\right] \frac{d}{d\left(k_0 r\right)}\left[k_0 r\, z^*_{n_2}\left(k_0 r\right)\right] \times \left(\delta_{m_1 m_2} - \delta_{m_1 0}\delta_{0 m_2}\right) \times$$

$$\times \left[\frac{2n_1(n_1+2)(n_1+m_1+1)}{(2n_1+3)(2n_1+1)} \frac{(n_1+m_1)!}{(n_1-m_1)!} \delta_{(n_1+1)n_2} + \frac{2(n_1^2-1)(n_1-m_1)}{(2n_1+1)(2n_1-1)} \frac{(n_1+m_1)!}{(n_1-m_1)!} \delta_{(n_1-1)n_2}\right]$$

Integrals of the dot product $\mathbf{N}_{em_1n_1} \cdot \mathbf{N}^*_{om_2n_2}$:

$$\oint_S \left(\mathbf{N}_{em_1n_1} \cdot \mathbf{N}^*_{om_2n_2}\right)\left(\hat{\mathbf{r}} \cdot \hat{\mathbf{x}}\right) dS = 0$$

$$\begin{aligned}
&\oint_S \left(\mathbf{N}_{em_1n_1} \cdot \mathbf{N}^*_{om_2n_2}\right)\left(\hat{\mathbf{r}} \cdot \hat{\mathbf{y}}\right) dS = \\
&= \left(1 + \delta_{m_1 0} - \delta_{0m_2}\right)\left[\begin{array}{l}
\delta_{n_1(n_2+1)}\delta_{m_1(m_2+1)} \dfrac{(n_1+m_1)!}{4n_1(n_1-m_1)!} + \delta_{n_1(n_2+1)}\delta_{m_1(m_2-1)} \dfrac{(n_2+m_2)!}{4n_1(n_2-m_2)!} + \\
-\delta_{n_2(n_1+1)}\delta_{m_1(m_2+1)} \dfrac{(n_1+m_1)!}{4n_2(n_1-m_1)!} - \delta_{n_2(n_1+1)}\delta_{m_1(m_2-1)} \dfrac{(n_2+m_2)!}{4n_2(n_2-m_2)!}
\end{array}\right] \times \\
&\times \oint_S \left(\mathbf{N}_{e0n_1} \cdot \mathbf{N}^*_{e0n_2}\right)\left(\hat{\mathbf{r}} \cdot \hat{\mathbf{z}}\right) dS =
\end{aligned}$$

$$\oint_S \left(\mathbf{N}_{em_1n_1} \cdot \mathbf{N}^*_{om_2n_2}\right)\left(\hat{\mathbf{r}} \cdot \hat{\mathbf{z}}\right) dS = 0$$

Integrals of the dot product $\mathbf{N}_{em_1n_1} \cdot \mathbf{M}^*_{em_2n_2}$:

$$\oint_S \left(\mathbf{N}_{em_1n_1} \cdot \mathbf{M}^*_{em_2n_2}\right)\left(\hat{\mathbf{r}} \cdot \hat{\mathbf{x}}\right) dS = 0$$

$$\begin{aligned}
&\oint_S \left(\mathbf{N}_{em_1n_1} \cdot \mathbf{M}^*_{em_2n_2}\right)\left(\hat{\mathbf{r}} \cdot \hat{\mathbf{y}}\right) dS = \frac{\pi r}{k_0} z^*_{n_1}\left(k_0 r\right) \frac{1}{k} \frac{d}{dr}\left[k_0 r\, z_{n_2}\left(k_0 r\right)\right] \times \\
&\times \delta_{n_1 n_2}\left[\left(\delta_{m_1(m_2+1)} + \delta_{m_1 1}\delta_{m_2 0}\right) \frac{1}{2n_1+1} \frac{(n_1+m_1)!}{(n_1-m_1)!} + \left(\delta_{m_2(m_1+1)} + \delta_{m_2 1}\delta_{m_1 0}\right) \frac{1}{2n_1+1} \frac{(n_1+m_2)!}{(n_1-m_2)!}\right]
\end{aligned}$$

$$\oint_S \left(\mathbf{N}_{em_1n_1} \cdot \mathbf{M}^*_{em_2n_2}\right)\left(\hat{\mathbf{r}} \cdot \hat{\mathbf{z}}\right) dS = 0$$

Integrals of the dot product $\mathbf{N}_{om_1n_1} \cdot \mathbf{M}^*_{om_2n_2}$:

$$\oint_S \left(\mathbf{N}_{om_1n_1} \cdot \mathbf{M}^*_{om_2n_2}\right)\left(\hat{\mathbf{r}} \cdot \hat{\mathbf{x}}\right) dS = 0$$

$$\oint_S \left(\mathbf{N}_{om_1n_1} \cdot \mathbf{M}^*_{om_2n_2}\right)\left(\hat{\mathbf{r}} \cdot \hat{\mathbf{y}}\right) dS = \frac{\pi r}{k_0} z^*_{n_1}\left(k_0 r\right)\frac{1}{k}\frac{d}{dr}\left[k_0 r\, z_{n_2}\left(k_0 r\right)\right]\times$$
$$\times\delta_{n_1n_2}\left[\left(\delta_{m_1(m_2+1)} - \delta_{m_11}\delta_{m_20}\right)\frac{1}{2n_1+1}\frac{\left(n_1+m_1\right)!}{\left(n_1-m_1\right)!} - \left(\delta_{m_2(m_1+1)} - \delta_{m_21}\delta_{m_10}\right)\frac{1}{2n_1+1}\frac{\left(n_1+m_2\right)!}{\left(n_1-m_2\right)!}\right]$$

$$\oint_S \left(\mathbf{N}_{om_1n_1} \cdot \mathbf{M}^*_{om_2n_2}\right)\left(\hat{\mathbf{r}} \cdot \hat{\mathbf{z}}\right) dS = 0$$

Integrals of the dot product $\mathbf{M}_{em_1n_1} \cdot \mathbf{M}^*_{em_2n_2}$:

$$\oint_S \left(\mathbf{M}_{em_1n_1} \cdot \mathbf{M}^*_{em_1n_2}\right)\left(\hat{\mathbf{r}} \cdot \hat{\mathbf{x}}\right) dS = \oint_S \left(\mathbf{M}_{e0n_1} \cdot \mathbf{M}^*_{e0n_2}\right)\left(\hat{\mathbf{r}} \cdot \hat{\mathbf{z}}\right) dS \times \left(1 + \delta_{m_10} + \delta_{0m_2}\right)\times$$
$$\times\left[\begin{array}{l} -\delta_{n_1(n_2+1)}\delta_{m_1(m_2+1)}\dfrac{\left(n_1+m_1\right)!}{4n_1\left(n_1-m_1\right)!} + \delta_{n_1(n_2+1)}\delta_{m_1(m_2-1)}\left(n_1-m_1-1\right)\left(n_1-m_1\right)\dfrac{\left(n_1+m_1\right)!}{4n_1\left(n_1-m_1\right)!} + \\ +\delta_{n_2(n_1+1)}\delta_{m_1(m_2+1)}\dfrac{\left(n_1+m_1\right)!}{4n_2\left(n_1-m_1\right)!} - \delta_{n_2(n_1+1)}\delta_{m_1(m_2-1)}\dfrac{\left(n_2+m_2\right)!}{4n_2\left(n_2-m_2\right)!} \end{array}\right]$$

$$\oint_S \left(\mathbf{M}_{em_1n_1} \cdot \mathbf{M}^*_{em_1n_2}\right)\left(\hat{\mathbf{r}} \cdot \hat{\mathbf{y}}\right) dS = 0$$

$$\oint_S \left(\mathbf{M}_{em_1n_1}\cdot\mathbf{M}^*_{em_1n_2}\right)\left(\hat{\mathbf{r}}\cdot\hat{\mathbf{z}}\right)dS =$$
$$= \pi\,\delta_{m_1m_2} z_{n_1}\left(k_0 r\right) z^*_{n_2}\left(k_0 r\right) r^2 \left[\frac{2n_1\left(n_1+2\right)\left(n_1+m_1+1\right)}{\left(2n_1+3\right)\left(2n_1+1\right)}\frac{\left(n_1+m_1\right)!}{\left(n_1-m_1\right)!}\delta_{(n_1+1)n_2} + \frac{2\left(n_1^2-1\right)\left(n_1-m_1\right)}{\left(2n_1+1\right)\left(2n_1-1\right)}\frac{\left(n_1+m_1\right)!}{\left(n_1-m_1\right)!}\delta_{(n_1-1)n_2}\right]$$

Integrals of the dot product $\mathbf{M}_{om_1n_1}\cdot\mathbf{M}^*_{om_2n_2}$:

$$\oint_S \left(\mathbf{M}_{om_1n_1}\cdot\mathbf{M}^*_{om_1n_2}\right)\left(\hat{\mathbf{r}}\cdot\hat{\mathbf{x}}\right)dS = \oint_S \left(\mathbf{M}_{e0n_1}\cdot\mathbf{M}^*_{e0n_2}\right)\left(\hat{\mathbf{r}}\cdot\hat{\mathbf{z}}\right)dS \times \left(1-\delta_{m_10}-\delta_{0m_2}\right)\times$$
$$\times\left[\begin{array}{l} -\delta_{n_1(n_2+1)}\delta_{m_1(m_2+1)}\dfrac{\left(n_1+m_1\right)!}{4n_1\left(n_1-m_1\right)!} + \delta_{n_1(n_2+1)}\delta_{m_1(m_2-1)}\left(n_1-m_1-1\right)\left(n_1-m_1\right)\dfrac{\left(n_1+m_1\right)!}{4n_1\left(n_1-m_1\right)!} + \\ +\delta_{n_2(n_1+1)}\delta_{m_1(m_2+1)}\dfrac{\left(n_1+m_1\right)!}{4n_2\left(n_1-m_1\right)!} - \delta_{n_2(n_1+1)}\delta_{m_1(m_2-1)}\dfrac{\left(n_2+m_2\right)!}{4n_2\left(n_2-m_2\right)!}\end{array}\right]$$

$$\oint_S \left(\mathbf{M}_{om_1n_1}\cdot\mathbf{M}^*_{om_1n_2}\right)\left(\hat{\mathbf{r}}\cdot\hat{\mathbf{y}}\right)dS = 0$$

$$\oint_S \left(\mathbf{M}_{om_1n_1}\cdot\mathbf{M}^*_{om_1n_2}\right)\left(\hat{\mathbf{r}}\cdot\hat{\mathbf{z}}\right)dS =$$
$$= \pi\,\delta_{m_1m_2} z_{n_1}\left(k_0 r\right) z^*_{n_2}\left(k_0 r\right) r^2 \left[\frac{2n_1\left(n_1+2\right)\left(n_1+m_1+1\right)}{\left(2n_1+3\right)\left(2n_1+1\right)}\frac{\left(n_1+m_1\right)!}{\left(n_1-m_1\right)!}\delta_{(n_1+1)n_2} + \frac{2\left(n_1^2-1\right)\left(n_1-m_1\right)}{\left(2n_1+1\right)\left(2n_1-1\right)}\frac{\left(n_1+m_1\right)!}{\left(n_1-m_1\right)!}\delta_{(n_1-1)n_2}\right]$$

Integrals of the dot product $\mathbf{M}_{em_1n_1} \cdot \mathbf{M}^*_{om_2n_2}$:

$$\oint_S \left(\mathbf{M}_{em_1n_1} \cdot \mathbf{M}^*_{om_1n_2}\right)\left(\hat{\mathbf{r}} \cdot \hat{\mathbf{x}}\right) dS = 0$$

$$\oint_S \left(\mathbf{M}_{em_1n_1} \cdot \mathbf{M}^*_{om_1n_2}\right)\left(\hat{\mathbf{r}} \cdot \hat{\mathbf{y}}\right) dS = \oint_S \left(\mathbf{M}_{e0n_1} \cdot \mathbf{M}^*_{e0n_2}\right)\left(\hat{\mathbf{r}} \cdot \hat{\mathbf{z}}\right) dS \times \left(1 + \delta_{m_1 0} - \delta_{0m_2}\right) \times$$
$$\times \left[\begin{array}{l} \delta_{n_1(n_2+1)}\delta_{m_1(m_2+1)} \dfrac{(n_1+m_1)!}{4n_1(n_1-m_1)!} + \delta_{n_1(n_2+1)}\delta_{m_1(m_2-1)}(n_1-m_1-1)(n_1-m_1)\dfrac{(n_1+m_1)!}{4n_1(n_1-m_1)!} + \\ -\delta_{n_2(n_1+1)}\delta_{m_1(m_2+1)} \dfrac{(n_1+m_1)!}{4n_2(n_1-m_1)!} - \delta_{n_2(n_1+1)}\delta_{m_1(m_2-1)} \dfrac{(n_2+m_2)!}{4n_2(n_2-m_2)!} \end{array} \right]$$

$$\oint_S \left(\mathbf{M}_{em_1n_1} \cdot \mathbf{M}^*_{om_1n_2}\right)\left(\hat{\mathbf{r}} \cdot \hat{\mathbf{z}}\right) dS = 0$$

Integrals of the dot product $\mathbf{N}_{em_1n_1} \cdot \mathbf{M}^*_{om_2n_2}$:

$$\oint_S \left(\mathbf{N}_{em_1n_1} \cdot \mathbf{M}^*_{om_2n_2}\right)\left(\hat{\mathbf{r}} \cdot \hat{\mathbf{x}}\right) dS = \frac{\pi r}{k_0} \frac{d}{d(k_0 r)}\left[k_0 r\, z^*_{n_2}(k_0 r)\right] z_{n_1}(k_0 r)\, \delta_{n_1 n_2}\left(1 - \delta_{0m_2}\right) \times$$
$$\times \left[\frac{2}{2n_1+1} \frac{(n_1+m_1)!}{(n_1-m_1)!} \delta_{m_1(m_2+1)} + \frac{2}{2n_1+1} \frac{(n_1+m_2)!}{(n_1-m_2)!} \left(\delta_{m_1(m_2-1)} + \delta_{m_1 0}\delta_{m_2 1}\right) \right]$$

$$\oint_S \left(\mathbf{N}_{em_1n_1} \cdot \mathbf{M}^*_{om_2n_2}\right)\left(\hat{\mathbf{r}} \cdot \hat{\mathbf{y}}\right) dS = 0$$

$$\oint_S \left(\mathbf{N}_{em_1n_1} \cdot \mathbf{M}^*_{om_2n_2}\right)\left(\hat{\mathbf{r}} \cdot \hat{\mathbf{z}}\right) dS = \pi\, \delta_{m_1 m_2} \frac{1}{k_0 r} \frac{d}{d(k_0 r)}\left[k_0 r\, z_{n_1}(k_0 r)\right] z^*_{n_1}(k_0 r)\, r^2 m_1 \frac{2}{2n_1+1} \frac{(n_1+m_1)!}{(n_1-m_1)!} \delta_{n_1 n_2}$$

Integrals of the dot product $\mathbf{N}_{om_1n_1} \cdot \mathbf{M}^*_{em_2n_2}$:

$$\oint_S \left(\mathbf{N}_{om_1n_1} \cdot \mathbf{M}^*_{em_2n_2}\right)\left(\hat{\mathbf{r}} \cdot \hat{\mathbf{x}}\right) dS = -\frac{\pi r}{k_0} \frac{d}{d\left(k_0 r\right)}\left[k_0 r\, z^*_{n_2}\left(k_0 r\right)\right] z_{n_1}\left(k_0 r\right) \delta_{n_1 n_2}\left(1-\delta_{0m_1}\right) \times$$
$$\times \left[\frac{2}{2n_1+1}\frac{\left(n_1+m_1\right)!}{\left(n_1-m_1\right)!}\left(\delta_{m_1(m_2+1)} + \delta_{m_1 1}\delta_{m_2 0}\right) + \frac{2}{2n_1+1}\frac{\left(n_1+m_2\right)!}{\left(n_1-m_2\right)!}\delta_{m_2(m_1+1)}\right]$$

$$\oint_S \left(\mathbf{N}_{om_1n_1} \cdot \mathbf{M}^*_{em_2n_2}\right)\left(\hat{\mathbf{r}} \cdot \hat{\mathbf{y}}\right) dS = 0$$

$$\oint_S \left(\mathbf{N}_{om_1n_1} \cdot \mathbf{M}^*_{em_2n_2}\right)\left(\hat{\mathbf{r}} \cdot \hat{\mathbf{z}}\right) dS = -\pi\, \delta_{m_1 m_2} \frac{1}{k_0 r} \frac{d}{d\left(k_0 r\right)}\left[k_0 r\, z_{n_1}\left(k_0 r\right)\right] z^*_{n_1}\left(k_0 r\right) r^2 m_1 \frac{2}{2n_1+1}\frac{\left(n_1+m_1\right)!}{\left(n_1-m_1\right)!}\delta_{n_1 n_2}$$

Integrals of the dyadic product $\mathbf{N}_{em_1n_1}\mathbf{N}^*_{em_2n_2}$:

$$\oint_S \left(\mathbf{N}_{em_1n_1}\mathbf{N}^*_{em_2n_2}\cdot\hat{\mathbf{r}}\right)\cdot\hat{\mathbf{x}}\,dS = \oint_S \left(\mathbf{N}_{e0n_1}\mathbf{N}^*_{e0n_2}\cdot\hat{\mathbf{r}}\right)\cdot\hat{\mathbf{z}}\,dS \times \left(1+\delta_{m_1 0}+\delta_{0m_2}\right)\times$$
$$\times\left[\begin{array}{l} -\delta_{n_1(n_2+1)}\delta_{m_1(m_2+1)}\dfrac{(n_1+m_1)!}{4n_1(n_1-m_1)!}+\delta_{n_1(n_2+1)}\delta_{m_1(m_2-1)}(n_1-m_1)(n_1-m_1-1)\dfrac{(n_1+m_1)!}{4n_1(n_1-m_1)!}+ \\ +\delta_{n_2(n_1+1)}\delta_{m_1(m_2+1)}\dfrac{(n_1+m_1)!}{4n_2(n_1-m_1)!}-\delta_{n_2(n_1+1)}\delta_{m_1(m_2-1)}\dfrac{(n_2+m_2)!}{4n_2(n_2-m_2)!} \end{array}\right]$$

$$\oint_S \left(\mathbf{N}_{em_1n_1}\mathbf{N}^*_{em_2n_2}\cdot\hat{\mathbf{r}}\right)\cdot\hat{\mathbf{y}}\,dS = 0$$

$$\oint_S \left(\mathbf{N}_{em_1n_1}\mathbf{N}^*_{em_2n_2}\cdot\hat{\mathbf{r}}\right)\cdot\hat{\mathbf{z}}\,dS =$$
$$= \frac{z_{n_1}(k_0r)\,z^*_{n_2}(k_0r)}{k_0^2}\pi\,\delta_{m_1m_2}\times$$
$$\times\left[\frac{2n_1(n_1+1)^2(n_1+2)(n_1+m_1+1)}{(2n_1+3)(2n_1+1)}\frac{(n_1+m_1)!}{(n_1-m_1)!}\delta_{(n_1+1)n_2}+\frac{2n_1^2(n_1^2-1)(n_1-m_1)}{(2n_1+1)(2n_1-1)}\frac{(n_1+m_1)!}{(n_1-m_1)!}\delta_{(n_1-1)n_2}\right]+$$
$$-\frac{d}{d(k_0r)}\left[k_0r\,z_{n_1}(k_0r)\right]\frac{z^*_{n_2}(k_0r)}{k_0^2}\pi\,\delta_{m_1m_2}\times$$
$$\times\left\{\left[\frac{2n_1(n_1+1)(n_1+2)(n_1+m_1+1)}{(2n_1+3)(2n_1+1)}\frac{(n_1+m_1)!}{(n_1-m_1)!}\delta_{(n_1+1)n_2}-\frac{2n_1(n_1^2-1)(n_1-m_1)}{(2n_1+1)(2n_1-1)}\frac{(n_1+m_1)!}{(n_1-m_1)!}\delta_{(n_1-1)n_2}\right]\right\}$$

Integrals of the dyadic product $\mathbf{N}_{om_1n_1}\mathbf{N}^*_{om_2n_2}$:

$$\oint_S \left(\mathbf{N}_{om_1n_1}\mathbf{N}^*_{om_2n_2}\cdot\hat{\mathbf{r}}\right)\cdot\hat{\mathbf{x}}\,dS = \oint_S \left(\mathbf{N}_{e0n_1}\mathbf{N}^*_{e0n_2}\cdot\hat{\mathbf{r}}\right)\cdot\hat{\mathbf{z}}\,dS \times \left(1-\delta_{m_1 0}-\delta_{0m_2}\right)\times$$
$$\times\left[\begin{array}{l} -\delta_{n_1(n_2+1)}\delta_{m_1(m_2+1)}\dfrac{(n_1+m_1)!}{4n_1(n_1-m_1)!}+\delta_{n_1(n_2+1)}\delta_{m_1(m_2-1)}(n_1-m_1)(n_1-m_1-1)\dfrac{(n_1+m_1)!}{4n_1(n_1-m_1)!}+ \\ +\delta_{n_2(n_1+1)}\delta_{m_1(m_2+1)}\dfrac{(n_1+m_1)!}{4n_2(n_1-m_1)!}-\delta_{n_2(n_1+1)}\delta_{m_1(m_2-1)}\dfrac{(n_2+m_2)!}{4n_2(n_2-m_2)!} \end{array}\right]$$

$$\oint_S \left(\mathbf{N}_{om_1n_1}\mathbf{N}^*_{om_2n_2}\cdot\hat{\mathbf{r}}\right)\cdot\hat{\mathbf{y}}\,dS = 0$$

$$\oint_S \left(\mathbf{N}_{om_1n_1}\mathbf{N}^*_{om_2n_2}\cdot\hat{\mathbf{r}}\right)\cdot\hat{\mathbf{z}}\,dS =$$
$$= \frac{z_{n_1}(k_0r)\,z^*_{n_2}(k_0r)}{k_0^2}\pi\,\delta_{m_1m_2}\times$$
$$\times\left[\frac{2n_1(n_1+1)^2(n_1+2)(n_1+m_1+1)}{(2n_1+3)(2n_1+1)}\frac{(n_1+m_1)!}{(n_1-m_1)!}\delta_{(n_1+1)n_2}+\frac{2n_1^2(n_1^2-1)(n_1-m_1)}{(2n_1+1)(2n_1-1)}\frac{(n_1+m_1)!}{(n_1-m_1)!}\delta_{(n_1-1)n_2}\right]+$$
$$-\frac{d}{d(k_0r)}\left[k_0r\,z_{n_1}(k_0r)\right]\frac{z^*_{n_2}(k_0r)}{k_0^2}\pi\,\delta_{m_1m_2}\times$$
$$\times\left\{\left[\frac{2n_1(n_1+1)(n_1+2)(n_1+m_1+1)}{(2n_1+3)(2n_1+1)}\frac{(n_1+m_1)!}{(n_1-m_1)!}\delta_{(n_1+1)n_2}-\frac{2n_1(n_1^2-1)(n_1-m_1)}{(2n_1+1)(2n_1-1)}\frac{(n_1+m_1)!}{(n_1-m_1)!}\delta_{(n_1-1)n_2}\right]\right\}$$

Integrals of the dyadic product $\mathbf{M}_{om_1n_1}\mathbf{N}^*_{em_2n_2}$:

$$\oint_S \left(\mathbf{M}_{om_1n_1}\mathbf{N}^*_{em_2n_2}\cdot\hat{\mathbf{r}}\right)\cdot\hat{\mathbf{x}}\,dS = -\left(1-\delta_{m_1 0}\right) r\, z_{n_1}\left(k_0 r\right)\frac{z^*_{n_2}\left(k_0 r\right)}{k_0}\pi\times$$
$$\times\left[\frac{2n_1\left(n_1+1\right)}{2n_1+1}\frac{\left(n_1+m_1\right)!}{\left(n_1-m_1\right)!}\left(\delta_{m_1(m_2+1)}+\delta_{m_1 1}\delta_{0m_2}\right)+\frac{2n_1\left(n_1+1\right)}{2n_1+1}\frac{\left(n_1+m_2\right)!}{\left(n_1-m_2\right)!}\delta_{m_2(m_1+1)}\right]$$

$$\oint_S \left(\mathbf{M}_{om_1n_1}\mathbf{N}^*_{em_2n_2}\cdot\hat{\mathbf{r}}\right)\cdot\hat{\mathbf{y}}\,dS = 0$$

$$\oint_S \left(\mathbf{M}_{om_1n_1}\mathbf{N}^*_{em_2n_2}\cdot\hat{\mathbf{r}}\right)\cdot\hat{\mathbf{z}}\,dS = -r\, z_{n_1}\left(k_0 r\right)\frac{z^*_{n_2}\left(k_0 r\right)}{k_0} m_1\pi\,\delta_{m_1m_2}\,\frac{2n_1\left(n_1+1\right)}{2n_1+1}\frac{\left(n_1+m_1\right)!}{\left(n_1-m_1\right)!}\delta_{n_1n_2}$$

Integrals of the dyadic product $\mathbf{M}_{em_1n_1}\mathbf{N}^*_{om_2n_2}$:

$$\oint_S \left(\mathbf{M}_{em_1n_1}\mathbf{N}^*_{om_2n_2}\cdot\hat{\mathbf{r}}\right)\cdot\hat{\mathbf{x}}\,dS = \left(1-\delta_{m_2 0}\right) r\, z_{n_1}\left(k_0 r\right)\frac{z^*_{n_2}\left(k_0 r\right)}{k_0}\pi\times$$
$$\times\left[\frac{2n_1\left(n_1+1\right)}{2n_1+1}\frac{\left(n_1+m_1\right)!}{\left(n_1-m_1\right)!}\delta_{m_1(m_2+1)}+\frac{2n_1\left(n_1+1\right)}{2n_1+1}\frac{\left(n_1+m_2\right)!}{\left(n_1-m_2\right)!}\left(\delta_{m_2(m_1+1)}+\delta_{m_2 1}\delta_{0m_1}\right)\right]$$

$$\oint_S \left(\mathbf{M}_{em_1n_1}\mathbf{N}^*_{om_2n_2}\cdot\hat{\mathbf{r}}\right)\cdot\hat{\mathbf{y}}\,dS = 0$$

$$\oint_S \left(\mathbf{M}_{em_1n_1}\mathbf{N}^*_{om_2n_2}\cdot\hat{\mathbf{r}}\right)\cdot\hat{\mathbf{z}}\,dS = r\, z_{n_1}\left(k_0 r\right)\frac{z^*_{n_2}\left(k_0 r\right)}{k_0} m_1\pi\,\delta_{m_1m_2}\,\frac{2n_1\left(n_1+1\right)}{2n_1+1}\frac{\left(n_1+m_1\right)!}{\left(n_1-m_1\right)!}\delta_{n_1n_2}$$

Integrals of the dyadic product $\mathbf{N}_{em_1n_1}\mathbf{N}^*_{om_2n_2}$:

$$\oint_S \left(\mathbf{N}_{em_1n_1}\mathbf{N}^*_{om_2n_2}\cdot\hat{\mathbf{r}}\right)\cdot\hat{\mathbf{x}}\,dS = 0$$

$$\oint_S \left(\mathbf{N}_{em_1n_1}\mathbf{N}^*_{om_2n_2}\cdot\hat{\mathbf{r}}\right)\cdot\hat{\mathbf{y}}\,dS = \oint_S \left(\mathbf{N}_{e0n_1}\mathbf{N}^*_{e0n_2}\cdot\hat{\mathbf{r}}\right)\cdot\hat{\mathbf{z}}\,dS \times \left(1+\delta_{m_1 0}-\delta_{m_2 0}\right)\times$$
$$\times\left[\begin{array}{l}\delta_{n_1(n_2+1)}\delta_{m_1(m_2+1)}\dfrac{(n_1+m_1)!}{4n_1(n_1-m_1)!}+\delta_{n_1(n_2+1)}\delta_{m_1(m_2-1)}\dfrac{(n_2+m_2)!}{4n_1(n_2-m_2)!}+\\ -\delta_{n_2(n_1+1)}\delta_{m_1(m_2+1)}\dfrac{(n_1+m_1)!}{4n_2(n_1-m_1)!}-\delta_{n_2(n_1+1)}\delta_{m_1(m_2-1)}\dfrac{(n_2+m_2)!}{4n_2(n_2-m_2)!}\end{array}\right]$$

$$\oint_S \left(\mathbf{N}_{em_1n_1}\mathbf{N}^*_{om_2n_2}\cdot\hat{\mathbf{r}}\right)\cdot\hat{\mathbf{z}}\,dS = 0$$

Integrals of the dyadic product $\mathbf{M}_{em_1n_1}\mathbf{N}^*_{em_2n_2}$:

$$\oint_S \left(\mathbf{M}_{em_1n_1}\mathbf{N}^*_{em_2n_2}\cdot\hat{\mathbf{r}}\right)\cdot\hat{\mathbf{x}}\,dS = 0$$

$$\oint_S \left(\mathbf{M}_{em_1n_1}\mathbf{N}^*_{em_2n_2}\cdot\hat{\mathbf{r}}\right)\cdot\hat{\mathbf{y}}\,dS = \delta_{n_1n_2}\frac{\pi r}{k_0}z_{n_1}\left(k_0 r\right)z^*_{n_2}\left(k_0 r\right)\times$$
$$\times\left[\frac{n_1(n_1+1)}{2n_1+1}\frac{(n_1+m_1)!}{(n_1-m_1)!}\left(\delta_{m_1(m_2+1)}+\delta_{m_1 1}\delta_{m_2 0}\right)+\frac{n_1(n_1+1)}{2n_1+1}\frac{(n_1+m_2)!}{(n_1-m_2)!}\left(\delta_{m_2(m_1+1)}+\delta_{m_2 1}\delta_{m_1 0}\right)\right]$$

$$\oint_S \left(\mathbf{M}_{em_1n_1}\mathbf{N}^*_{em_2n_2}\cdot\hat{\mathbf{r}}\right)\cdot\hat{\mathbf{z}}\,dS = 0$$

Integrals of the dyadic product $\mathbf{M}_{om_1n_1}\mathbf{N}^*_{om_2n_2}$:

$$\oint_S \left(\mathbf{M}_{om_1n_1}\mathbf{N}^*_{om_2n_2}\cdot\hat{\mathbf{r}}\right)\cdot\hat{\mathbf{x}}\,dS = 0$$

$$\oint_S \left(\mathbf{M}_{om_1n_1}\mathbf{N}^*_{om_2n_2}\cdot\hat{\mathbf{r}}\right)\cdot\hat{\mathbf{y}}\,dS = \delta_{n_1n_2}\frac{\pi r}{k_0}z_{n_1}\left(k_0r\right)z^*_{n_2}\left(k_0r\right)\times$$
$$\times\left[\frac{n_1\left(n_1+1\right)}{2n_1+1}\frac{\left(n_1+m_1\right)!}{\left(n_1-m_1\right)!}\left(\delta_{m_1(m_2+1)}-\delta_{m_11}\delta_{m_20}\right)+\frac{n_1\left(n_1+1\right)}{2n_1+1}\frac{\left(n_1+m_2\right)!}{\left(n_1-m_2\right)!}\left(\delta_{m_2(m_1+1)}-\delta_{m_21}\delta_{m_10}\right)\right]$$

$$\oint_S \left(\mathbf{M}_{om_1n_1}\mathbf{N}^*_{om_2n_2}\cdot\hat{\mathbf{r}}\right)\cdot\hat{\mathbf{z}}\,dS = 0$$

REFERENCES

1. Berini, P., et al., *Long-range surface plasmon-polariton waveguides and devices in lithium niobate.* Journal of Applied Physics, 2007. **101**(11): p. -.
2. Berini, P., et al., *Characterization of long-range surface-plasmon-polariton waveguides.* Journal of Applied Physics, 2005. **98**(4): p. -.
3. Charbonneau, R., et al., *Demonstration of integrated optics elements based on long-ranging surface plasmon polaritons.* Opt. Express, 2005. **13**(3): p. 977-984.
4. Charbonneau, R., et al., *Passive integrated optics elements used on long-range surface plasmon polaritons.* Journal of Lightwave Technology, 2006. **24**(1): p. 477-494.
5. Jette-Charbonneau, S., et al., *Demonstration of Bragg gratings based on long-ranging surface plasmon polariton waveguides.* Optics Express, 2005. **13**(12): p. 4674-4682.
6. Jette-Charbonneau, S., et al., *Bragg gratings based on long-range surface plasmon-polariton waveguides: Comparison of theory and experiment.* Ieee Journal of Quantum Electronics, 2005. **41**(12): p. 1480-1491.
7. Mattiussi, G., et al., *Fabrication of long-range surface plasmon-polariton waveguides in lithium niobate on silicon.* Journal of Vacuum Science & Technology A, 2007. **25**(4): p. 692-700.
8. Alu, A. and N. Engheta, *Input impedance, nanocircuit loading, and radiation tuning of optical nanoantennas.* Physical Review Letters, 2008. **101**(4): p. -.

9. Boriskina, S.V. and L. Dal Negro, *Multiple-wavelength plasmonic nanoantennas.* Optics Letters, 2010. **35**(4): p. 538-540.

10. Brongersma, M.L., *Plasmonics - Engineering optical nanoantennas.* Nature Photonics, 2008. **2**(5): p. 270-272.

11. Encina, E.R. and E.A. Coronado, *Plasmonic nanoantennas: Angular scattering properties of multipole resonances in noble metal nanorods.* Journal of Physical Chemistry C, 2008. **112**(26): p. 9586-9594.

12. Fischer, H. and O.J.F. Martin, *Engineering the optical response of plasmonic nanoantennas.* Optics Express, 2008. **16**(12): p. 9144-9154.

13. Pakizeh, T. and M. Kall, *Unidirectional Ultracompact Optical Nanoantennas.* Nano Letters, 2009. **9**(6): p. 2343-2349.

14. Pucci, A., et al., *Surface enhanced infrared spectroscopy using gold nanoantennas.* Physica Status Solidi B-Basic Solid State Physics, 2010. **247**(8): p. 2071-2074.

15. Schnell, M., et al., *Controlling the near-field oscillations of loaded plasmonic nanoantennas.* Nature Photonics, 2009. **3**(5): p. 287-291.

16. Cubukcu, E., et al., *Plasmonic laser antenna.* Applied Physics Letters, 2006. **89**(9): p. -.

17. Cubukcu, E., et al., *Plasmonic Laser Antennas and Related Devices.* Ieee Journal of Selected Topics in Quantum Electronics, 2008. **14**(6): p. 1448-1461.

18. Yu, N.F., et al., *Small divergence edge-emitting semiconductor lasers with two-dimensional plasmonic collimators.* Applied Physics Letters, 2008. **93**(18): p. -.

19. Yu, N.F., et al., *Small-divergence semiconductor lasers by plasmonic collimation.* Nature Photonics, 2008. **2**(9): p. 564-570.

20. Durnin, J., J.J. Miceli, and J.H. Eberly, *Diffraction-Free Beams.* Physical Review Letters, 1987. **58**(15): p. 1499-1501.

21. Gutierrez-Vega, J.C., M.D. Iturbe-Castillo, and S. Chavez-Cerda, *Alternative formulation for invariant optical fields: Mathieu beams.* Optics Letters, 2000. **25**(20): p. 1493-1495.

22. Siviloglou, G.A. and D.N. Christodoulides, *Accelerating finite energy Airy beams.* Optics Letters, 2007. **32**(8): p. 979-981.

23. Siviloglou, G.A., et al., *Observation of accelerating airy beams.* Physical Review Letters, 2007. **99**(21): p. -.

24. Siviloglou, G.A., et al., *Ballistic dynamics of Airy beams.* Optics Letters, 2008. **33**(3): p. 207-209.

25. Broky, J., et al., *Self-healing properties of optical Airy beams.* Optics Express, 2008. **16**(17): p. 12880-12891.

26. Eichelkraut, T.J., et al., *Oblique Airy wave packets in bidispersive optical media.* Optics Letters, 2010. **35**(21): p. 3655-3657.

27. Bandres, M.A., *Accelerating beams.* Optics Letters, 2009. **34**(24): p. 3791-3793.

28. Davis, J.A., et al., *Generation of accelerating Airy and accelerating parabolic beams using phase-only patterns.* Applied Optics, 2009. **48**(17): p. 3170-3176.

29. Dolev, I., et al., *Control of free space propagation of Airy beams generated by quadratic nonlinear photonic crystals.* Applied Physics Letters, 2009. **95**(20): p. -.

30. Ellenbogen, T., et al., *Nonlinear generation and manipulation of Airy beams.* Nature Photonics, 2009. **3**(7): p. 395-398.

31. Berry, M.V. and N.L. Balazs, *Non-Spreading Wave Packets.* American Journal of Physics, 1979. **47**(3): p. 264-267.

32. Besieris, I.M. and A.M. Shaarawi, *A note on an accelerating finite energy Airy beam.* Optics Letters, 2007. **32**(16): p. 2447-2449.

33. Baumgartl, J., M. Mazilu, and K. Dholakia, *Optically mediated particle clearing using Airy wavepackets.* Nature Photonics, 2008. **2**(11): p. 675-678.

34. Polynkin, P., et al., *Curved Plasma Channel Generation Using Ultraintense Airy Beams.* Science, 2009. **324**(5924): p. 229-232.

35. Chong, A., et al., *Airy-Bessel wave packets as versatile linear light bullets.* Nature Photonics, 2010. **4**(2): p. 103-106.

36. Otto, A., *Excitation of Nonradiative Surface Plasma Waves in Silver by Method of Frustrated Total Reflection.* Zeitschrift Fur Physik, 1968. **216**(4): p. 398-&.

37. Abbe, E., *Beitrage zur theorie des microscopes und der mikroskopischen wahrnehmung.* Schultzes Arch. Mikr. Anat., 1873. **9**.

38. Ash, E.A. and G. Nicholls, *Super-Resolution Aperture Scanning Microscope.* Nature, 1972. **237**(5357): p. 510-&.

39. Lewis, A., et al., *Development of a 500-a Spatial-Resolution Light-Microscope .1. Light Is Efficiently Transmitted through Gamma-16 Diameter Apertures.* Ultramicroscopy, 1984. **13**(3): p. 227-231.

40. Pohl, D.W., W. Denk, and M. Lanz, *Optical Stethoscopy - Image Recording with Resolution Lambda/20.* Applied Physics Letters, 1984. **44**(7): p. 651-653.

41. Synge, E., H., *A suggested method for extending the microscopic resolution into the ultramicroscopic region.* Phil. Mag., 1928. **6**.

42. Hell, S.W. and J. Wichmann, *Breaking the Diffraction Resolution Limit by Stimulated-Emission - Stimulated-Emission-Depletion Fluorescence Microscopy*. Optics Letters, 1994. **19**(11): p. 780-782.

43. Salandrino, A. and N. Engheta, *Far-field subdiffraction optical microscopy using metamaterial crystals: Theory and simulations.* Physical Review B, 2006. **74**(7): p. -.

44. Jacob, Z., L.V. Alekseyev, and E. Narimanov, *Optical hyperlens: Far-field imaging beyond the diffraction limit.* Optics Express, 2006. **14**(18): p. 8247-8256.

45. Lee, H., et al., *Development of optical hyperlens for imaging below the diffraction limit.* Optics Express, 2007. **15**(24): p. 15886-15891.

46. Liu, Z.W., et al., *Experimental studies of Far-field SuperLens for sub-diffractional optical imaging.* Optics Express, 2007. **15**(11): p. 6947-6954.

47. Liu, Z.W., et al., *Far-field optical hyperlens magnifying sub-diffraction-limited objects.* Science, 2007. **315**(5819): p. 1686-1686.

48. Rho, J., et al., *Spherical hyperlens for two-dimensional sub-diffractional imaging at visible frequencies.* Nat Commun, 2010. **1**: p. 143.

49. Gazit, S., et al., *Super-resolution and reconstruction of sparse sub-wavelength images.* Opt. Express, 2009. **17**(26): p. 23920-23946.

50. Veselago, V.G., *Properties of Materials Having Simultaneously Negative Values of Dielectric (Xi) and Magnetic (Mu) Susceptibilities.* Soviet Physics Solid State,Ussr, 1967. **8**(12): p. 2854-&.

51. Smith, D.R., et al., *Composite medium with simultaneously negative permeability and permittivity.* Physical Review Letters, 2000. **84**(18): p. 4184-4187.

52. Pendry, J.B., et al., *Magnetism from conductors and enhanced nonlinear phenomena.* Ieee Transactions on Microwave Theory and Techniques, 1999. **47**(11): p. 2075-2084.

53. Siddiqui, O.F., M. Mojahedi, and G.V. Eleftheriades, *Periodically loaded transmission line with effective negative refractive index and negative group velocity.* Ieee Transactions on Antennas and Propagation, 2003. **51**(10): p. 2619-2625.

54. Shalaev, V.M., *Optical negative-index metamaterials.* Nature Photonics, 2007. **1**(1): p. 41-48.

55. Eleftheriades, G.V., A.K. Iyer, and P.C. Kremer, *Planar negative refractive index media using periodically L-C loaded transmission lines.* Ieee Transactions on Microwave Theory and Techniques, 2002. **50**(12): p. 2702-2712.

56. Clarricoats, P.J.B. and R.A. Waldron, *Non-periodic slow-wave and backward-wave structures.* Electron. Control 1960. **8**.

57. R.E., C., *Field Theory of Guided Waves*. 2 ed. 1991, New York: IEEE Press.

58. Clarricoats, P.J.B., *Backward waves in waveguides containing dielectrics.* Proc. IEE, 1961. **108**: p. 496–501.

59. Clarricoats, P.J.B. and A.B. Birtles, *Circular Waveguide Backward-wave Experiments.* J. Electron Contr., 1963. **15**: p. 325–330.

60. Ibanescu, M., et al., *Anomalous dispersion relations by symmetry breaking in axially uniform waveguides.* Physical Review Letters, 2004. **92**(6): p. -.

61. Tsandoulas, G.N., *Propagation in Dielectric-Lined Square Waveguides.* Ieee Transactions on Microwave Theory and Techniques, 1975. **Mt23**(5): p. 406-410.

62. Waldron, R.A., *Theory and potential applications of backward-waves in non-periodic inhomogeneous waveguides.* Proc. IEE, 1964. **111**: p. 1659–1667.

63. Lee, C.S., S.W. Lee, and S.L. Chuang, *Plot of Modal Field Distribution in Rectangular and Circular Wave-Guides.* Ieee Transactions on Microwave Theory and Techniques, 1985. **33**(3): p. 271-274.

64. Gillespie, E.F.F., *Power flow and negative impedance in the dielectric rod waveguide.* Proc. Inst. Electr. Eng., 1960. **107c**: p. 198–201.

65. Mokhov, S., R. El-Ganainy, and D.N. Christodoulides, *Power circulation via negative energy-flux wormholes in optical nanowaveguides.* Optics Express, 2006. **14**(8): p. 3255-3262.

66. Bolivar, P.H., et al., *Measurement of the dielectric constant and loss tangent of high dielectric-constant materials at terahertz frequencies.* Ieee Transactions on Microwave Theory and Techniques, 2003. **51**(4): p. 1062-1066.

67. Potter, R.F., *Germanim (Ge),* in *Handbook of Optical Constants of Solids*, E.D. Palik, Editor. 1985, Academic: Orlando, FL.

68. Nam, S.H., A.J. Taylor, and A. Efimov, *Subwavelength hybrid terahertz waveguides.* Optics Express, 2009. **17**(25): p. 22890-22897.

69. Huang, W.P., *Coupled-Mode Theory for Optical Wave-Guides - an Overview.* Journal of the Optical Society of America a-Optics Image Science and Vision, 1994. **11**(3): p. 963-983.

70. Marcuse, D., *Coupled Mode Theory of Round Optical Fibers.* Bell System Technical Journal, 1973. **52**(6): p. 817-842.

71. Snyder, A.W. and J.D. Love, *Optical Waveguide Theory*. 1983, London: Wiley and Chapman and Hall.

72. Yariv, A., *Coupled-Mode Theory for Guided-Wave Optics.* Ieee Journal of Quantum Electronics, 1973. **Qe 9**(9): p. 919-933.

73. Lahini, Y., et al., *Effect of Nonlinearity on Adiabatic Evolution of Light.* Physical Review Letters, 2008. **101**(19): p. -.

74. Longhi, S., et al., *Coherent tunneling by adiabatic passage in an optical waveguide system.* Physical Review B, 2007. **76**(20): p. 201101.

75. Paspalakis, E., *Adiabatic three-waveguide directional coupler.* Optics Communications, 2006. **258**(1): p. 30-34.

76. Gaubatz, U., et al., *Population Transfer between Molecular Vibrational Levels by Stimulated Raman-Scattering with Partially Overlapping Laserfields - a New Concept and Experimental Results.* Journal of Chemical Physics, 1990. **92**(9): p. 5363-5376.

77. Yariv, A., *Quantum electronics*. 3 ed. 1989: John wiley and Sons.

78. Bender, C.M. and S.A. Orszag, *Advaced Mathematical Methods for Scientists and Engineers*. 1999: Springer.

79. Gradshteyn, I.S. and I.M. Ryzhik, *Table of Integrals, Series and Products*. 6 ed. 2000: Academic Press.

80. Lebedev, P., *Experimental examination of light pressure.* Annals of Physics, 1901. **6**.

81. Nichols, E.F. and G.F. Hull, *A Preliminary Communication on the Pressure of Heat and Light Radiation.* Physical Review, 1901. **13**.

82. Ashkin, A., *History of optical trapping and manipulation of small-neutral particle, atoms, and molecules.* Ieee Journal of Selected Topics in Quantum Electronics, 2000. **6**(6): p. 841-856.

83. Ashkin, A., *Optical trapping and manipulation of neutral particles using lasers.* Proceedings of the National Academy of Sciences of the United States of America, 1997. **94**(10): p. 4853-4860.

84. Ashkin, A., *Trapping and Cooling of Neutral Atoms by Light.* Journal of the Optical Society of America a-Optics Image Science and Vision, 1985. **2**(13): p. P50-P50.

85. Ashkin, A., *Trapping and Cooling of Neutral Atoms by Resonance Radiation Pressure.* Bulletin of the American Physical Society, 1979. **24**(4): p. 634-635.

86. Ashkin, A., *Trapping of Atoms by Resonance Radiation Pressure.* Physical Review Letters, 1978. **40**(12): p. 729-732.

87. Ashkin, A., *Acceleration and Trapping of Particles by Radiation Pressure.* Physical Review Letters, 1970. **24**(4): p. 156-&.

88. Ashkin, A. and J.M. Dziedzic, *Optical Trapping and Manipulation of Single Living Cells Using Infrared-Laser Beams.* Berichte Der Bunsen-Gesellschaft-Physical Chemistry Chemical Physics, 1989. **93**(3): p. 254-260.

89. Albaladejo, S., et al., *Scattering Forces from the Curl of the Spin Angular Momentum of a Light Field.* Physical Review Letters, 2009. **102**(11): p. -.

90. Lee, S.H., Y. Roichman, and D.G. Grier, *Optical solenoid beams.* Optics Express, 2010. **18**(7): p. 6988-6993.

91. Sukhov, S. and A. Dogariu, *On the concept of "tractor beams".* Optics Letters, 2010. **35**(22): p. 3847-3849.

92. Mizrahi, A. and Y. Fainman, *Negative radiation pressure on gain medium structures.* Optics Letters, 2010. **35**(20): p. 3405-3407.

93. Bohren , C.F. and D.R. Huffman, *Absorption and Scattering of Light by Small Particles*. 1983: Wiley.

94. Salandrino, A., A. Alu, and N. Engheta, *Parallel, series, and intermediate interconnections of optical nanocircuit elements. 1. Analytical solution.* Journal of the Optical Society of America B-Optical Physics, 2007. **24**(12): p. 3007-3013.

95. Valentine, J., et al., *Three-dimensional optical metamaterial with a negative refractive index.* Nature, 2008. **455**(7211): p. 376-U32.

96. Kittel, C., *Introduction to solid state Physics*. 7 ed. 1995.

97. Cubukcu, E., et al., *Negative refraction by photonic crystals.* Nature, 2003. **423**(6940): p. 604-605.

98. Salandrino, A. and D.N. Christodoulides, *Negative index Clarricoats-Waldron waveguides for terahertz and far infrared applications.* Optics Express, 2010. **18**(4): p. 3626-3631.

99. Debye, P., *Der Lichtdruck auf Kugeln von beliebigem Material.* Annalen der Physik, 1909. **335**(11): p. 57-136.